UNIVERSITEIT VAN PRETORIA
UNIVERSITY OF PRETORIA
YUNIBESITHI YA PRETORIA

MODELLING SUBJECT-SPECIFIC ELECTRICALLY EVOKED AUDITORY NEURAL RESPONSES IN THE GUINEA PIG

by

Ramana Govindasamy

Submitted in partial fulfillment of the requirements for the degree
Master of Engineering (Bio-Engineering) in the
Faculty of Engineering, the Built Environment and Information Technology
UNIVERSITY OF PRETORIA

March 2012

© University of Pretoria

SUMMARY

MODELLING SUBJECT-SPECIFIC ELECTRICALLY EVOKED AUDITORY NEURAL RESPONSES IN THE GUINEA PIG

by

Ramana Govindasamy

Supervisor: Prof T Hanekom

Co-supervisor: Prof JJ Hanekom

Department: Electrical, Electronic and Computer Engineering

University: University of Pretoria

Degree: Master of Engineering (Bio-Engineering)

The degree of hearing restoration provided by the cochlear implant is prone to inter-subject variance. The objective of this study is to account for some of the factors influencing this through a subject-specific model of the guinea pig inner ear. Electrically evoked auditory neural responses, a common measure of threshold activity, are used to quantify the accuracy of the model. The model expands on the existing guinea pig subject-specific model through the implementation of added parameters. It was found that modeling the return electrode, silicon carrier and hook region has the greatest effect on improving the accuracy of the model.

These findings provide insight into the various parameters that affect neural excitation behaviour in the electrically stimulated auditory system and also lay the foundation for the development of subject-specific human models. It is expected that these models could potentially provide a tool to individualise implant parameters.

© University of Pretoria

OPSOMMING

DIE MODELLERING VAN SUBJEK-SPESIFIEKE ELEKTRIES OPGEWEGTE GEHOORSENUWEERESPONSE IN DIE MARMOTKOGLEA

deur

Ramana Govindasamy

Studieleier: Prof T Hanekom

Mede-studieleier: Prof JJ Hanekom

Departement: Elektriese, Elektroniese en Rekenaaringenieurswese

Universiteit: Universiteit van Pretoria

Graad: Magister in Ingenieurswese (Bio-Ingenieurswese)

Die vlak van gehoorherwinning wat deur kogleêre inplantings verskaf word, wissel van persoon tot persoon. Die doel van hierdie navorsing is om faktore onderliggend aan hierdie variasie te ondersoek deur middel van 'n onderwerpspesifieke model van die marmotkoglea. Elektries-opgewekte gehoorsenuweereaksies, wat 'n kritieke stap in die gehoorherwinningsproses verteenwoordig, is gebruik om die akkuraatheid van die model te meet. Die model brei uit op die bestaande onderwerpspesifieke model deur bykomende veranderlikes te implemteer. Die modellering van die terugkeerelektrode, die silikoondraer en die haakarea het die meeste bygedra tot die verbetering van die model.

Hierdie bevindinge werp lig op die verskeie veranderlikes wat die gedrag van senuwees in die elektries-gestimuleerde gehoorstelsel beïnvloed en lê 'n grondslag vir die ontwikkeling van onderwerpspesifieke modelle van menskogleas. Sulke modelle kan bydra tot gereedskap vir die berekening van veranderlikes vir individuele inplantinggebruikers.

© University of Pretoria

CONTENTS

© University of Pretoria

© University of Pretoria

© University of Pretoria

UNIVERSITEIT VAN PRETORIA
UNIVERSITY OF PRETORIA
YUNIBESITHI YA PRETORIA

CHAPTER 1: INTRODUCTION

1.1 PROBLEM STATEMENT

1.1.1 Background and context

Cochlear implants are successful and useful devices enabling thousands of people to regain some perception of hearing by the controlled electrical stimulation of the auditory nerve fibers. Unfortunately speech and music perception show significant variance across subjects (Kunisue et al. 2007). Age of implantation (Hassanzadeh et al. 2002), duration of hearing loss (Blamey et al. 1996a), design of the electrodes (Rebscher et al. 2007), electrode insertion depth (Finley et al. 2008) and other pre-operative variables (Gantz et al. 1993) are some of the factors which influence this. Their effects form an integral part of the research aimed at optimally restoring a subject's hearing. A subject-specific model could provide clarity on some of these effects, through simulation, supplementing time consuming physical procedures.

To predict perceptual behaviour based on physical variables[1] a model that is both anatomical and neural in nature is required. This is realised, where a volume conduction model and neural model are integrated to simulate the response to a cochlear implant (Frijns, Briaire, & Schoonhoven 2000; Frijns, Mooij, & Ten Kate 1994). First the potential distribution within the spiralling volume conduction model is computed. These potentials are then applied to a nerve fiber model to reconstruct excitation profiles of the auditory nerve. The predicted results are compared with actual electrically evoked brainstem responses. The nerve fiber model is a non-linear SEF (Schwarz, Eikhof and Frijns) model and represents essential mammalian nerve properties[2] while also treating the myelin sheath as a perfect insulator. In total the 30 000 actual nerve fibers found in the cochlea are represented by 365 model fibers[3]. Similar models have been constructed (Hanekom 2001b; Hanekom 2005). These are generic models and do not accommodate for subject-specific variances. This accommodation is necessary to understand an individual's cochlear environment post implantation. The need for subject-specific models is further substantiated by the effects of insertion trauma, a surgical risk, which can cause neural

[1] Electrode configuration etc.
[2] Action potential conduction velocity, repetitive firing and refractory behaviour
[3] Each one represents 85 actual fibers

© University of Pretoria

degeneration and altered performance of the implant. Studies investigated the anatomy of the cochlear spiral and examined the potential for certain areas to undergo trauma during implantation (Adunka & Kiefer 2006; Briaire & Frijns 2006; Verbist et al. 2009). It is shown that the intrinsic three-dimensional (3D) morphology of the cochlea contributes to the risk of insertion trauma at the basilar membrane and at the floor of the scala tympani.

The design of the electrodes and their insertion depth are known hence it is possible to gauge their effect on a subject's perception. Repeated surgical procedures to test different configurations in human implantees is ill advised as it is complex, costly and could cause damage to the cochlea. A common practice in the medical field is to use an animal model for humans. Guinea pigs are favoured due to their similar cochlea anatomy and physiology, although the shape of the guinea pig cochlea and thickness of the bone capsule are considerably different. Inferior colliculus central nucleus responses (ICC) have been used to detect neural activation within the cochlea (Snyder, Bierer, & Middlebrooks 2004a; Snyder, Bierer, & Middlebrooks 2004b; Snyder, Middlebrooks, & Bonham 2008), as perception cannot be inferred from animal subjects. Understanding of the spatial spread and consequent neural activation has been fast-tracked by the incorporation of computational models. The generic computational models are of both human and guinea pig cochleae but are exclusive of the geometric variations among subjects, hence they cannot be used to investigate the individual factors which influence perception and performance. This can only be realised through the construction of a subject-specific model.

1.1.2 Research Gap

The correct prediction of ICC response data should give an estimate of the activation spread within the cochlea, the overlap of activation profiles and the independence of cochlear implant channels, i.e. channel interaction. It would also give confidence in understanding the biophysical, anatomical and neural factors which influence ICC in the guinea pig. The results will be applicable in developing similar models for human subjects. Once established, the models may be used to provide a basis for individualising a subject's map, which is necessary due to anatomical, neural survival and electrode location variations across subjects. The map defines perceptual thresholds (T-levels), comfort levels (C-levels), dynamic ranges and characteristic frequencies as a function of electrode number (longitudinal position) for a specific subject. This information could be used to tailor the

© University of Pretoria

implant in a manner which restores maximum hearing objectively. As a research tool, the model could facilitate research on the effects of electrode design and position on neural excitation which are important for auditory perception. An accurate prediction of the spatial spread within the cochlea may also assist research into current steering in cochlear implants (Bonham & Litvak 2008).

1.2. RESEARCH OBJECTIVES AND QUESTIONS

The primary objective is to improve the accuracy of the existing subject-specific guinea pig cochlea model (Malherbe 2009), in its ability to correctly predict evoked auditory brain stem responses. The primary research questions that will be addressed are thus; Do subject-specific models allow a more accurate prediction of ICC data than generic models? Which added model parameters have the greatest impact on the accuracy of the prediction? How can we apply the subject-specific model approach to humans?

1.3 HYPOTHESIS AND APPROACH

The hypotheses are that it is possible to improve the accuracy of the subject-specific cochlear model, through the incorporation of additional model parameters and that the model's prediction of ICC data will be more accurate than a generic model.

The proposed research builds on (Malherbe 2009), where a subject-specific model of the guinea pig cochlea is used to determine some of the factors influencing variability in implant performance. The primary objective will be addressed by expanding the model to include an accurate reconstruction of the bone encasing the cochlea, modelling of the hook area, modelling of the electrode carrier, assessment of neuron damage and implementation thereof, modelling of "leaky holes" arising during implantation (insertion trauma) and an accurate positioning of the ground electrode for monopolar stimulation only[4]. The model parameters will be assessed on their influence in correctly predicting ICC responses and also in terms of their contribution to model complexity.

[4] Only monopolar stimulation is used in this study as it has the widest distribution, thus allowing the researchers to capture the effects of multiple parameters simultaneously

© University of Pretoria

1.4 OVERVIEW OF STUDY

A modelling study will be conducted aimed at improving an existing model so that it is more accurate in its predictions of neural responses. The model's prediction will be assessed against physical ICC data, inferred from the brain stem of the specific guinea pig used in this investigation. The study utilises both a finite element method (FEM) volume conduction model, derived from μ-CT scan data and a generalised Schwarz-Eikhof-Frijns (GSEF) neural model. The measured neural responses are of single nerve fibers, although these are comparable to a population, as single nerve fiber responses are discernable from a population recording where isolation is poor (Snyder, Bierer, & Middlebrooks 2004a). The additional model parameters e.g. electrode carrier, are modelled sequentially with their impact on the accuracy assessed after each implementation. The parameters are also combined and assessed in conjunction. Figure 1.1 provides an overview of the research components associated with this study.

© University of Pretoria

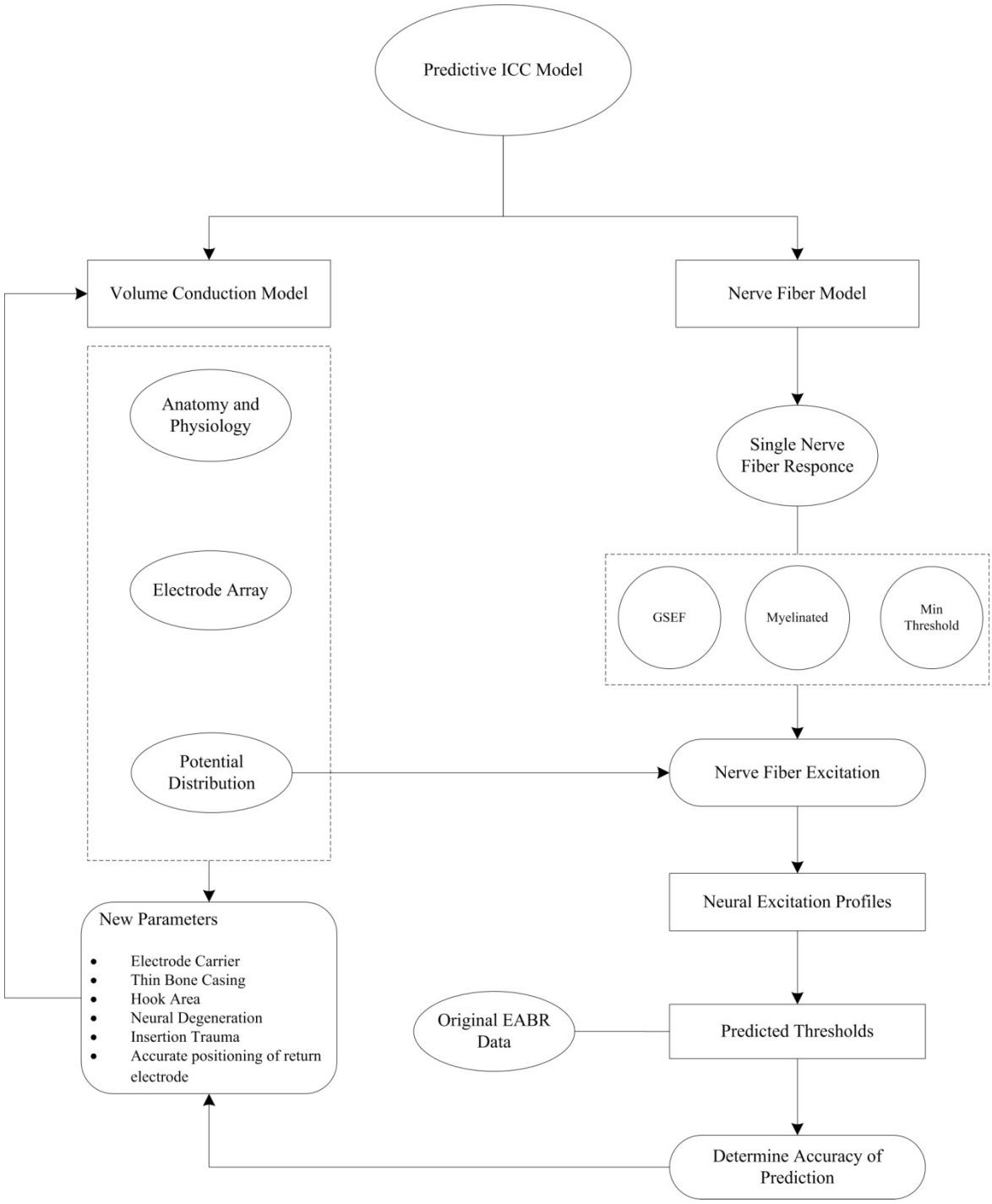

Figure 1.1 Diagram illustrating the two models in this study and how they are used in conjunction to realise the research outcomes. The square blocks show structural components while the rounded blocks depict activity steps. Key aspects of each model are contained in dashed lines.

© University of Pretoria

1.5 OUTLINE

This dissertation spans six chapters, each with a specific focus outlined below:

Chapter 1: Introduction- the current chapter which provides a context for the study, the hypotheses and approach

Chapter 2: Literature Review – gives a detailed description of the existing body of knowledge surrounding this study

Chapter 3: Models and Methods – describes how the various parameters were added to the existing model

Chapter 4: Results– exposes the results and impact of each of the parameters

Chapter 5: Discussion– qualifies and describes the implication of the results

Chapter 6: Conclusion – summarises the findings, answers the research questions and proves/ disproves the hypotheses

© University of Pretoria

CHAPTER 2: LITERATURE STUDY

2.1 PROCESSES OF THE INNER EAR (COCHLEA):

The auditory system is remarkable in its engineering complexities and elevates the hearing process to one of the pinnacles of anatomical achievement. In the vicinity of the inner ear lies the cochlea (Latin for "snail shell"), which is responsible for the conversion of three-dimensional sound waves into neural impulses. This transduction is inclusive of displacements in the nanometer range and can occur at a fast rate, corresponding to the processing of high pitch tones. Signal engineers are familiar with the Fourier transform, which enables the decomposition of complex signals into fundamental sinusoids. This spectral decomposition is explanatory of the cochlea's ability to represent audible frequencies as a function of length along the cochlea (tonotopy). This organisational structure is maintained to the inferior colliculus, a metabolically vibrant region in the midbrain involved in acoustic integration and linked to the cochlea via the auditory nerve.

Cochlear morphology

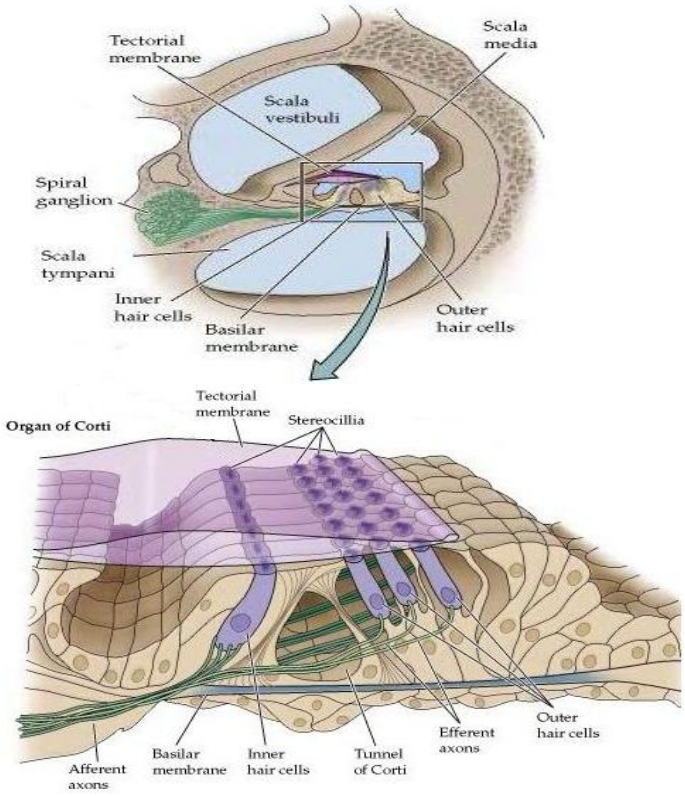

Figure 2.1: Cross-section of the cochlea with magnified Organ of Corti. (Purves, Augustine, & Fitzpatrick 2001) with permission from UP copyright office

© University of Pretoria

The frequency range of humans is between 20 Hz - 20 kHz while guinea pigs have a range of 125 Hz – 33 kHz[5]. The lowest sound pressure level (SPL) that humans can hear is 0 dB at 1 kHz (hearing threshold) with the dynamic range of human hearing being 120 dB (threshold of pain).

The components of the cochlea and their associated physical properties give rise to auditory perceptions[6], derived from interaction between the cochlea (figure 2.1) and the central auditory system. The human cochlea is a spiralling structure, 3.5cm in length and tapering from base to apex. It has three large fluid-filled ducts separated by the basilar membrane, Organ of Corti, Reissner's membrane and tectorial membrane. The scala vestibuli and scala tympani form the large outer ducts while the scala media forms the smaller inner duct. At the apical end, the scala vestibuli and scala tympani are joined via an opening known as the helicotrema. This juncture assists in pressure equalisation, although the main contributors to this equalisation are movements in the basilar membrane and the round and oval windows. The scala media is filled with potassium rich endolymph, excreted by the stria vascularis, while the scala tympani and scala vestibuli are filled with a sodium rich perilymph, secreted by the cochlea with contribution from cerebrospinal fluid. An extension of the basal region forms the hook area whose walls are perforated giving rise to both the round window and oval window.

Of particular interest is the basilar membrane that traverses the length of the cochlea. It is broader and more flexible at the apex while being narrower and less flexible at the base(Gelfand 2004). It lies below the Organ of Corti, from which hair cells protrude. These provide the sensory cells of the inner ear and are innervated by the auditory nerve. The physiology of these two structures will now be discussed to illustrate the process of sensory transduction.

Sensory Transduction

Sensory transduction is initiated by a travelling wave along the basilar membrane in response to an acoustic stimulus. The travelling wave is a result of the shape of the basilar membrane, which reacts by always propagating energy from base to apex regardless of the

[5] Suspected they can hear up to 40-50 KHz
[6] Pitch, loudness, timbre etc.

© University of Pretoria

position of the source along its length. Another attribute derived from its shape is the occurrence of maximum vibration at a position relating to the stimulus frequency. This results in a highly tuned response that is mimicked by the auditory fibers which fire at a maximum rate at the point of greatest displacement. The displacement causes tiny structures on the apical end of the hair cells (stereocilia) to bend upon contact with the tectorial membrane. A consequence of this is a change in the voltage across the hair cell membrane. This rapid depolarisation causes the afferent nerve fibers attached to the hair cells to fire thus completing the sensory transduction process. A topographical frequency map is possible due to high frequencies being processed at the base and low frequencies at the apex.

The human cochlea has two types of hair cells, one row of inner and three rows of outer. The inner hair cells (IHC) are the sensory receptors with 95% of the auditory nerve fibers innervating these hair cells. The outer hair cells are believed to enhance the frequency resolving ability of the inner hair cells by contracting and relaxing, thus changing the stiffness of the tectorial membrane (Purves, Augustine, & Fitzpatrick 2001). When deplorisation of the IHC occurs, a neurotransmitter at the basal end of the IHC is released eliciting an action potential in the dendrites of the 8th cranial nerve (auditory nerve) which transmits this impulse to the ICC.

The **inferior colliculus central nucleus** (ICC) is one third[7] of the inferior colliculus (IC), the prominent midbrain nucleus of the auditory pathway. Inferior colliculi are large auditory nuclei on the right and left sides of the midbrain with the ICC being the principal juncture for ascending auditory information. The input connections to the IC comprise of many brainstem nuclei, with the majority of auditory fibers ascending in the lateral lemniscus terminating in the ICC[8]. The IC also receives input from the ears via the ipsilateral and contralateral cochlear nucleus. The IC's bimodal neurons may be responsible for filtering self-effected sounds from vocalisation, chewing, or respiration activities. The IC is the first place where vertically orientated data from the fusiform cells in the dorsal cochlear nucleus finally fuses with horizontally orientated data. This

[7] The inferior colliculus has three subdivisions: the central nucleus, a dorsal cortex and an external cortex
[8] In addition, the IC receives inputs from the auditory cortex, the medial division of the medial geniculate body, the posterior limitans, suprapeduncular nucleus and subparafascicular intralaminar nuclei of the thalamus, the substantia nigra, pars compacta lateralis, the dorsolateral periaqueductal gray, the nucleus of the brachium of the inferior colliculus and the colliculus

© University of Pretoria

reconciliation of the aural dimensions allows the IC to fully integrate all sound location data (Gelfand 2004; Shore 2009).

The IC acts as an integrative station involved in the integration and routing of multi-modal sensory perception. It is also responds to specific amplitude modulation frequencies which may enable pitch detection. Spatial localisation by binaural hearing is a related function of the IC as well.

Sensorineural hearing loss

The sensory transduction process described above, when compromised, results in a disability known as *sensorineural hearing loss.* It is particularly debilitating as it leads to the brain being, effectively, 'unplugged' from the peripheral auditory system. A primary cause is the exposure to loud sounds which damages the stereocilia by causing them to either break off or join together hindering lateral movement. Hair cells are also destroyed by certain antibiotics e.g. kanamycin and gentamycin found in ototoxic drugs. Another cause is ethacrynic acid which kills off cells responsible for the excretion of potassium in the stria vascularis. This disrupts the role of the potassium rich endolymph, which is integral in providing the potential difference required for action potential generation. The common pathology here is the inability of the auditory nerve fibers to fire, thus the 'digital' encoding of acoustic information is not possible. Traditional hearing aids (acoustic amplifiers) used in conductive hearing loss cannot combat this problem when the loss is large. A detailed account of the *Cochlear Implant* and its function in restoring partial hearing to those with severe sensorineural loss is given in the next section.

2.2 COCHLEAR IMPLANTS

Cochlear implants are successful and useful devices enabling thousands of people to regain some perception of hearing by the controlled electrical stimulation of the auditory nerve fibers. They are aimed at individuals who lack the hair cells required for transduction but have their auditory nerve intact. Existing implants provide varying degrees of speech reception enabling some users to engage in telephonic communication without associative lip-reading. In addition they have been clinically proven to enhance the implantees quality of life (Klop et al. 2008).

© University of Pretoria

2.2.1 How do they work?

The implant exploits the tonotopic arrangement of the cochlea with progression from high frequencies at the base to lower frequencies in more apical regions. It comprises of an implanted electrode array and external speech processor coupled through a transcutaneous link. The speech processor in turn, receives its input from a microphone which converts acoustic signals into analog voltages. Modern devices are capable of fully implantable (experimental) or behind-the-ear (BTE) speech processors (Wilson 2004). Figure 2.2 illustrates the individual components orientated around the auditory headspace (Wilson & Dorman 2008).

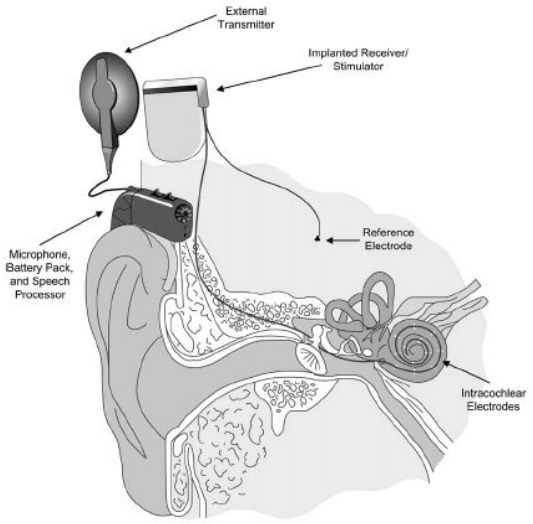

Figure 2.2: Components of the cochlear implant system. (Wilson & Dorman 2008) with permission from UP copyright office

Components

The fundamental requirement for a cochlear microphone is that it has a wide frequency response up to 6 kHz, but not extending to the low frequencies induced by head movement or walking (< 20Hz) (Wilson 2004). The availability of piezoelectric materials has allowed for microphones to be placed within the BTE housing with modern versions offering improved signal quality. The speech processor forms the 'intelligent' part of the CI system. It is responsible for converting the complex auditory signal from the microphone into a signal that can be applied as a stimulus to the electrodes, while preserving as much of the acoustic information as possible. There are multiple processing strategies employed by

© University of Pretoria

current speech processors with all of them subscribing to some form of frequency decomposition and compression (amplitude modulation) (Rubinstein 2004). The transcutaneous link comprises of an external transmitting coil and implanted receiving coil, embedded in the temporal bone above the pinna. The pair is aligned using magnets placed at their respective centers, which keeps the external coil adjacent to its interior half. In most curremt CI's the link is bi-directional allowing for measurement of evoked potentials and electrode impedance, useful for ascertaining the integrity of the auditory nerve and programming the speech processor (Wilson 2004). Electrodes deliver the stimulating pulses to surviving neurons and provide the physical interface for acoustic information transfer from the speech processor to the auditory system. Information transfer is influenced by the number of distinct channels, dynamic range, neural thresholds and channel interaction. These performance indicators have a proven relation to electrode design parameters such as size, shape, orientation and proximity to neural fibers (Rebscher et al. 2007). A typical array consists of between 4 and 22 spherical / square, half-band or banded (ring) electrodes[9]. This low resolution encapsulates the workings of the cochlear implant whose purpose is to provide speech intelligibility and modest music perception with very few separate channels. The number of information transfer channels appears to only be six to eight, independent from the number of electrodes in the array (Friesen et al. 2001).

2.2.2 Problems

The cochlear implant has restored partial hearing to over 200 000 profoundly deaf people, making it the most widely distributed and successful neural prosthetic by several orders of magnitude (Wilson & Dorman 2008). It has also proven useful as a research tool, in expanding the understanding of neural plasticity in children and the mechanisms involved in auditory pattern recognition.

Despite its widespread success, the level of hearing restoration, speech intelligibility and music perception provided by the CI varies greatly amongst subjects (Kunisue et al. 2007). Speech intelligibility is particularly difficult in noise, while music perception is generally poor although quiet environments also lead to variance in speech perception, suggesting that there may be inherent subject-specific variables influencing this.

[9] MedEl and Advanced Bionic implants have square electrodes

© University of Pretoria

2.2.3 Variation of speech and music perception

In this section some of the physical pre-operative factors influencing variability in speech perception and their impact on the biophysical parameters such as neural threshold, dynamic range and excitation spread are examined.

2.2.3.1 Age of implantation and duration of deafness

Age of implantation is an important factor in determining the degree of restored speech perception (Boons et al. 2012; Niparko et al. 2010), although under certain circumstances there is evidence to support otherwise (Tobey et al. 2003). The duration of deafness is of primary concern as it results in physiological and morphological changes in the cochlea and auditory brainstem (Hardie & Shepherd 1999). Speech perception has been shown to decrease with a longer duration of deafness (Blamey et al. 1996b). Reduced spiral ganglion density at the cochlea seems to have little effect on speech perception (Blamey 1997), it is rather the compromising of more central auditory pathways that has the greatest impact (Eggermont et al. 1997; Friedland, Venick, & Niparko 2003; Van Dijk et al. 1999). It has been demonstrated that children implanted at an early age show better results than those implanted at a later age (Dettman et al. 2007; Geers 2004; Manrique et al. 2004; Robbins et al. 2004; Svirsky, Teoh, & Neuburger 2004). Animal and human studies have revealed that a lack of acoustic stimulation causes degeneration of the higher auditory system (Hardie & Shepherd 1999; Leake et al. 1993; Moore 1994; Nadol, Adams, & O'Malley 2011; Ponton & Eggermont 2001; Ryugo et al. 1998). The compromising of central processes can be directly attributed to the duration of deafness. The age of implantation however is also significant in the sense that children below the age of 7 have a 3.5 year period over which their central auditory system remains non-degenerative and exhibits maximum plasticity (Sharma, Dorman, & Spahr 2002). Support for implantation at an early age also stems from cross-modal recruitment of the auditory cortex by the visual system, which is much harder to reverse after 6.5 years of age (Finney, Fine, & Dobkins 2001; Lee et al. 2001; Nishimura et al. 1999). Early implantation is also imperative in prelingually deaf children to encourage future speech intelligibility (Nikolopoulos, O'Donoghue, & Archbold 1999). Recent research (Colletti et al.) shows that the earliest implantees, children less than 12 months old, outperform those implanted below the age of 7. This study indicates that infants have the best chance of developing as close to normal hearing as possible, as early implantation takes advantage of the period of neural plasticity. The age of implantation and

© University of Pretoria

duration of deafness affect the central auditory processes, hence the influence of biophysical parameters controlled through stimulation at the periphery (cochlea) has little effect (Rebscher, Snyder, & Leake 2001). Since this study is concerned with the peripheral factors influencing subject-specific hearing restoration, this parameter has been excluded.

2.2.3.2 Electrode array, insertion depth and spatial selectivity

The design of the electrode array and its insertion depth are known hence it is possible to gauge the effect on a subject's perception. The modern array aims to achieve minimum trauma during insertion, increased penetration depth and lower stimulation thresholds for increased efficiency (Rebscher et al. 2007).

CI users have reported a mismatch of frequencies at the lower end of the speech spectrum, where the perceived frequency is higher than the original acoustic frequency. This is due to the tonotopic range of the lower speech frequencies being out of range of the inserted electrode array (Baskent & Shannon 2003; Faulkner 2006; Fu & Shannon 1999; Fu, Shannon, & Galvin III 2002; Oxenham, Bernstein, & Penagos 2004). The electrodes at the apical end excite neurons in a higher frequency band than intended, due to their positional mismatch with the sites at which the lower frequencies are encoded. With the knowledge and clinical methods now available, it is possible to determine an accurate frequency-position map and gauge where each electrode is placed relative to this map on an individual basis. Modern electrode arrays strive to take advantage of this and accurately match the insertion depth with the tonotopic arrangement of the cochlear, for improved speech perception at lower frequencies (Escude. et al. 2006; Stakhovskaya et al. 2007). The CI is also assisted by a psychophysical property known as "residue pitch" which allows the auditory cortex to determine the fundamental frequency from higher harmonics, particularly relevant for lower frequencies encoded at the apical end[10](Rauschecker & Shannon 2002). The tonotopic relation between the electrode contacts and the cochlea has commonly been defined by Greenwood's function (Greenwood 1990), relating place to characteristic frequency. Carolyn et al. interrogated this relationship using three different techniques: pitch adjustment, constant stimuli and interleaved adaptive procedures. Results showed that all three techniques are subject to non-sensory range biases, supporting earlier studies that frequencies deviate from Greenwood's function by one or two octaves (Boëx

[10] The electrode array is prevented from recruiting theses sights due to the narrow cross-sectional area of the most apical regions

© University of Pretoria

et al. 2006; Dorman et al. 2007). Nevertheless, it is possible to obtain reliable matches which do not deviate from Greenwood's prediction under certain conditions. A detailed breakdown of these conditions is beyond the scope of this study but may be found in (Carlyon et al. 2010)

It is possible to achieve higher information transfer by increasing the dynamic range. A lowering of the threshold level increases the dynamic range and studies have shown that placing the electrode array in a more modiolar position lowers the thresholds (Frijns, Briaire, & Grote 2001; Ho, Wiet, & Richter 2004). The proximity of the stimulating contacts to the modiolus minimises the effect of dendric neural degeneration, with stimulation occurring in the axons at lower thresholds. Smaller electrodes have a higher current density when stimulated, which may lower thresholds, but they also significantly increase the impedance at the electrode-tissue interface. This is not encouraged due to the potential for harmful chemical reactions to occur, hence most ball electrodes are between 200-300µm in diameter.

The number of electrodes and their spatial selectivity is integral in increasing the number of discrete channels and minimising channel interaction leading to greater information transfer (Rebscher et al. 2007). The mode of stimulation exercises extensive control over neural thresholds and spatial spread. The spatial spread influences pitch, critical in music perception (Spahr et al. 2008), and the ability to differentiate between multiple speakers (Drullman & Bronkhorst 2004).

Modes of stimulation:

The mode of stimulation at the stimulating sites (electrodes) has an effect on certain biophysical parameters e.g. neural threshold, dynamic range, excitation spread. There are three overarching modes namely, monopolar (MP), bipolar (BP) and tripolar (TP). MP is used to describe a mode where the stimulating electrode is within the cochlea while the return electrode is located outside. It is associated with low neural thresholds, broad excitation spread and conservative dynamic ranges. BP describes a mode where both active electrodes are within the cochlea. They are either adjacent or separated by other electrodes e.g. BP + 1 describes two active electrodes separated by one passive electrode in between the two. BP stimulation results in increased neural thresholds, narrower excitation spread

© University of Pretoria

and greater dynamic range (Chatterjee 1999; Chatterjee et al. 2006; Kileny et al. 1998; Rebscher, Snyder, & Leake 2001; Zwolan et al. 1996). TP describes a configuration utilising one active and two return flanking electrodes located within the cochlear. It has been shown to exhibit the highest thresholds, narrowest excitation spread and a greater dynamic range than MP but one comparable to that of BP (Bierer 2007; Bierer & Middlebrooks 2002; Snyder, Middlebrooks, & Bonham 2008).

All the above protocols affect stimulation through a symmetric bi-phasic current pulse (Figure 2.3). It consists of a first phase of one polarity followed closely by a phase of opposite polarity (charge-balanced). Monophasic pulses exhibit significantly lower thresholds (Shepherd & Javel 1999) but their unbalanced nature causes charge build up at the electrode-tissue interface. This has the potential to release noxious products into the surrounding area causing degradation (Shepherd et al. 1999). There is, however, research investigating pulse shapes that elicit lower thresholds while being charge-balanced (van Wieringen et al. 2008).

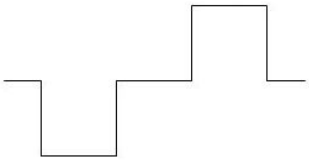

Figure 2.3: Cathodic-first bi-phasic waveform

Another criterion to consider is the orientation of the electrodes. A study by (Snyder, Bierer, & Middlebrooks 2004b) showed that for BP stimulation, radially orientated pairs produced a far more restricted spatial spread compared to longitudinal pairs. Their results also show that electrode separation has little effect on spatial spread for radially placed electrodes, but confirmed the contribution in longitudinal pairs, with the spread increasing with an increase in separation (Snyder et al. 1990). An increase in separation also results in an associated lowering of neural thresholds for longitudinal pairs, although this finding is disputed by a model based study (Frijns, De Snoo, & Ten Kate 1996).

2.2.4 EABR data

The electrically evoked auditory brainstem response (EABR) is a measure of central auditory neural activity elicited by an electrical stimulus. It is indicative of a gross response by a group of fibers as opposed to data from a single auditory nerve fiber

© University of Pretoria

(ANF)(Miller et al. 2008). The earliest EABR recordings used animal subjects to gauge the effects of various stimulation protocols on neural responses (Gyo & Yanagihara 1980; Nagel 1974; Stypulkowski & Van den Honert 1984). The recordings also provided insight into the relationship between evoked potentials and neural degeneration, important for comparison to the response characteristics of healthy fibers. Another key attribute of animal studies is their capability of providing gross response data, comparable to human recordings, as well as single ANF data, which is difficult to obtain from humans(Miller et al. 1999). Single ANF responses provide evidence of the underlying physiology and interactions of the gross response, with the amplitude of the gross response indicating the number of synchronous ANF firings.

2.2.4.1 Measurement of EABR

EABR is recorded as a time-varying voltage with the EABR threshold defined as the lowest level where a replicable response can be identified. The parameter of interest corresponding to this is the stimulus intensity and signifies the minimum current necessary (μA) to elicit a replicable response. Its definition stems from the finding that it consistently represents neither the behavioural threshold (T-level) nor comfort level (C-level), but rather a response in-between these two extremes. The T-level is the minimum stimulus current at which a sound is perceived, while the C-level is the maximum stimulus current before discomfort. The EABR magnitude may be explained by the fact that its response represents a population of neurons, rather than individual fibers which may have lower thresholds than the group.

In humans the EABR recordings usually take place via scalp electrodes. The positive electrode is placed at the vertex, the reference at the contra lateral / ipsilateral mastoid and the ground on the forehead. A high-gain, RF shielded amplifier and digital filter are usually found between the electrodes and the receiving computer (Brown et al. 1994). The super-dermal placement of electrodes gives a far-field recording of central neural activity with some delays due to propagation. The spontaneous firings of cranial neurons create noise which may compromise the integrity of brainstem data. This non-invasive measurement technique does, however, allow for recordings without the need to access the stimulating electrodes, as is the case with ECAP, allowing for a much broader subject base (Miller et al. 2008).When using animal subjects it is possible to obtain EABR data from a position adjacent to the source (McCreery, Lossinsky, & Pikov 2007; Middlebrooks & Snyder

© University of Pretoria

2007; Shivdasani et al. 2008). This is achieved through the clinical insertion of a measuring probe into the inferior colliculus (IC). The recording probe is inserted longitudinally into the IC and houses contacts to monitor neural activity. The data obtained using this method provides far greater accuracy in terms of the stimulus site in the cochlea, due to the preservation of the tonotopic arrangement into the IC. This can effectively be used to determine tonotopic selectivity and thresholds (Rebscher, Snyder, & Leake 2001; Snyder, Bonham, & Sinex 2008; Snyder, Middlebrooks, & Bonham 2008; Vollmer et al. 2007). The next section details the application of EABR data in objectively optimising a subject's map and determining psychophysical factors influencing perception.

2.2.4.2 EABR applications

Electrical stimuli evoke highly synchronous activity in nerve fibers, hence one expects good correlation between EABR and psychophysical thresholds (Goldstein & Kiang 1958). A study(Brown et al. 1994) measured EABR data from 12 adults and 14 children during CI implantation surgery and a few months after and presents a strong case for the use of EABR as a measure to assist audiologists. The study revealed that the EABR was consistently greater than T-levels (current stimulus proportional to the first instance of auditory perception) but less than C-levels (current level associated with the first degree of pain), even though these varied across subjects. The extensive inter-subject variability is supported by Mason et al. (Mason et al. 1993).These findings exclude EABR as a predictive measure of either T-or C-levels as it can only be used to indicate a level that is audible. EABR may also reduce the time it takes to programme the remaining electrodes once the T-and C-levels have been determined for the first. This is due to the EABR profile being similar to the T- and C-level profiles, hence it provides an indication of the respective levels for corresponding electrodes. This attribute may also afford the audiologist the ability to interpolate T-and C-levels for electrodes located between those for which behavioural measures exist. The role of EABR in understanding some of the processes of the central auditory system is presented in a study by Miller et al. (Miller, Woodruff, & Pfingst 1995). The results show that the slopes of EABR strength-duration functions are less than psychophysical functions, suggesting the existence of a central mode of integration (temporal) in addition to that occurring at the auditory nerve. Strength-duration also varied with mode of stimulation with monopolar producing a steeper function than bi-polar. Finally, the degree of correlation between EABR and psychophysical measures was shown to be dependent on pulse duration. A follow up study (Miller,

© University of Pretoria

Faulkner, & Pfingst 1995) hypothesised that that the strength-duration function will change over time thus EABR and psychophysical responses may provide insight into neural degeneration. Analysis of the data showed little change over time in either the psychophysical or EABR thresholds (Beitel et al. 2000), but the slopes of both strength-duration functions decreased with time. Clinically EABR could be used to assess neural degeneration over time through examination of its strength-duration function, particularly in cases where it is impractical to use behavioural measures. These findings are supported by (Kubo et al. 2001) where is it suggested that the EABR amplitude-growth curve may also be used as an indicator for neural degeneration.

2.2.4.3 Limitations

The credibility of EABR as a predictive measure is assessed in a study (Aubert & Clarke 1994) which exposes some of the limitations. In particular, there was poor correlation between the psychophysical and EABR thresholds when different pulse rates were used. Due to the nature of the EABR waveform, responses can only be elicited at relatively low frequencies (10-30Hz). When the psychophysical threshold was measured at these lower frequencies the correlation was good. Increasing the pulse rate to 500Hz for psychophysical measures showed poor correlation with EABR thresholds. Since the behavioural mapping is carried out at these higher pulse rates, the study encourages caution when using EABR as a predictive measure and proposes that a correction formula be applied to compensate for the error, corroborated by (Tavartkiladze et al. 2000).

The recording of EABR data during or post surgery may pose a problem (Brown et al. 2000). Post implant measurement requires sedation[11] of the child and extended time in the operating room, if measured during surgery. In addition, the actual recording via the surface electrodes requires specialised averaging systems. An alternative to EABR is the electrically evoked compound action potential (ECAP). This is measured via the implanted electrodes, using passive sites to measure the distributions around the active one (Brown, Abbas, & Gantz 1990). The data is extracted via the bi-directional transcutaneous link supplied with the implant. ECAPs are immune from compromise by muscle artefacts, thus sedation is not required before extraction (Miller et al. 2008). The ECAP data do pose potential complexities, one being that the ECAP profile is influenced by the shape of the evoking stimulus (Macherey et al. 2006; van Wieringen et al. 2008)

[11]Anaesthetic has an inherent risk

© University of Pretoria

EABR and ECAP have both been used as a predictive measure of auditory response characteristics and are both clinically accepted. ECAP is practically to EABR having larger amplitude, requires no additional devices and is shielded from muscular metabolic activity. EABR, despite its limitations, provides a better understanding of central auditory processing and displays greater rigidity. It is also suggestive of the mechanisms underlying audio signal processing and whether these may be compromised. Thus, it may be used as an indicator of cochlear neural responses and as an indicator of how physical parameter changes influences neural excitation (Snyder, Middlebrooks, & Bonham 2008). The single fiber ICC's examined in this study allows one to understand some of these effects, but more complex neural models are required before one is able to develop human models, characterised by the integrated behaviour of neural populations. The relationship between EABR and fitting parameters in human CI users is weak and not yet applicable in individual recipients but this model may be a start in understanding why.

2.3 COMPUTATIONAL MODELLING OF BIOLOGICAL SYSTEMS

Modelling has widespread application in biomedical research and is integral to the formulation of theory from observation. Models in biomedical research are complex, as the interdisciplinary nature of the environment requires the use of techniques from previously disparate scientific fields. Models also allow for computer simulations to be used to test certain phenomena, as opposed to direct experimentation on live specimens.

The integrity of a model can be measured to a certain extent by the properties associated with a robust biological system. Firstly, the functional elements involved in the complex processing should transition their responsibilities smoothly and effectively to produce a coherent behaviour. This is exemplified by the different behaviours of physiological systems underpinned by the interactions between similar composite cells or by an embedded microprocessor, processing instructions in a single-cycle, multi-cycle or pipelined fashion by manipulating only the data paths between its respective components. The notion of feedback, however, for regulation or stability, even though common to both biological and engineered systems, is difficult to implement when modelling a biological system. This is due mainly to the nature of the control variable which is revisable by the biological system itself, while such evolution is beyond the realisation of engineering control theory (Kitano 2002a; Kitano 2002b). For compliance with the scientific method a biological model should embrace the structure and linkages of figure 2.4 (Massoud et al.

© University of Pretoria

1998). The *semantic link* is used as a term to describe the process leading to the construction of a model representing measured data. Once constructed the model is adjusted through the *syntactic link* to behave in a general fashion, capable of generating outcomes comparable to the real-world. Finally, the *pragmatic link* represents the process of using the model's output to estimate the behavioural response of the real-world. This predicted behaviour has to be validated by physical data to complete the process.

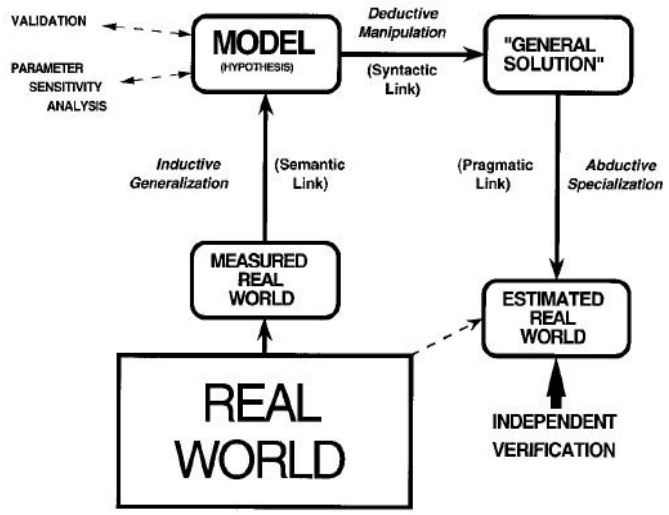

Figure 2.4: The scientific method of modelling. (Massoud et al. 1998) with permission from UP copyright office

The next section explores some of the computational models in existence in the auditory research space and the techniques utilised in representing the functions of a modelled system. Finite element models are developed and solved using various methods to address the design of the electrodes, electric fields surrounding the electrode and nerve fibers excited by the electrode. Perceptual or neural models are used to investigate the relationship between acoustic stimulation and perception. The signal processing capabilities between the normal auditory system and an electrically stimulated one are compared. Computer models of these systems are created with the goal of understanding how one can bridge the gaps between normal human hearing and electrically stimulated hearing. The models are supported by experimental work involving normal users and those with cochlear implants. They are exposed to the same acoustic stimulus and their perception of the generated sound is analysed. Acoustic models of cochlear implants are created to enable normal people to hear the sounds perceived by an implantee. The idea is

© University of Pretoria

to use these models to create speech processing algorithms that generate electrical signals in such a manner as to mimic normal human hearing.

2.3.1 Volume conduction techniques

Volume conduction is defined in biomedical application as the transmission of electric fields from an electric current source, through biological tissue, to target tissues away from the source. The conductivity distribution of the different tissue elements represents the volume conductor. If it is assumed that the frequency is low (<1KHz) then one can ignore the capacitive and inductive components of tissue impedance. This then allows for the transmission to be modeled using quasi-static Maxwell equations. In cochlear implant research various volume conduction methods have been utilized to assess the potential distribution within the electrically stimulated cochlea (Frijns, De Snoo, & Schoonhoven 1995; Frijns, De Snoo, & Ten Kate 1996; Hanekom 2001b). They vary from crude, resource friendly lumped parameter models to the more complex finite element methods.

2.3.1.1 Lumped parameter models

The lumped parameter model represents the impedance of the tissue medium by a capacitive and resistive network. This allows for reactive effects to be incorporated if necessary and computer simulations to be executed quickly due to the 'bulk' nature of the model. This method is capable of determining the voltage distribution in the unrolled cochlea. A series of lumped parameter models are concatenated along the length of the cochlea. An electric circuit simulation package is then be used to determine the voltage at a point in this distributed network (Strelioff 1973). Due to the 'bulk' nature of the model, it is not detailed enough to represent voltages at specific points along a neuron and gives only a general description of voltages in a tissue area (Suesserman & Spelman 1993).One could theoretically extend the model to represent voltages at a higher resolution that could include prediction of voltages along the neural elements. However, the models in literature are not this detailed.

2.3.1.2 Finite element models

Two commonly used numerical modeling techniques are the Finite Element Method (FEM) and Boundary Element Method (BEM). FEM is a technique used for finding approximate solutions to Partial Differential Equations (PDE). The solution involves reducing the PDE to approximate ordinary differential equations or eliminating the

© University of Pretoria

differential equation entirely and then using numerical integration techniques to solve i.e. Euler etc. This technique can be used to solve a volume conduction problem by first generating a mesh that represents the geometric and electric properties of the volume conductor(Clough 1990). Each element in the mesh is modeled using equations. A trial solution is then formulated using an optimizing criterion dependent on the type of equations used. The *variation approach,* if integral equations are used or the *weighted residual approach* for differential equations (Mattiussi 2000). The system is solved for different optimizing criteria until convergence between the different solutions is achieved leading to the final solution. The accuracy of the solution may be estimated by the closeness in the convergence during iteration. The FEM is capable of generating solutions for small anisotropic volumes making it powerful in its application. Another volume discretisation method similar to FEM is the FDM (Finite Difference Method).FDM approximates the differential equation rather than the solution allowing for easy implementation. It is not suitable for modeling biological anatomy due to its low spatial resolution and simple mesh structure which has to be made extremely small to incorporate membranous regions, leading to intensive memory use and long computational times.

The BEM is used to solve linear PDE's that have been formulated in boundary integral form (Cheng & Cheng 2005). BEM uses the boundary conditions to fit boundary values to the integral equations as opposed to values throughout the space defined by the PDE. The application in volume conduction problems is the same as the FEM, which involves "meshing" of the medium. It has the advantage of not having to re-mesh the entire system if a new geometry is added. It also saves on computational processing power for problems that have a small surface to volume ratio (Gibson 2008) but only provides accurate solutions on the surfaces and not throughout the medium. It is capable of anisotropy in only one direction when used exclusively but can be expanded to incorporate full anisotropy when combined with the FDM (Briaire & Frijns 2000; Zhou & Van Oosterom 1994).

The chosen numerical solution for this study is FEM as its accuracy and spatial resolution are to BEM, due to the solution being valid throughout the volume. It also places less strain on computational resources when modeling a biological system. Even though FEM mesh generation is repetitive when new geometries are added to the system, newer

© University of Pretoria

versions of Comsol[12] provide extensive meshing protocols capable of handling these additions. Furthermore, the integration with a neural model is supported by its ability to provide accurate electric field potentials at various inter-nodal lengths along the neuron.

2.3.2 Neural models

A neural model serves the purpose of mathematically representing the response of a neuron to a stimulus. Initially this was only over a very small area with understanding and modelling derived from a *patch clamp* experiment. This has been expanded to represent an entire nerve fiber, via various cable models and most recently the combined response of a population (Jonsson.R, Hanekom.T, & Hanekom.J.J 2007). The neural modelling process is able to provide insight into neural thresholds, delays, neural degeneration and the neural encoding process.

Seminal work in the field of neural modelling was published in 1952 by Hodgkin and Huxley (HODGKIN & HUXLEY 1952). The Hodgkin-Huxley (H-H) model uses simple circuit theory to represent each component of the cell membrane, which has a biophysical analog. The model describes how action potentials in neurons are initiated and propagated using a set of nonlinear differential equations. The main equation (1) gives the membrane current density as a sum of the capacity current plus the ionic currents flowing through the resistive elements (channels for K^+, Na^+ and leakage). The model links ion channels to currents and action potentials. The H-H equations provide the foundation for all subsequent models and are powerful in their application.

$$I_{total} = C_M . \frac{dV}{dt} + \bar{g}_K . n^4 (V - V_K) + \bar{g}_{Na} . m^3 . h (V - V_{Na}) + \bar{g}_L . (V - V_L). \quad (1)$$

The original work carried out by Hodgkin and Huxley was on a giant squid axon at a temperature of 6.3°C. It was later discovered that the rate variables α and β are affected by temperature(Chandler & Meves 1970), hence one has to modify the HH equations by introducing the temperate co-efficient (k). This co-efficient is factored into the equations for the gating variables (n,m,h) to more closely mimic the response of mammalian nerve fibers:

$$k = 1.5 \times exp^{\frac{(T-6.3)}{10}}. \quad (2)$$

[12] A multiphysics finite element modelling and simulation package
Website: http://www.Comsol.com/

© University of Pretoria

There have been other models developed similar to the HH (Chiu et al. 1979; Fitzhugh 1969; Schwartz & Eikhof 1987; Sweeney, Mortimer, & Durand 1987) but all these are only valid over a small portion of the neural membrane. An expansion into expressing the behaviour of an entire neuron is given by cable models which account for physical properties such as propagation, nodal lengths, myelin sheaths, dendrites, somas and axons. Two cable models used in the cochlear research space are (Rattay, Lutter, & Felix 2001) by Rattay and the generalised Schwarz-Eikhof-Frijns (GSEF) model (Frijns, De Snoo, & Schoonhoven 1995).

2.3.3 Integration of VC and Neuron models

To predict perceptual behaviour based on physical variables[13] a model that is both anatomical and neural in nature is required. This is realised, where a volume conduction model and neural model are integrated to simulate the response to a cochlear implant (Briaire & Frijns 2005; Frijns, Briaire, & Schoonhoven 2000; Frijns, Mooij, & Ten Kate 1994). First the potential distribution within the spiralling volume conduction model is computed. These potentials are then applied to a nerve fiber model to reconstruct excitation profiles of the auditory nerve. The predicted results are compared with actual electrically evoked brainstem responses. The nerve fiber model is a non-linear SEF (Schwarz, Eikhof and Frijns) model and represents essential mammalian nerve fiber properties[14] while also treating the myelin sheath as a perfect insulator. In total the approximately 30 000 actual nerve fibers found in the cochlea are represented by 365 model fibers[15]. Similar models have been constructed (Hanekom 2001b; Hanekom 2005). In this study, the combination of a VC and neural model is used to predict ICC responses, however this type of model is also capable of predicting eCAP signals (Briaire & Frijns 2005; Westen et al. 2011)

These are generic models and do not accommodate for subject-specific variances. This accommodation is necessary to understand an individual's cochlear environment post implantation. The need for subject-specific models is further substantiated by the effects of insertion trauma, a surgical risk, which can cause neural degeneration and altered performance of the implant. Studies investigated the anatomy of the cochlear spiral and examined the potential for certain areas to undergo trauma during implantation (Adunka &

[13] Electrode configuration, etc.
[14] Action potential conduction velocity, repetitive firing and refractory behaviour
[15] Each one represents 85 actual fibers.

© University of Pretoria

Kiefer 2006; Briaire & Frijns 2006; Verbist et al. 2009). It is shown that the intrinsic three-dimensional (3D) morphology of the cochlea contributes to the risk of insertion trauma at the basilar membrane and at the floor of the scala tympani.

Since repeated surgical procedures to test different electrode designs in human subjects is ill advised (as it is complex, costly and could cause damage to the cochlea) animal models are commonly used to extrapolate outcomes for human users.

2.3.6 Subject-specific models

A three-dimensional subject-specific computer model of the guinea pig cochlea has been realised (Malherbe 2009). The model incorporates a spiralling volume conduction component constructed from μCT scans of a specific guinea pig cochlea, coupled with a neural model which represents the 30 000 auditory nerve fibers with 505 model fibers. The FEM was used to determine the potential distribution in the cochlear for various stimulus protocols and electrode configurations. Excitation profiles were generated from this data using a GSEF neural model. The results were then compared to physical ICC data captured from the guinea pig. Although the model did not predict the ICC responses with a high degree of accuracy, it was validated as a scientific research tool with significant potential.

The model is powerful in its ability to represent a subject-specific geometry of the cochlea. It also highlights that subject-specific variances do make a difference when predicting ICC data, relative to generic models. In retrospect it was revealed that increasing the complexity of the subject-specific representation may improve the model's predictions. The key areas that were identified are discussed in the following section.

2.4 MODEL REFINEMENTS

2.4.1 Bone encasing the cochlea

The osseous labyrinth (bone capsule) is a network of passages defined by bony walls and air filled spaces. The immediate region surrounding the cochlea comprises of a thin bone capsule and an air filled bulla. The current model depicts this entire region as solid bone with the return electrode for monopolar stimulation comprising of the outer walls of this cylindrical bone capsule. This may influence the potential distribution in the cochlea for monopolar stimulation and a realistic depiction of this bony space should be implemented and the results investigated. The osseous labyrinth forms part of the larger guinea pig

© University of Pretoria

temporal bone which is a complex lattice of bone interlaced with fluid and air filled chambers, but bears little resemblance to the topography of the human temporal bone (Wysocki 2005). The osseous labyrinth should thus be constructed from anatomical representations of the guinea pig temporal bone (Voie 2002), should the subject-specific data prove incomplete in its representation of the area surrounding the cochlea.

2.4.2 Silicon electrode carrier

Modelling of the silicon carrier could affect the output of the model as it influences the current spread within the cochlea. Research showed that lower thresholds and more selective current distributions are achieved when using space filling arrays(Snyder, Middlebrooks, & Bonham 2008). The silicon carrier could also limit shunting of the current between electrodes. The symmetric nature of the guinea pig cochlea increases the chances of cross-turn stimulation for more apical turns (Fig 2.5A) (Frijns, Briaire, & Grote 2001). Basal turns are less likely to be affected (Fig 2.5B). The presence of a carrier could shield untargeted dendrites from the stimulating electrode, with varying degrees of success depending on the orientation of the carrier but may promote cross-turn stimulation in the axons if current is focused toward the modiolus.

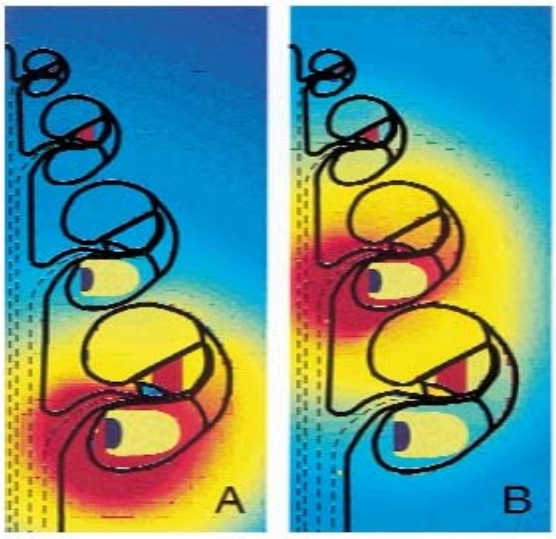

Figure 2.5: The effects of cross-turn stimulation are more prominent in basal regions through axonal excitation of apical fibers (A) Basal electrode contact (B) Apical electrode contact. (Frijns, Briaire, & Grote 2001) with permission from UP copyright office

2.4.3 Insertion trauma and neuron - damage

The trajectory of the electrode carrier causes it to pass through multiple cochlear structures. This causes trauma as the carrier penetrates the walls of the cochlear ducts. The cochlear

© University of Pretoria

ducts contain fluid which accounts for their resistive properties. Perforation of the containing walls may cause exchange of this fluid and blending of resistances, which could lead to changes in the current paths. A more pressing concern is the possibility of neural degeneration as endolymph of the scala media is neurotoxic (Thalmann & Thalmann 1999). A cross-sectional view of the cochlea shows that the scala media lies just above the Organ of Corti in close proximity to the nerve fibers. Perforation by the carrier may cause endolymph to leak onto the fibers with subsequent damage to the dendrites close to the breach.

2.4.4 Accurate positioning of return electrode for MP stimulation

MP stimulation elicits the widest current spread with the current paths to the return electrode being governed by the media surrounding the cochlea (Snyder, Middlebrooks, & Bonham 2008). The original model (Malherbe 2009) did not include a discrete return electrode, but used the entire exterior surface of a cylindrical bone volume surrounding the cochlea as the ground reference. An accurate positioning of the return electrode is expected to give a more realistic representation of the current paths associated with MP stimulation and the consequent neural excitation. The return electrode is usually positioned as far away from the cochlea as possible and closer to the skin surface, although there is support for placement within the modiolus as this may yield lower neural thresholds (Ho, Wiet, & Richter 2004).

2.4.6 Cochlear Hook Region

The cochlear hook region is an extension of the basal portion of the cochlea and tapers as it approaches the round window. The round window provides the insertion point for most cochlear electrode arrays as it grants direct access to the scala tympani (Li et al. 2007). Modelling the hook region could influence the current distribution within the cochlea for MP stimulation, as it affects tissue composition, thus potentially affecting neural thresholds.

2.5 AREAS OF APPLICATION

A subject-specific model of the guinea pig cochlea has multiple areas of application. It may be used to accelerate research and understanding of a subject's cochlear infrastructure post implantation (Pfingst et al. 2011). The prediction of ICC data could facilitate

© University of Pretoria

estimation of activation spread, overlapping of activation profiles and the independence of cochlear implant channels. The results could be applicable in developing similar models for humans. Once established, these models could provide a basis for objectively individualising a subject's map through their ability to predict T-levels, C-levels, dynamic ranges and characteristic frequencies as a function of longitudinal position for a specific subject. This information could be used to tailor the implant in a manner which restores maximum hearing objectively.

It could also facilitate research on the effects of electrode design and position on neural excitation which is important for auditory perception. This could be done through exclusive use of the model once it has been validated to correctly represent an individual's cochlear environment. Another area of application is assisting research into current steering in cochlear implants which relies on a correct prediction of spatial spread within the cochlea (Berenstein et al. 2008; Bonham & Litvak 2008). Finally, it would add to the knowledge base regarding the biophysical, anatomical and neural factors which influence the prediction of ICC data.

© University of Pretoria

CHAPTER 3: MODELS AND METHODS

3.1 INTRODUCTION AND OVERVIEW

The original subject-specific guinea pig model is constructed from μ-CT scan images, supplied by Bonham *et.al.*[16] and includes a representation of the electrodes from the customised electrode array. The model was verified against ICC responses (obtained from the inferior colliculus of the guinea pig, before conclusion of the physiological study). This chapter details how the existing model was augmented with the additional parameters, their detailed construction and a description of how they were evaluated with regard to their influence on neural excitation patterns.

The original model was reconstructed in Matlab and then exported directly to Comsol excluding the previously deployed "GMSH" step. GMSH[17] is a three-dimensional finite element generator that was previously used to mesh the spiralling geometries before exporting to Comsol. Once the original had been reconstructed, the additional parameters were then implemented sequentially in the following order:

1. Modelling of the electrode carrier
2. Accurate reconstruction of the bone capsule
3. Identifying areas of insertion trauma
4. Implementation of neuron damage
5. Modelling of the hook area
6. Accurate placement of the ground electrode for MP stimulation

In order to gauge the effect of each of these parameters; their implementation was followed by:

a) Determination of the current distribution in the cochlea
b) Modelling of neural responses
c) Comparison of neural responses to original model predictions and ICC data

The chapter starts with a description of the Matlab-Comsol model and other general procedures before migrating into the detail surrounding parameter implementation.

[16]Unpublished data through relation with Ben H. Bonham and colleagues – Epstein Laboratory, Department of Otolaryngology – HNS, Box 0526, U490, University of California, San Francisco, CA 94143-0526, United States
[17]Website: http://geuz.org/gmsh/

© University of Pretoria

3.2 GENERAL PROCEDURES

3.2.1 Matlab-Comsol model

A key component of this study is the compatibility between Matlab and Comsol and the seamless transfer of binaries [18] between these two platforms. The spiralling volume conduction model consists of nine separate geometries each representing a component of the cochlear anatomy. These were constructed through discretisation of the cochlear slices[19] into linear faces forming a framework for the modelled cross-sectional area (Figure 3.1).

Each slice has 36 vertices representing a data point, with sequential points for each vertex forming an upward spiral that tapers from base to tip (Figure 3.1c).There are 42 line segments in a single cross-sectional "slice" (Figure 3.1b), with pairs of flanking vertices creating the "faces" between consecutive line segments. In total there are 505 points and 168 faces from base to apex as each side is represented by 3 data points as one ascends vertically. Spline interpolation was used to generate the points between cross-sectional slices (Figure 3.1c).

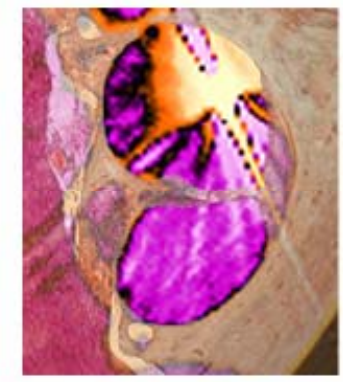

a)

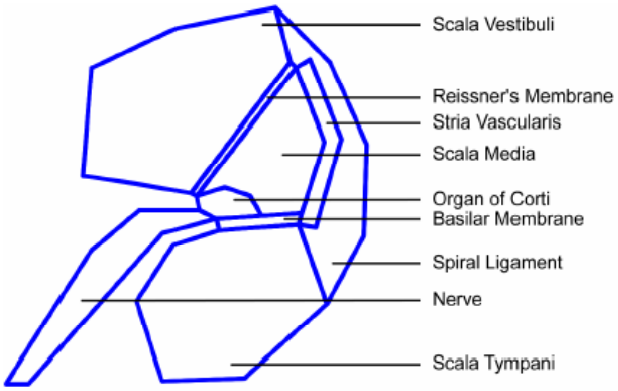

b)

[18] A data file encoded in binary form
[19] Cross-sectional slices of the guinea pig cochlear prepared by B.Bonham and colleagues

© University of Pretoria

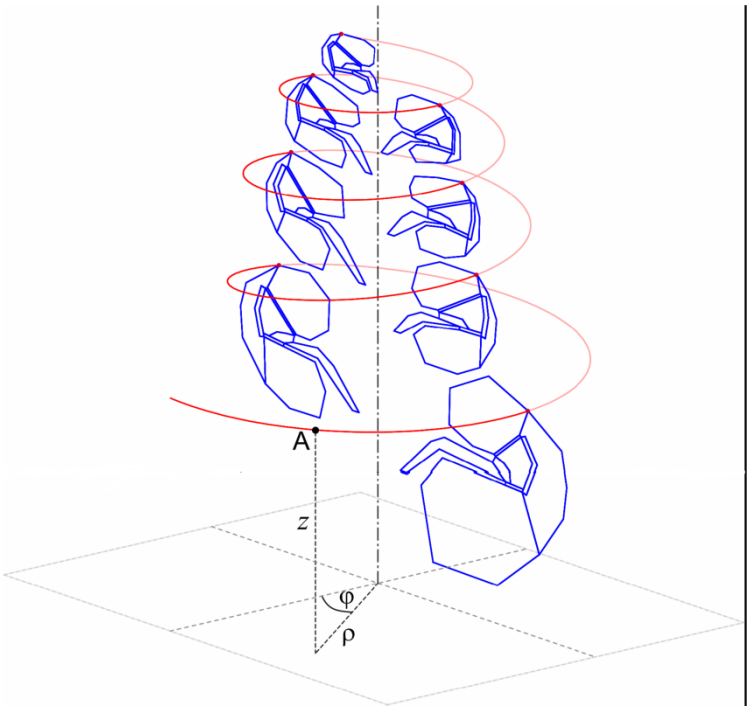

Figure 3.1: µ-CT slice to software representation. (Malherbe 2009) with permission from UP copyright office

The processing and construction of the nine geometries from µ-CT images into a virtual representation was carried out in Matlab with assistance from *ImageJ*[20] (used to retrieve data points from raw cross-sectional images). Once established, the independent geometries were exported directly into Comsol and meshed using the tetrahedral mesh algorithm in Comsol. This removed the step of meshing the structures in GMSH before export into Comsol, thus speeding up the process and allowing Matlab geometry changes to be easily propagated through to Comsol. The integrity of the representation was vetted through comparison of the neural excitation patterns produced for MP stimulation (Figure 3.2).

[20] A freely available image processing program developed by the National Institutes of Health (NIH)
Website: http://rsbweb.nih.gov/ij/

© University of Pretoria

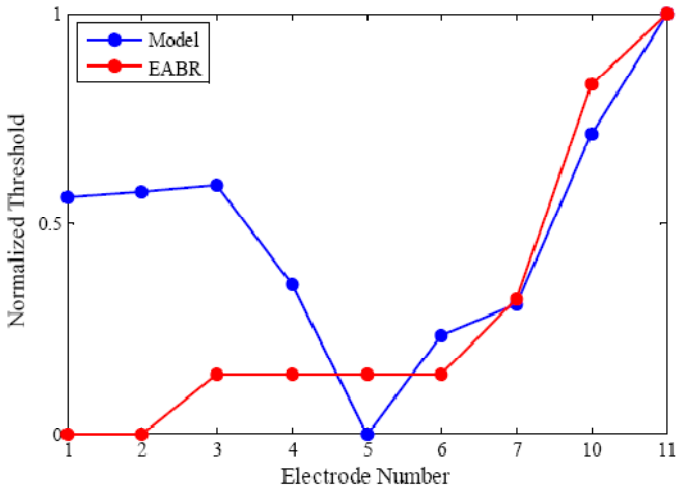

Figure 3.2: Predicted neural response (blue line) using Matlab-GMSH-Comsol model

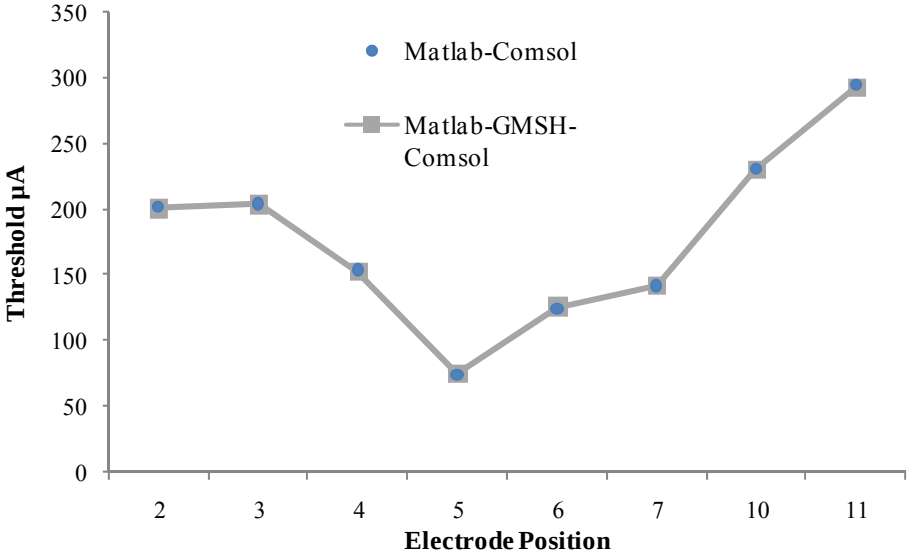

Figure 3.3: Predicted neural response using Matlab-Comsol model

One can gauge from Figures 3.2 and 3.3 that the neural outputs of the models are the same, except at electrodes 2,4,6 and 11 where there is a mean square error of 0.5 (1 µA difference). This may be due to mesh tolerances between GMSH and Comsol, but the error is within an acceptable range for this study. The GMSH step is not utilised due to the iterative nature of the modelling process requiring frequent exchange of data between Matlab and Comsol. It was previously used as older versions of Comsol were unable to mesh the complex and intricate spiralling geometries of the cochlea.

© University of Pretoria

3.2.2 Current distribution in the cochlea

The multiphysics finite element package Comsol is capable of simulating electric properties such as the voltage and current distributions in a resistive medium. The cochlear volume is modelled to a relative size and with impedance properties reflecting the conductivities of the various structures. A simulated current source will thus generate a distribution propagating outward from the source. The instantaneous value of this field may be extracted at any point where the FEM solution is valid. Figure 3.4 is exemplary of such a distribution observed across a single plane.

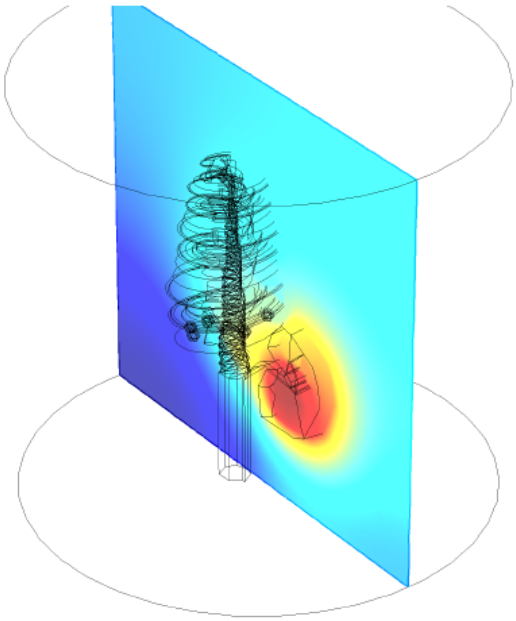

Figure 3.4: Current distribution in the cochlea

3.2.3 Modelling Neural Responses

The neuron model used throughout this study is the Generalised Schwarz-Eikhof-Frijns (GSEF) model (Frijns, De Snoo, & Schoonhoven 1995). The model obeys the Schwarz-Eikhof equations and is chosen as it describes the behaviour of mammalian nerve fibers instead of that of amphibian or squid nerve fibers-. A more detailed explanation of the kinetics is given in (Frijns, Mooij, & Ten Kate 1994). The model comprises of 26 inter-nodal compartments and is representative of a single guinea pig high spontaneous rate fiber. The fiber has a dendric and axonal diameter of 3 µm and a soma measuring 10 µm in diameter. Figure 3.5 illustrates the internodal lengths for the first 9 compartments with the

© University of Pretoria

remaining 17 compartments each measuring 350 µm in length. The fiber may only be stimulated in the un-myelinated portions (27 nodes) between respective compartments. The modiolus consists of approximately 30 000 active nerve fibers. In this study each model fiber represents 60 actual neurons resulting in 505 modelled neurons, each having 27 nodes.

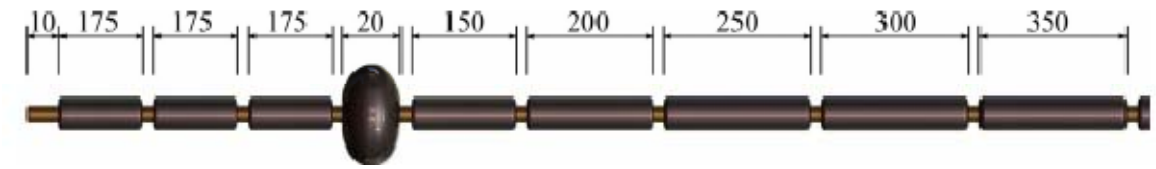

Figure 3.5: Modelled nerve fiber with inter-nodal lengths in µm. (Frijns, De Snoo, & Schoonhoven 1995) with permission from UP copyright office

The implementation of the neuron model in C++ is legacy software developed in-house and accepts initial values and input through a text file. It is inclusive of the properties listed in Table 3.1 and also allows for neural degeneration (Momin et al. 2010; Semaan & Megerian 2010), through truncation of the model, i.e. by removing inter-nodal compartments. The stimulating waveform is hard-coded as a cathodic-first bi-phasic pulse with a 0.2 ms phase and an interphase gap of 0.02 ms. The cathodic-first waveform was used in all experiments.

Table 3.1: GSEF Model Parameters

Parameter	Value	Unit
Nodal length	0.001	cm
Axonal diameter	0.0003	cm
Axoplasm resistivity	0.07	kΩ-cm
Leak conductance	25.78	$k\Omega^{-1}/cm^2$
Potassium permeability	0.000067	Ωcm/s
Sodium permeability	0.00172	Ωcm/s
Intracellular potassium concentration	141	$mmol/cm^3$
Extracellular potassium concentration	4.2	$mmol/cm^3$
Intracellular sodium concentration	10	$mmol/cm^3$
Extracellular sodium concentration	142	$mmol/cm^3$
Simulation Temperature	310.15	K

© University of Pretoria

The model's input is derived from the voltage distribution, extracted from the volume conduction model (Comsol model). The voltages are representative of the resistances between inter-nodal compartments and the stimulating electrode allowing a resistance matrix to be defined. The resistance matrix is then applied to the neural model for each of the 505 neurons. The amplitude of the stimulating current is varied in software until it converges upon a value, which is the minimum current required for the neuron to fire along any one of its 27 nodes[21]. This is defined as the minimum threshold (T_{stim}). The T_{stim} values were used to construct neural excitation profiles (threshold curves) for MP stimulation, with these then being compared to the ICC data.

3.2.4 Comparison of neural responses to ICC data

The predicted neural responses are compared to the physical ICC data[22] from the inferior colliculus (IC) of the guinea pig. The presence of spontaneous firing makes it difficult to determine an absolute minimum threshold, hence the threshold level inferred from this data is described as the minimum current which elicits a normalised response of 0.2 (Snyder, Middlebrooks, & Bonham 2008). The formula used to achieve this is:

$$RN = \frac{R - S}{M - S}$$

S is the spontaneous rate, R the recorded rate, M the maximum recorded rate and RN the normalised rate. Figure 3.6 illustrates the normalised ICC responses for monopolar stimulation of electrode 7 without spontaneous firing. Dark blue represents sub-threshold activity while dark red is indicative of the maximum firing rate. The ordinate reflects the recording position within the ICC and abscissa the stimulus level. The threshold (μA) is calculated by antilog of the dB value corresponding to the first instance of supra-threshold activity.

[21]Stimulation may occur in the dendrite soma or axon
[22]Unpublished data through relationwith Ben H. Bonham and colleagues– Epstein Laboratory,Department of Otolaryngology – HNS, Box 0526, U490, University of California, San Francisco, CA 94143-0526, United States

© University of Pretoria

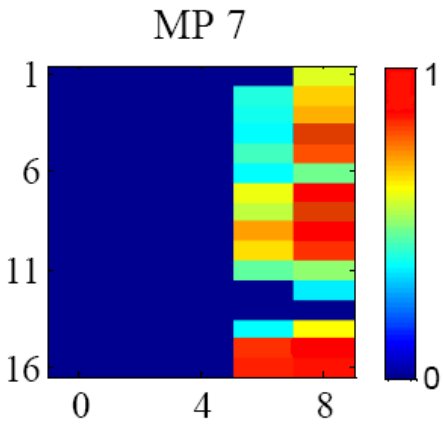

Figure 3.6: ICC recording for monopolar stimulation of electrode 7

This concludes the description pertaining to the general procedures executed after implementation of each new parameter. The next section justifies the inclusion of each parameter and describes their implementation.

3.3 PARAMETER IMPLEMENTATION

3.3.1 Modelling the electrode carrier

The carrier is modelled from images of the implanted carrier (Figure 3.7) and the carrier mould (Figure 3.8). There are 12 ball electrodes, each with a radius of 75µm that are spaced in three groups of four along the carrier. There are 500µm spacing's between electrodes within a group and 1mmspacings between groups. Theoretically, the electrodes should be positioned under the peripheral processes, with the carrier oriented such that it exposes the top of each electrode. This would channel current upward towards the targeted dendrites. The exact orientation of the carrier, as it spirals upward, cannot be deduced from the µCT scans due to the carrier's low density. It is thus modelled to expose the hemisphere of each electrode.

© University of Pretoria

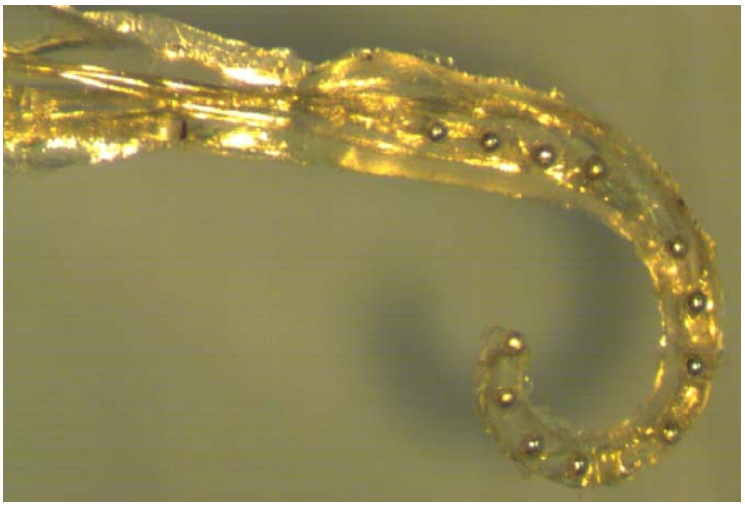

Figure 3.7: Actual carrier that was inserted. Image supplied with permission by B.Bonham et.al

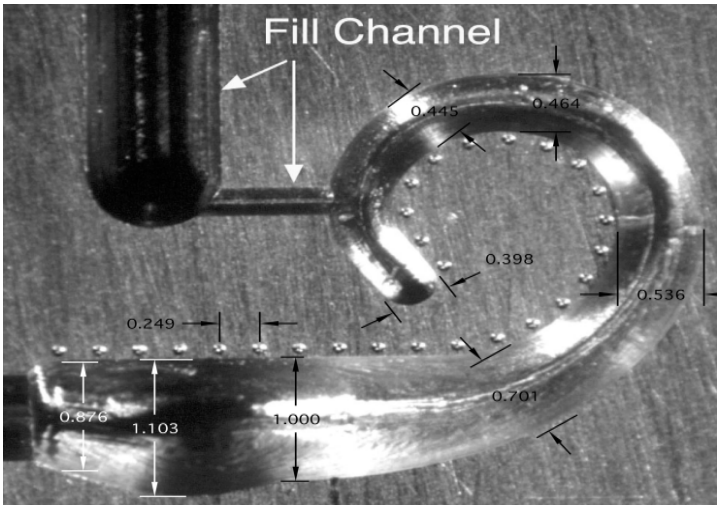

Figure 3.8: Carrier mould. Image supplied with permission by B.Bonham et.al

ImageJ and known dimensions were used to determine the physical diameters of the carrier. A known dimension (radius of electrode) was divided by its "pixel width" to determine the relationship between pixels and micrometers. It was derived from the carrier images that 1 pixel represents 8.67 µm. The carrier has a length of 8.775mm with a base diameter of 553µm and apex diameter of 398µm.Examination of the carrier cross section shows that it tapers from base to tip. The relationship between carrier cross section and length is determined by taking five lengths and five diameters along the carrier. These were plotted with length on the abscissa and diameter on the ordinate. Matlab was used to fit a line to these points. The relationship is linear with the diameter increasing by 17.8µm for every millimetre from apex to base:

© University of Pretoria

$$Diamater = (0.0177 \times Length) + 0.3968. \quad (1)$$

Table 3.2: Length and Diameter measurements

Length	Diameter
0	0.398
2.675	0.445
3.975	0.464
7.7475	0.536
9.675	0.701

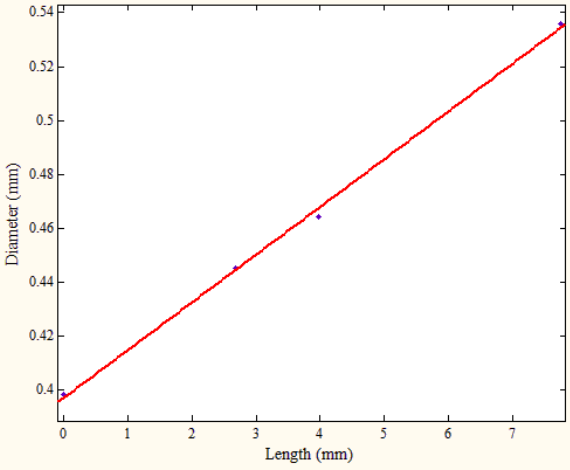

Figure 3.9: Linear approximation of Length vs. Diameter along the carrier

The second requirement for modelling the carrier is an accurate measure of its trajectory as it spirals upward through the cochlea. This was achieved by using the electrode positions, determined previously from µCT scans, as reference points and spline interpolation to produce a smooth projection of the carrier's trajectory. The electrode positions are defined by x,y and z coordinates (Table 3.2). These values were converted to cylindrical co-ordinates (r, θ), interpolated and then converted back to Cartesian representations. The *cart2pol, interp1* and *pol2cart*Matlab functions were respectively used to achieve this. Figure 3.10 illustrates the smooth curve plotted in a three-dimensional space, using *plot3.*

© University of Pretoria

Table 3.3: Cartesian co-ordinates of electrode positions

Electrode Number	X	Y	Z
1	0.81	-2.36	1.32
2	0.86	-1.77	1.26
3	1.07	-1.59	1.06
4	1.28	-1.24	0.93
5	1.15	-0.27	0.84
6	0.97	0.21	1.02
7	0.68	0.51	1.09
8	0.31	0.74	1.26
9	-0.51	0.82	1.78
10	-0.83	0.63	2.04
11	-0.84	0.12	2.36
12	-0.69	-0.31	2.48

© University of Pretoria

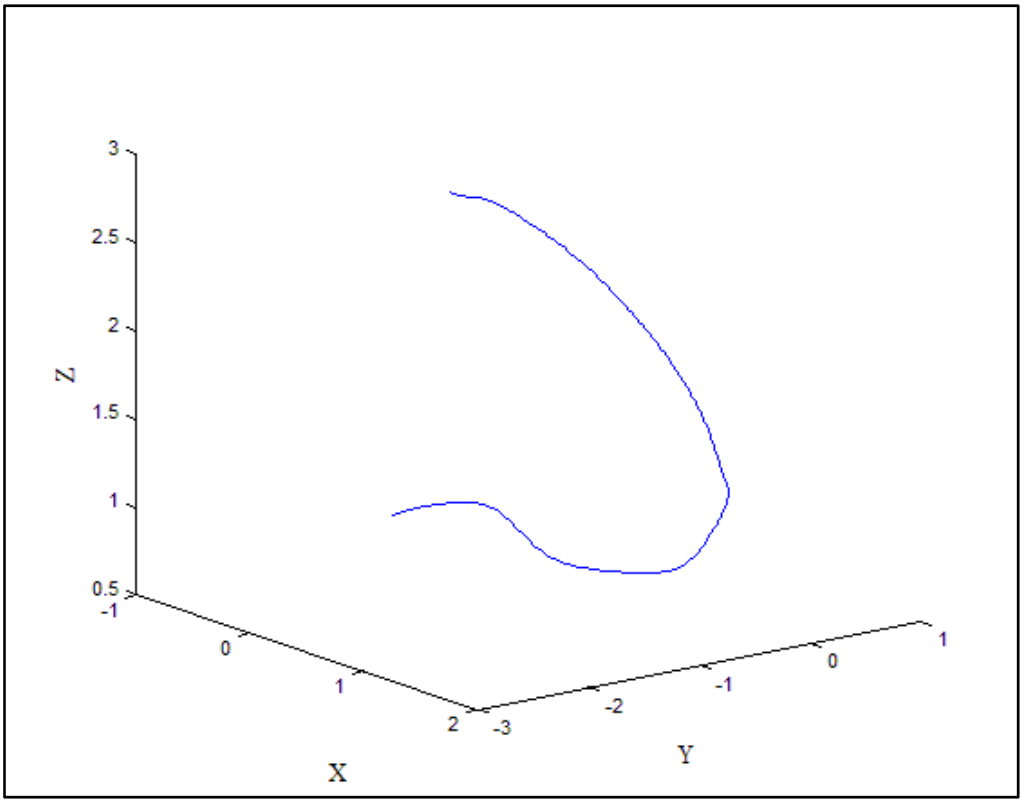

Figure 3.10: Trajectory of the electrode carrier

© University of Pretoria

A modified *Rodrigues Rotation Formula* (Koks 2006) was then used to revolve and extrude the tapering carrier along this curve.

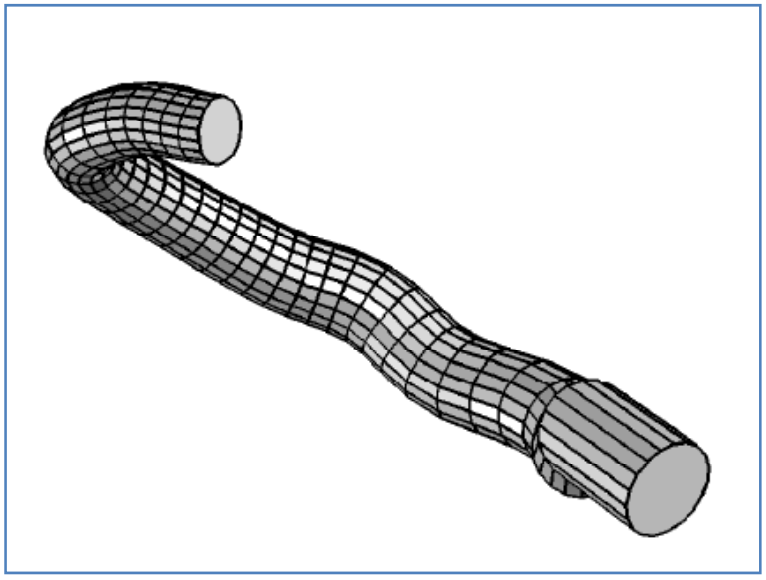

Figure 3.11: Carrier extruded

The carrier coupled with the electrodes is finally 'inserted' into the cochlea. This proved a complex process due to the multiple intersections of the carrier with existing structures, especially where minimal overlap occurred between domains. The carrier was thus shifted submissively in certain regions to allow for complete integration.

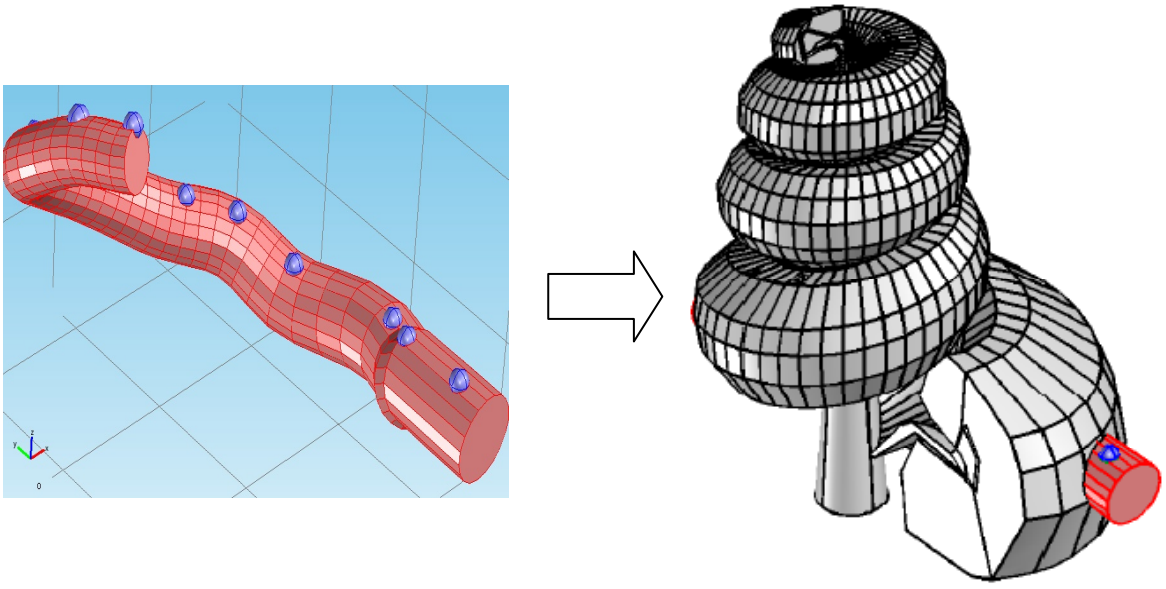

Figure 3.12: Carrier with electrodes
'inserted' into the cochlea

© University of Pretoria

3.3.2 Identifying areas of insertion trauma

The trajectory of the electrode carrier causes it to pass through multiple cochlear structures. This could lead to trauma as the carrier penetrates the walls of the cochlear ducts. The areas of insertion trauma can thus be identified by first "inserting" the modelled carrier into the cochlear model. The process involves the partial removal of existing structures should they lie in the path of the carrier. This is carried out in Comsol through use of the *"Difference"* function. The function is used to subtract a portion of one solid from the other should the two intersect. The subtraction of solid *B* from solid *A* (A-B), will result in solid A being reduced in volume, by an amount proportional to the intersection between A and B. The internal boundaries of the intersection are kept in-tact, thus ensuring that the resulting domains remain clearly defined (Figure 3.13).

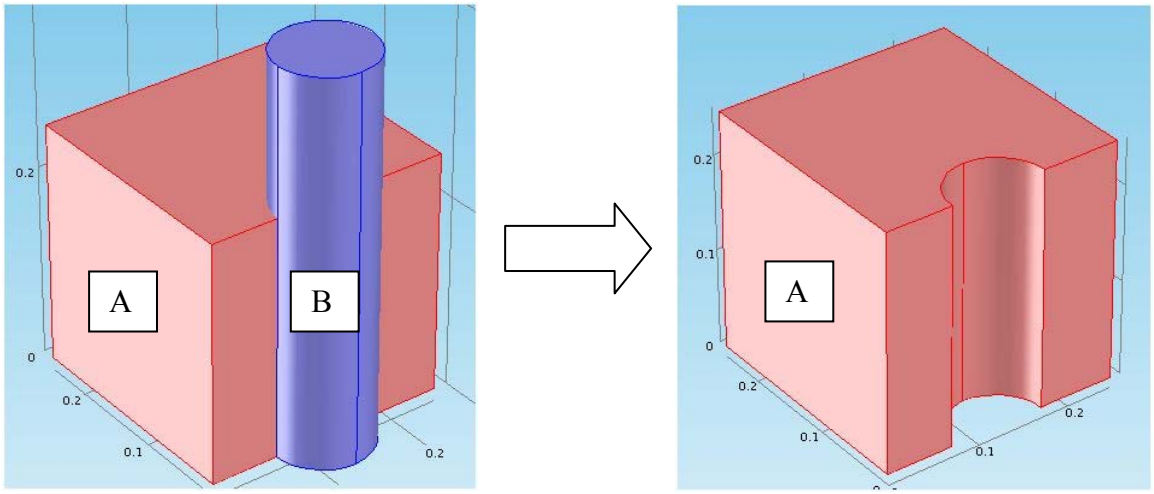

Figure 3.13: The subtraction of solid B from solid A

The method described above is used extensively in identifying areas of insertion trauma. The structures through which the carrier traverses are analogous to the solid *A* and the carrier to solid *B*. In cases where the intersection is complex i.e. when multiple intersections occur between two solids or when the intersection is minor, the "*Relative repair tolerance"* variable is adjusted in Comsol to prevent system error[23].

[23] "*Changing the default relative repair tolerance does not affect the tolerances in existing features. The absolute repair tolerance is the relative repair tolerance times the maximum coordinate of the input object".*

© University of Pretoria

3.3.3 Implementing neuron damage

The neuron damage referred to in this study is damage that may have been caused by the surgical procedure and does not account for any damage that may have occurred prior to implant insertion.

The method is intuitive in that examines the possibility of neuron damage occurring due to contact with neurotoxic endolymph. The fluid is a constituent of the scala media which lies in close proximity to the nerve fibers innervating the cochlea. It is assumed that a structural compromise of the scala media, by the electrode carrier, will cause this endolymph to leak onto the dendric portions of fibers close to the breach. This would destroy these projections, with stimulation then only occurring in the axonal portions.

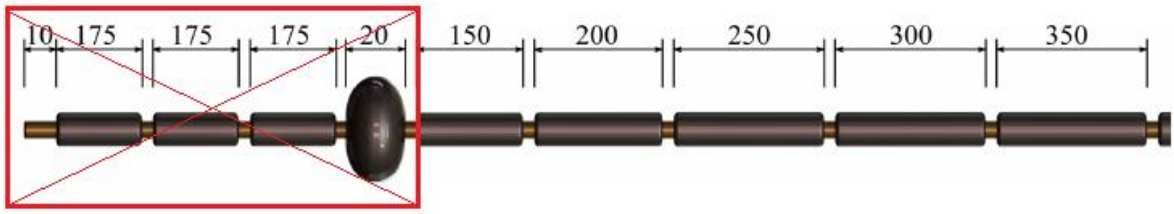

Figure 3.14: Illustration of neural degeneration adapted from (Frijns, De Snoo, & Schoonhoven 1995) with permission from UP copyright office

3.3.4 Accurate reconstruction of the bone capsule

The guinea pig cochlea is encased by a thin bone layer surrounded by an air filled tympanic bulla. This section describes how this anatomy is partially re-constructed in Comsol.

The first step is ascertaining the thickness of the bone capsule through examination of the µCT scans supplied by *Bonham et al.* The dimensions were confirmed through comparison with data derived from another tympanic bulla, image courtesy of (Voie 2002). Figure 3.15 is a cross-sectional slice of the subject's cochlea, with a clear depiction of the thin bone capsule. In this particular image, the resolution is 20 µm (1 pixel represents 20 µm[24]). One can also notice the artefacts produced by the electrodes, which causes blurring around these metal contacts as the reflected X-rays are scattered. There are multiple techniques

Geometric entities that have a distance less than the absolute repair tolerance are merged" – COMSOL help file.
[24]Scaling supplied by *Bonham et al.*

© University of Pretoria

designed to 'deblur' these artefacts(Jiang et al. 2003; Wang & Vannier 1998; Xu et al. 2000).

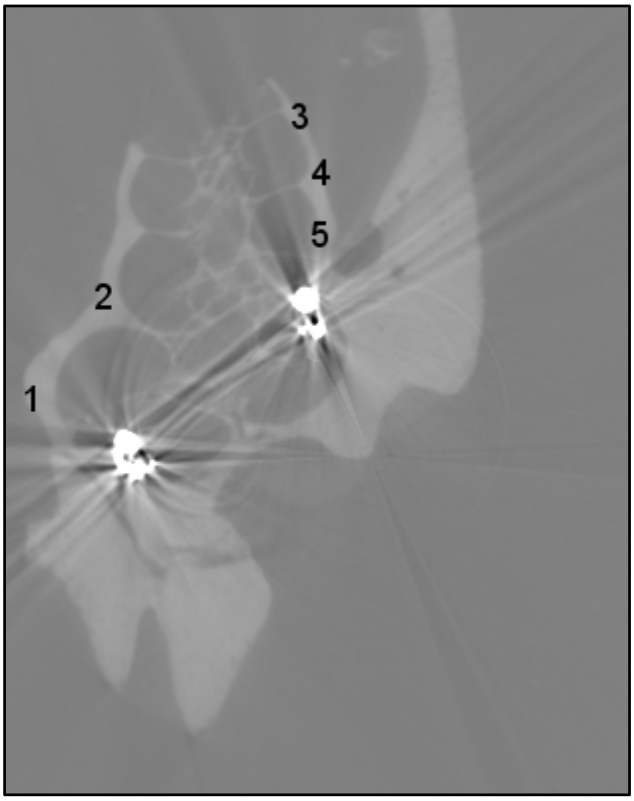

Figure 3.15: CT slice of the cochlea supplied by Bonham et al.

ImageJ is used to measure the number of pixels constituting the thickness of the bone capsule, which is then converted into a μm value. The same protocol is followed when measuring the thickness derived from the image of a guinea pig's temporal bulla (Figure 3.16). The *Orthogonal-plane fluorescence optical sectioning (OPFOS)* technique used in obtaining this image has a resolution of 27 μm. Table 3.3 displays values taken at comparative regions in the two images and their averages. The **8%** difference in the two averages validates the thickness of the bone capsule.

© University of Pretoria

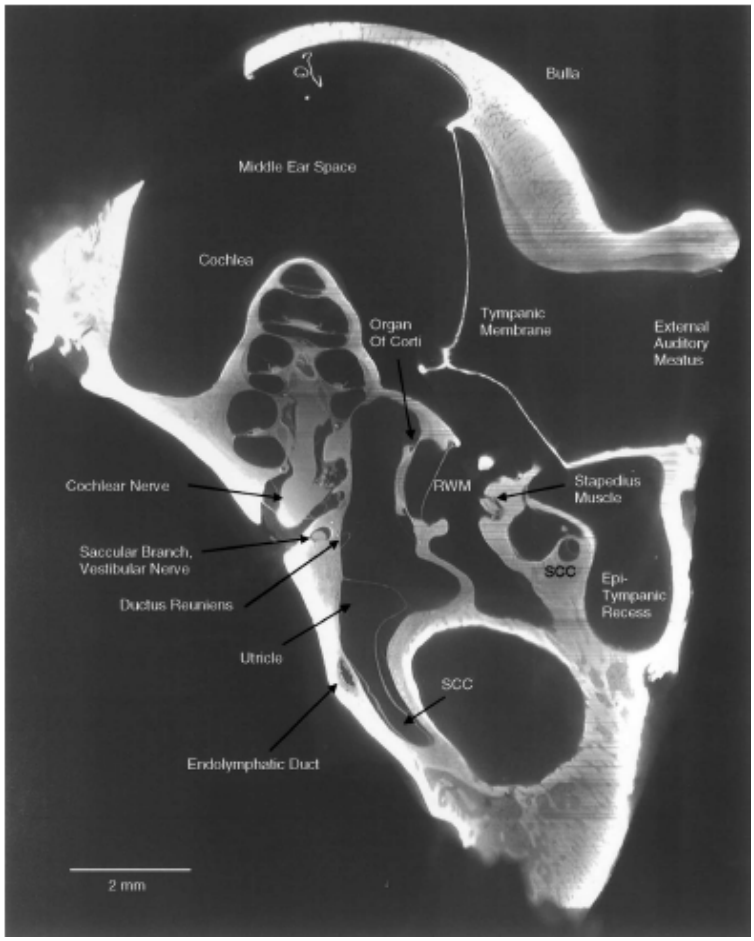

Figure 3.16: OPFOS imaging used to obtain an image of a guinea pig temporal bulla. (Voie 2002) with permission from UP copyright office

Table 3.3: Comparative thickness in the two images

Position	**Thickness µm** (CT Image)	**Thickness µm (**OPFOS Image)
1	380	367
2	200	162
3	100	81
4	180	170.1
5	220	224.1
Average	**216**	**200**

A uniform thickness of 200 µm is chosen for the thin bone capsule to simplify the modelling process. The modelling is carried out in Comsol, using the *Bezier Polygon*

© University of Pretoria

function to first trace an outline of the cochlea following the silhouette of the spirals (Figure 3.17). To accommodate this, the 3D model is 'cut' along the y-z plane.

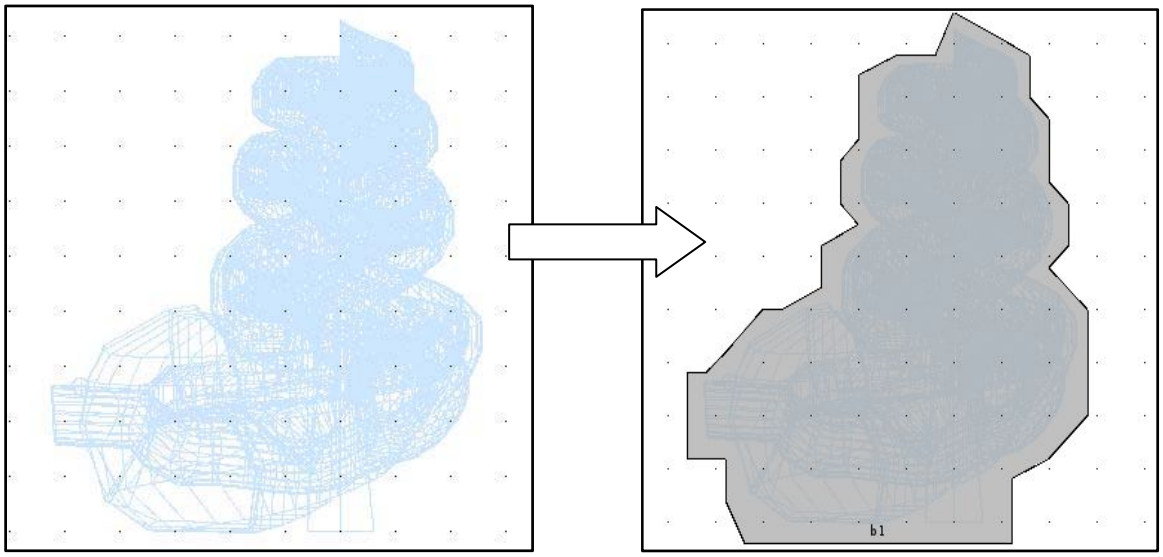

Figure 3.17: An outline trace of the bone capsule

Once established, the polygon is extruded along the x-axis to form a solid bone structure. The solid structure is then adjusted in regions that exceed 200 μm to remove excess bone and maintain a uniform thickness (Figure 3.18).

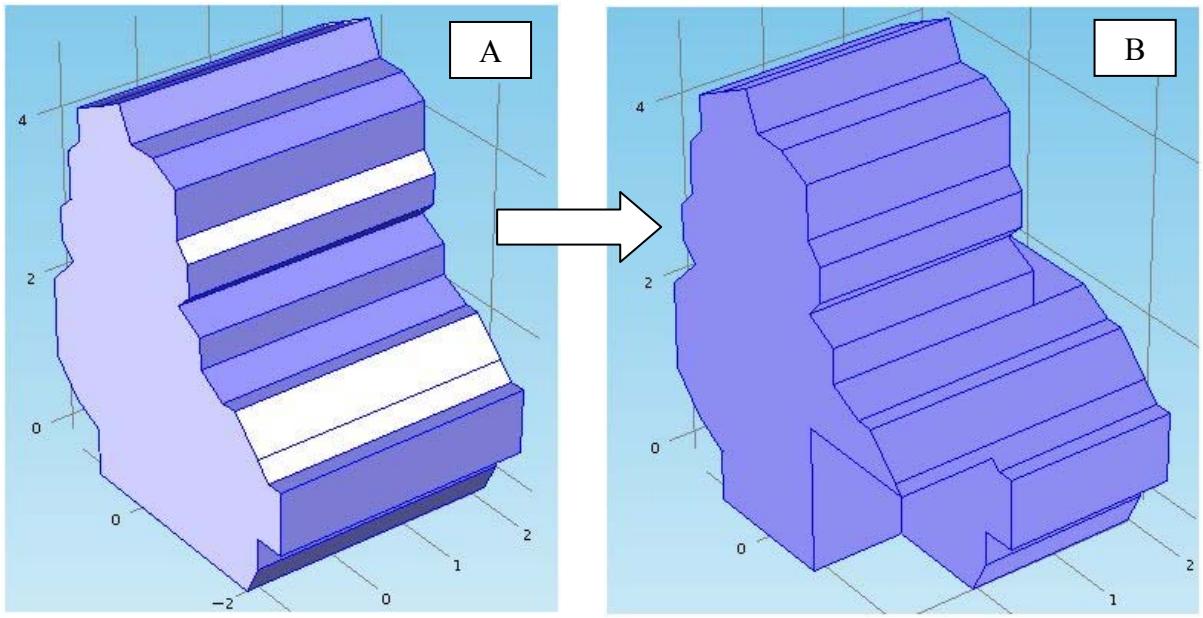

Figure 3.18: A - Solid Bone. B - Uniform Thickness

© University of Pretoria

The final realisation can be seen in a trasparent image viewed from the y-z plane (Figure 3.19).It shows the spiraling cochlea, electrode carrier and bone capsule. Comsol resolves the domains in such a manner that all the cavities inbetween the cochlear spirals are represented by bone, while the cochlear structures retain their definition.

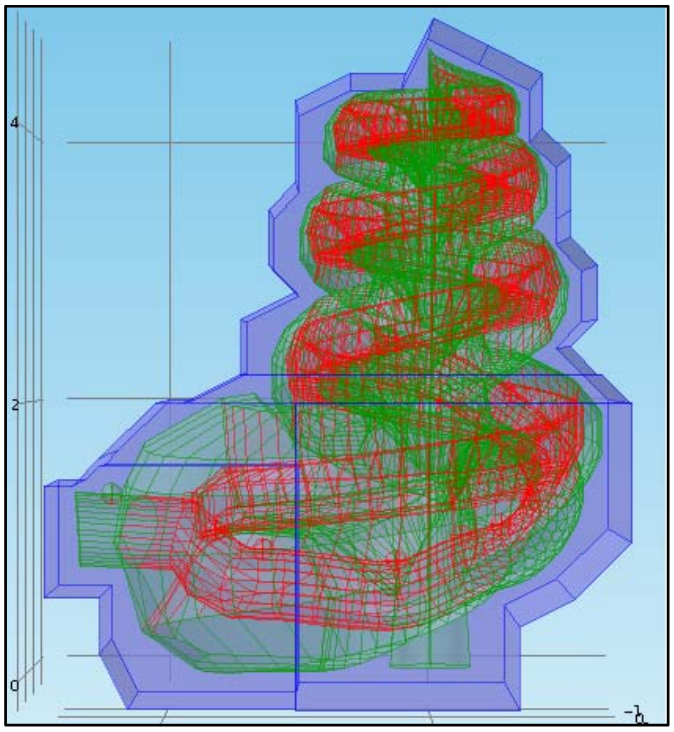

Figure 3.19: Final bone capsule

3.3.5 Modelling the hook region

The hook region is an extension of the basal portion of the cochlea and derives its name from its shape. The region extends over the round window, a common entry point for CI insertion. A feature of the hook is a tapering of the dimensions as it extends outward from the base. The hook region is modelled using both µCT scan data and intuition, as the images do not provide a detailed account of the individual cochlear structures in the vicinity of the hook region. The structures were extruded from the base of the cochlea with a trajectory that matched a profile derived from the µCT scan data.

ImageJ is used to concatenate the µCT slices to form a virtual volume of the cochlea (Figure 3.20). The volume is then orientated to display a view (x-y plane). The depth

© University of Pretoria

perception is adjusted until one can clearly observe a profile of the hook region (Figure 3.21).

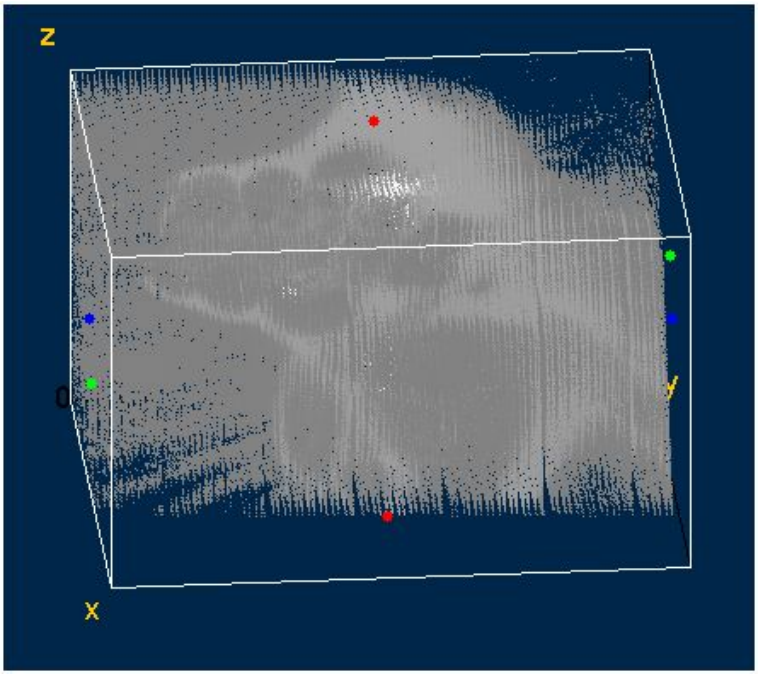

Figure 3.20: CT slices concatenated to form a volume

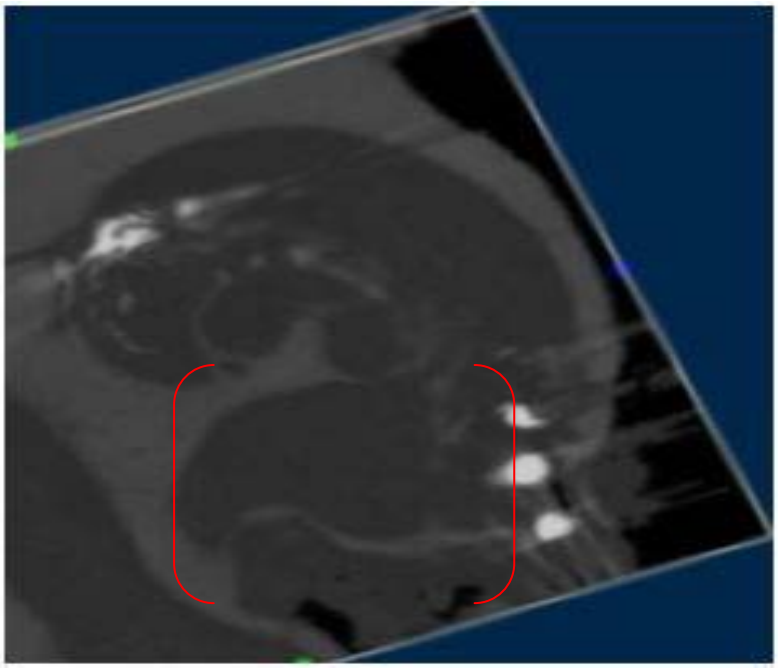

Figure 3.21: Hook region viewed from above

© University of Pretoria

Once established, pixel widths are taken along the hook's length and converted to micrometers (Table 3.4). These provide a series of cross-sections spanning the length of the hook. The cochlear structures are then extruded in stages with a ratio matching these cross-sections and with a profile matching the x-y view (Figure 22). A total of 10 segments are extruded before they are fused together. The solid is then appended to the basal region of the cochlea, to form continuous domains from cochlear apex to hook apex. The hook region is modelled to contain all 8 cochlear structures [25] each with equivalent conductivities.

Table 3.4: Cross-sectional lengths along the hook region (1 is closest to the base)

Cross Section	Width (Pixels)	Width (µm)
1	60.8	1216
2	70.5	1410
3	63.1	1262
4	50.3	1006
5	44.3	886
6	37.5	750
7	26.6	532
8	15.7	314
9	9.0	180
10	3.7	74

[25] Scala Tympani, Scala Media, Scala Vestibuli, Organ of Corti, Stria Vascularis, Spiral Ligament, Reissner's Membrane and Basilar Membrane

© University of Pretoria

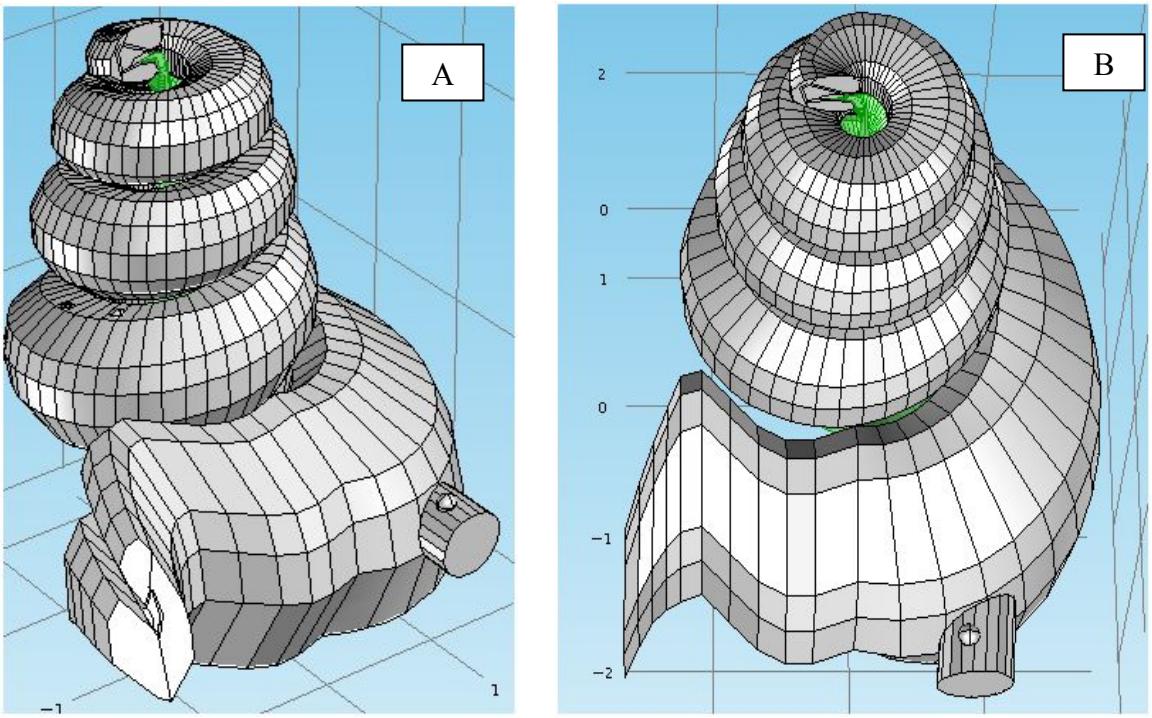

Figure 3.22: A - Cochlea with hook region B - Hook region viewed from above

3.3.6 Accurate positioning of the return electrode (MP stimulation)

MP stimulation relies on the return electrode being placed in the exterior of the cochlea, thus creating maximum distance to the stimulating electrode. The existing model (Malherbe 2009) is not inclusive of a return electrode as the entire surface of the surrounding bone capsule is assigned to ground. An accurate representation of the return electrode is described below.

In the current subject, the return electrode is placed 1cm under the surface of the skin, orientated such that it lies posterior to the cochlea (Figure 3.23.a). This positioning is implemented in Comsol by inserting an electrode at the left basal region of the model within the thin bone capsule (Figure 3.23.b). The surface of the electrode is modelled as having zero potential and the surface off the bone as charge conservation. The precise distance away from the cochlea is unknown and figure 3.23.b illustrates a qualitative estimate, based on the insertion procedure, as to where the return electrode may lie. The accuracy should suffice to model the effect on the current paths.

© University of Pretoria

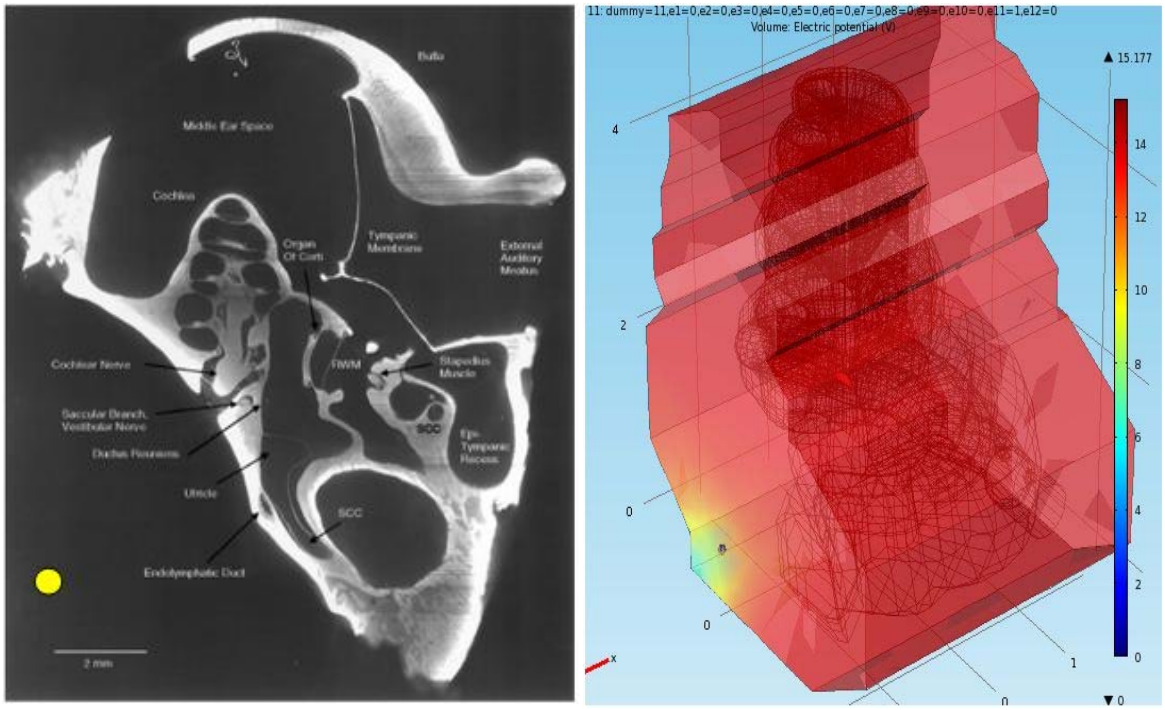

a) b)

Figure 3.23: Accurate positioning of the return electrode

The procedures described in this chapter illustrate the technical steps involved in modelling each of the parameters and how they were implemented in Comsol. The next chapter assesses the results of the various models once the Comsol simulations have been executed.

© University of Pretoria

CHAPTER 4: RESULTS

4.1 OBJECTIVES AND OVERVIEW

This chapter details the results of the incremental modelling process as each new parameter is added. The effect of each parameter is assessed individually and then in combination. The final set of results is inclusive of all additional parameters. The predicted neural thresholds are compared to physical ICC data, the original model's prediction and a generic model.

The effect of each parameter is quantified in terms of its ability to improve the accuracy of the prediction relative to the ICC data. When necessary, the neural predictions are augmented with 3-dimensional distributions of the current spread in the cochlea. This is carried out on a discretionary basis to support any derived understandings.

The inserted electrode array contains 12 ball electrodes, although results are only presented for electrodes 2-7 and 10-11. Electrodes 1 and 12 are outside the cochlea hence, their results are not valid for the purposes of this study, while electrodes 8 and 9 were disconnected from the stimulus source during the insertion procedure. The predicted results are thus generated for only the electrodes where valid ICC data exists.

4.2 TERMINOLOGY USED

Electrodes are numbered from apex to base with only *monopole stimulation* (MP) applied to each electrode. The electrodes are referred to as *e1, e2….e12.* In all cases the return electrode is represented by the outer wall of the bone capsule, except for the results in which it is modelled explicitly. The model's prediction is quantified in terms of an *Impact Factor*, which is determined by dividing the percentage error, of the original prediction, by the percentage error after implementation of the parameter in question. An Impact Factor less than one implies a reduction in predictive accuracy, with a positive value implying an increase in accuracy.

© University of Pretoria

4.3 COMPARISON TO ICC DATA AND ORIGINAL PREDICTION

The neural predictions after adding each new parameter to the volume conduction model are expressed in this section. Voltage distributions are determined in Comsol using a parametric sweep which creates a distribution for each electrode in a sequential fashion. The values are then exported to Matlab and resistance matrices are created. These are then utilised by the neural model to determine the minimum firing threshold for each electrode.

4.3.1 Thin bone capsule

The infinite cylindrical bone is replaced by a thin bone capsule which is modelled using a profile that resembles that of the µCT image. Table 4.1 is illustrative of the comparative metrics. It is evident from the data and Figure 4.2 that an increase in accuracy occurs only at *e5* and *e7*. The most apical and basal electrodes (*e2, e11)*have the highest reduction in accuracy. Figure 4.1 depicts the current distribution around electrodes 2, 5 and 11. Stimulation of *e2* results in most of the current being shunted away from the modiolus toward the thin bone capsule. A similar dispersion occurs at *e11*. The distribution is slightly more favourable at *e5* as a larger percentage of the current flows upward, toward the dendric portions of neurons in the vicinity. The thin bone capsule has an aggregated IF of 0.89 summarising its adverse effect on the accuracy of the prediction. This is visually expressed by the green line in figure 4.2.

Table 4.1: Comparative data for thin bone capsule

Electrode Position	ICC	Original prediction	Thin Bone	%Error (Original)	%Error (Bone)	Impact Factor
(Apex) 2	25.18	202	269	702	968	0.73
3	31.70	204	231	544	629	0.86
4	31.70	154	190	386	499	0.77
5	31.70	75	70	137	121	1.13
6	31.70	125	127	294	301	0.98
7	39.91	142	133	256	233	1.10
10	63.40	231	257	264	305	0.87
(Base) 11	71.13	294	399	313	461	0.68

© University of Pretoria

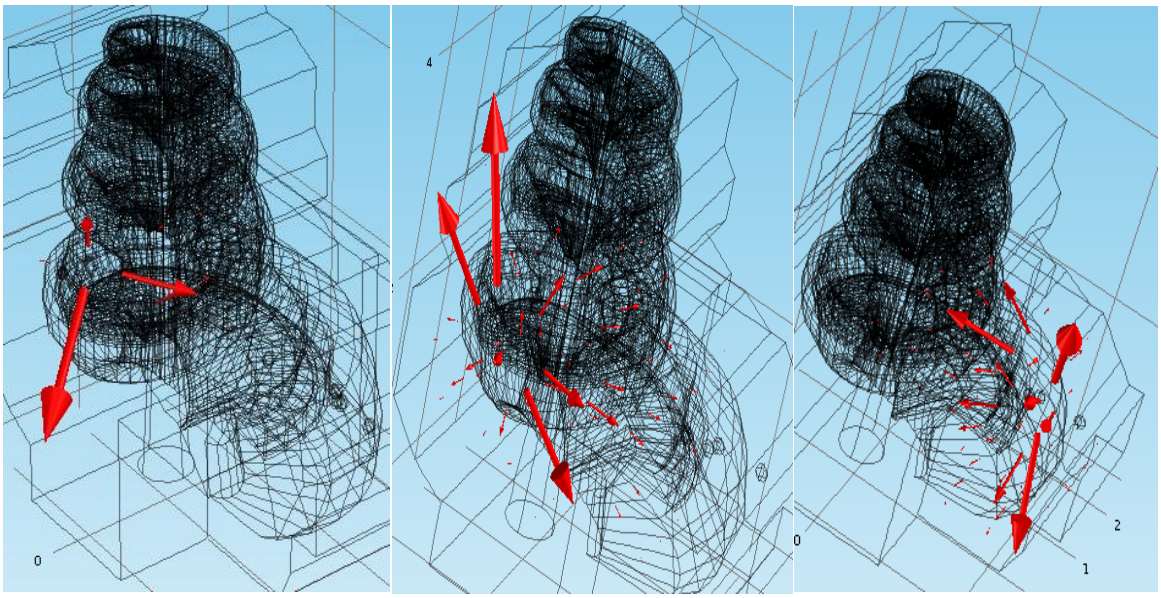

a) b) c)

Figure 4.1: Current distributions showing the dispersion at *e2* and *e11* with better concentration around the modiolus at *e5*

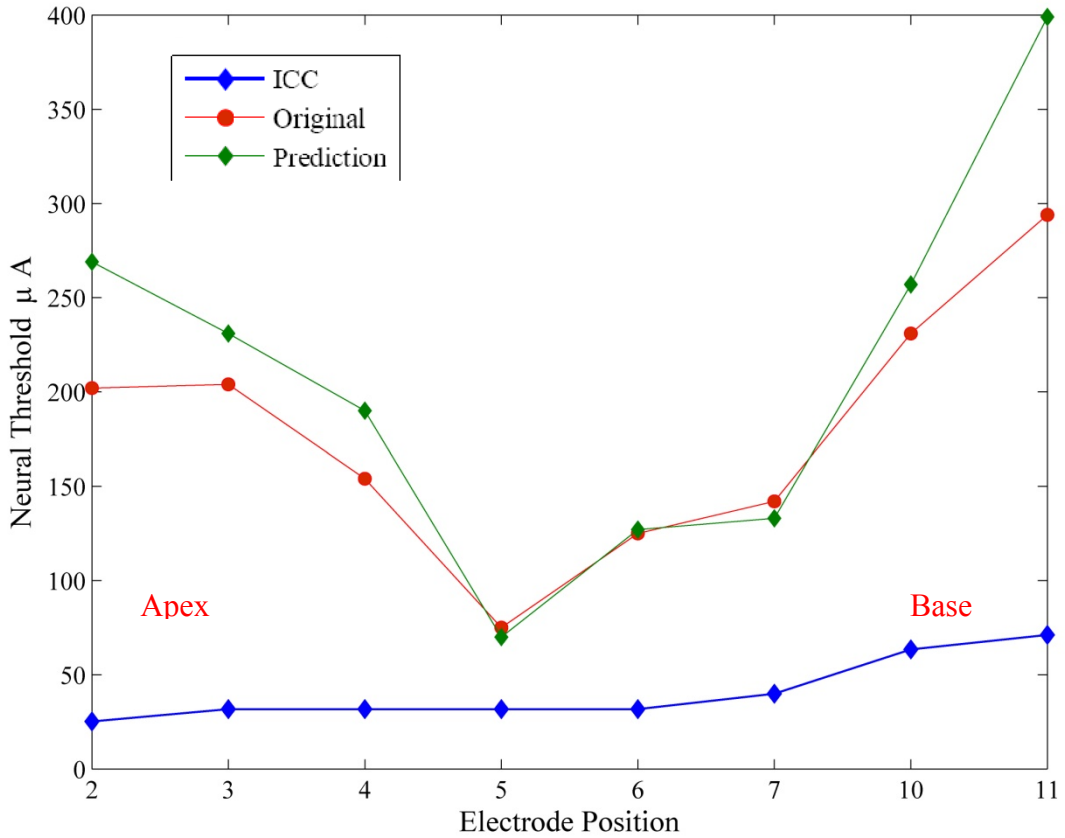

Figure 4.2: Predicted neural response using thin bone capsule

© University of Pretoria

4.3.2 Carrier

Modelling of the electrode carrier in conjunction with the thin bone capsule yields an improvement in accuracy across six electrodes (*e4,e5,e6,e7,e10,e11*). The apical electrodes (*e2, e3*), however, have a further reduction in accuracy. Figure 4.3 illustrates that majority of the current is shunted away from the nerve fibers toward the bone capsule upon stimulation of *e2*. The insulative nature of the carrier and orientation of the electrode could influence this shunting of the current toward the bone capsule. Table 4.2 reflects the increase in accuracy with an aggregated Impact Factor of 1.36 for the carrier; a 150% improvement compared to modelling only the thin bone capsule.

Table 4.2: Comparative metrics for the electrode carrier

Electrode Position	ICC	Original prediction	Carrier	%Error (Original)	%Error (Carrier)	Impact Factor
(Apex) 2	25.18	202	298	702	1084	0.65
3	31.70	204	256	544	708	0.77
4	31.70	154	126	386	298	1.30
5	31.70	75	58	137	83	1.65
6	31.70	125	81	294	156	1.89
7	39.91	142	87	256	118	2.17
10	63.40	231	219	264	245	1.08
(Base) 11	71.13	294	232	313	226	1.39

© University of Pretoria

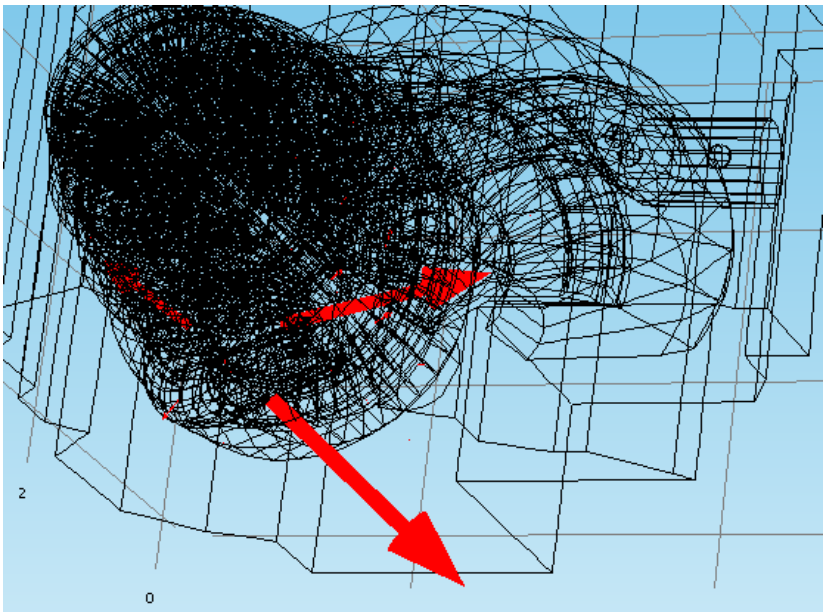

Figure 4.3: Current distribution around *e2* where most of the current is shunted away from the nerve fibers

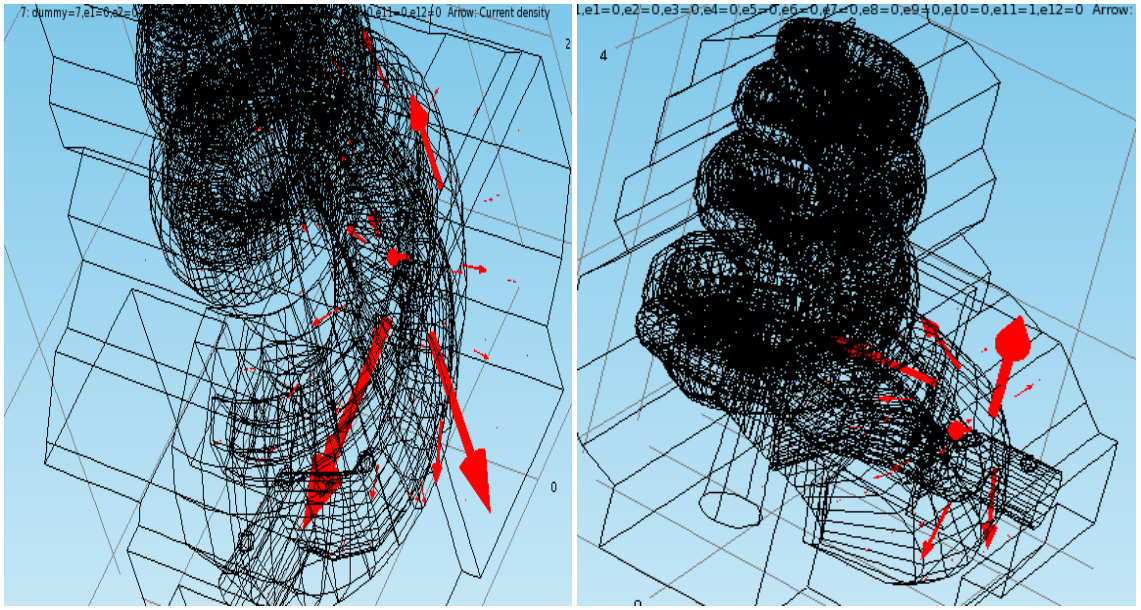

a) b)

Figure 4.4: Current distributions around *e7* and *e11*showing how the carrier prevents lateral shunting with direction toward the modiolus

The increased accuracy over electrodes *e5*-*e7* may be attributed to the distribution exemplified by figure 4.4a. The carrier positively influences the isolation of the current and causes a greater portion to flow toward the nerve fibers. A significant improvement in accuracy, 0.68 to 1.39, occurs at *e11*. Again, the carrier greatly reduces the amount of

© University of Pretoria

current shunted laterally toward the bone and channels current toward the modiolus. Exposure of the hemisphere of *e11* and its proximity to the ground surface, however, still results in a portion of the current returning to ground without excitational influence (Figure 4.4b).

Figure 4.5 illustrates the improved neural prediction by depicting the results of Table 4.2. The prediction (green) is closer to the ICC data across all electrodes except for*e2* and *e3*. The profile of the prediction is different from the original (red), indicating that the carrier does not only influence the magnitude of the prediction but also relative gradients between electrodes. This may be translated as a direct influence on the current paths within the cochlea and not a mere current density influence. This is supported through inspection of figures 4.4 and 4.11 which indicates varying trajectories in the current paths.

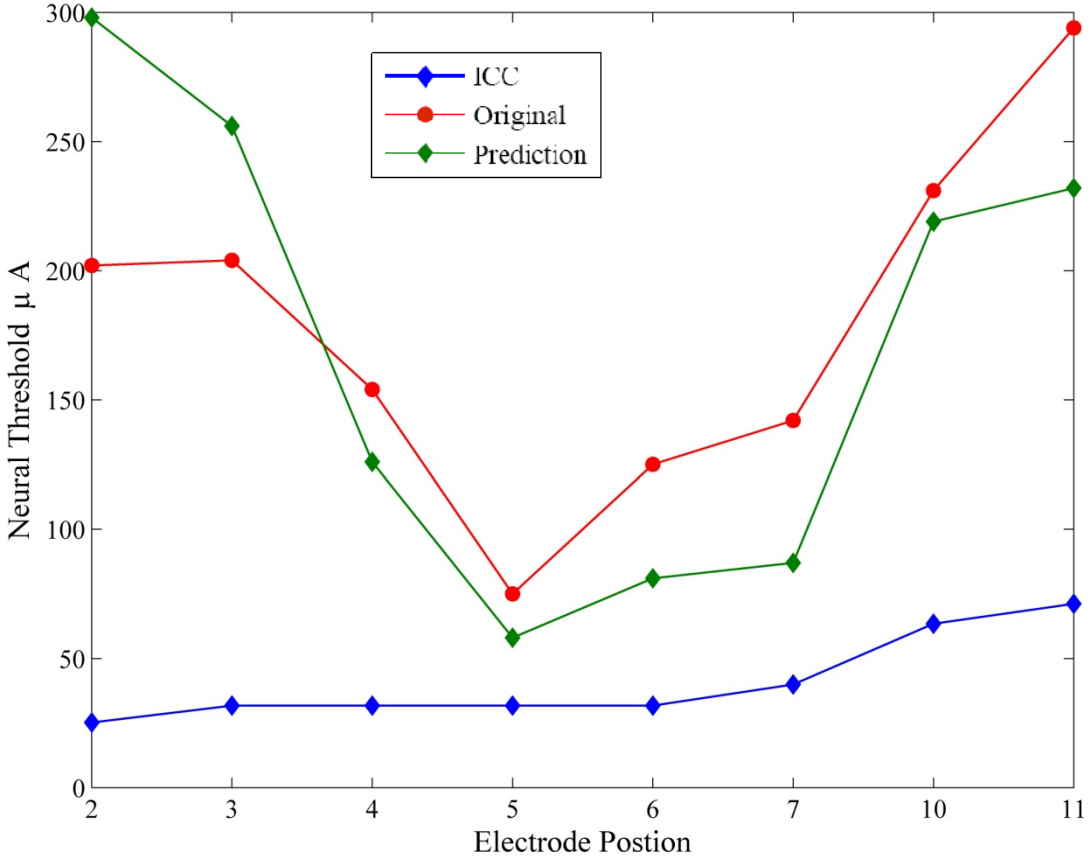

Figure 4.5: Predicted neural response with electrode carrier and thin bone capsule

© University of Pretoria

4.3.3 Hook

Table 4.3 illustrates the impact of modelling the hook region. An improvement is only evident for *e7*, although this is the same as that for the thin bone capsule indicating that the hook region has no influence on the neural thresholds at *e7*,when modelled only with the bone capsule. The impact over all other electrodes is negative with an aggregated Impact Factor of 0.85.

Table 4.3: Comparative metrics: Hook region and thin bone capsule

Electrode Position	ICC	Original prediction	HC	%Error (Original)	%Error (HC)	Impact Factor
(Apex) 2	25.18	202	271	702	976	0.72
3	31.70	204	241	544	660	0.82
4	31.70	154	184	386	480	0.80
5	31.70	75	55	137	74	1.86
6	31.70	125	82	294	159	1.85
7	39.91	142	91	256	128	2.00
10	63.40	231	208	264	228	1.16
(Base) 11	71.13	294	501	313	604	0.52

This may be explained by the hook region acting as a current ‘sink’ due to its higher conductivity relative to bone. Due to complexity in meshing, only four of the cochlear structures were modelled in the hook region. Their combined conductivity is 9 times higher than the bone which would otherwise occupy that space. This creates an attractive current path which draws current away from the nerve fibers toward the periphery. A more detailed description is given in section 4.3.4.

Table 4.4: Conductivities

Cochlear Structure	Conductivity (S/m)
Spiral Ligament	1.67
Scala Vestibuli	1.43
Scala Tympani	1.43
Reissners Membrane	0.00115
Average	**1.13**
Average (-RM)	**1.51**

© University of Pretoria

The conductivities in table 4.4 are for the structures that have been modelled in the hook region. Relative to the bone conductivity (0.156 S /m) the average conductivity of the modelled structures is between 7.3 and 9.7 times higher. This range is determined by inclusion or exclusion of Reissners' Membrane in the averaging. Although the conductivity is much lower, relative to the surrounding structures, Reissners membrane is narrow and its presence may be negligible.

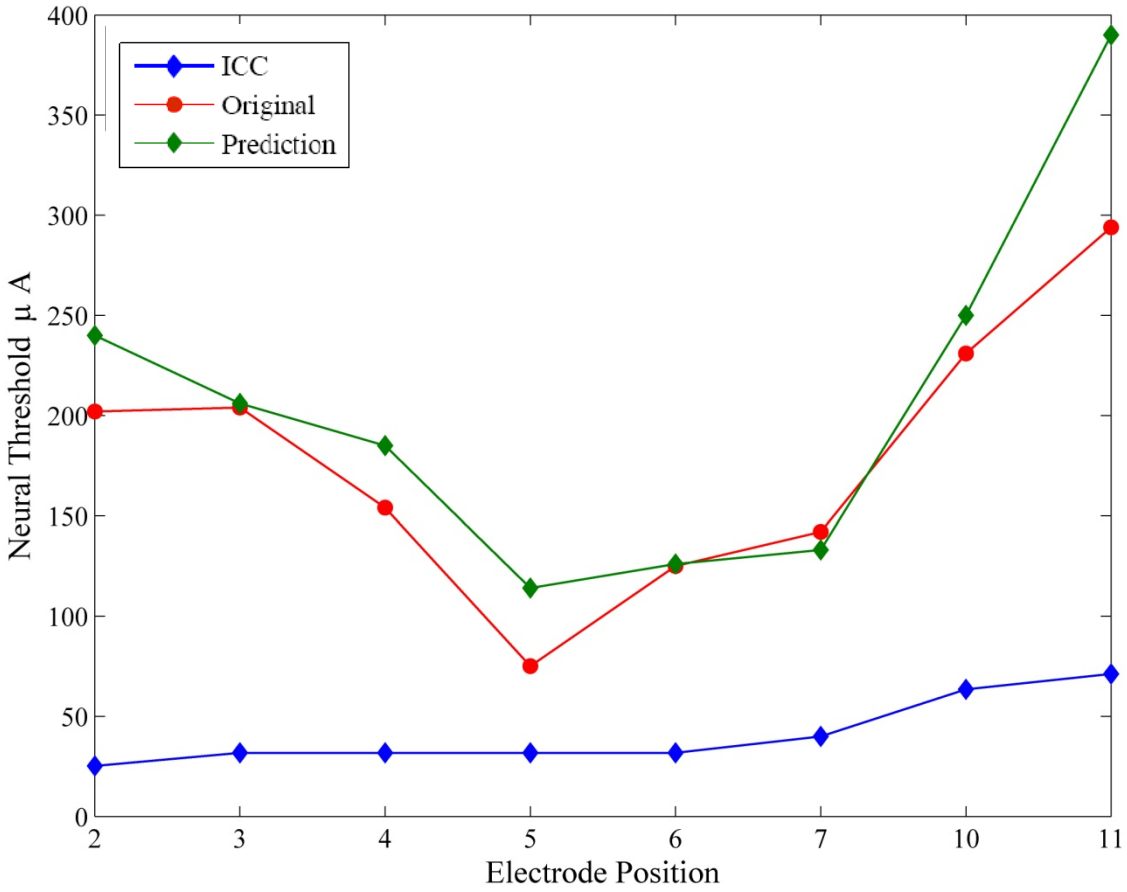

Figure 4.6: Predicted neural response with the hook region and thin bone capsule

The negative influence of the hook region is confirmed by the neural response above (figure 4.6). The magnitudes of the predicted neural thresholds are all above the original prediction with *e6* and *e7* being the exception. Their exclusion may be explained by their distance away from the hook region and their proximity to the nerve fibers, which may isolate these electrodes from the hook's influence.

© University of Pretoria

4.3.4 Hook-carrier

The results detailed in this section are a consequence of combining both the hook region and carrier into the model. The aggregated Impact Factor of this combination is 1.22. Although lower than the Impact Factor of the carrier alone (1.36), the addition of the hook region does improve the accuracy at four electrode positions (*e2,e3,e5,e10*). The relative improvement, however, at these locations is slight.

Table 4.5: Comparative metrics – Hook, carrier and thin bone capsule

Electrode Position	ICC	Original prediction	HC	%Error (Original)	%Error (HC)	Impact Factor
(Apex) 2	25.18	202	271	702	976	0.72
3	31.70	204	241	544	660	0.82
4	31.70	154	184	386	480	0.80
5	31.70	75	55	137	74	1.86
6	31.70	125	82	294	159	1.85
7	39.91	142	91	256	128	2.00
10	63.40	231	208	264	228	1.16
(Base) 11	71.13	294	501	313	604	0.52

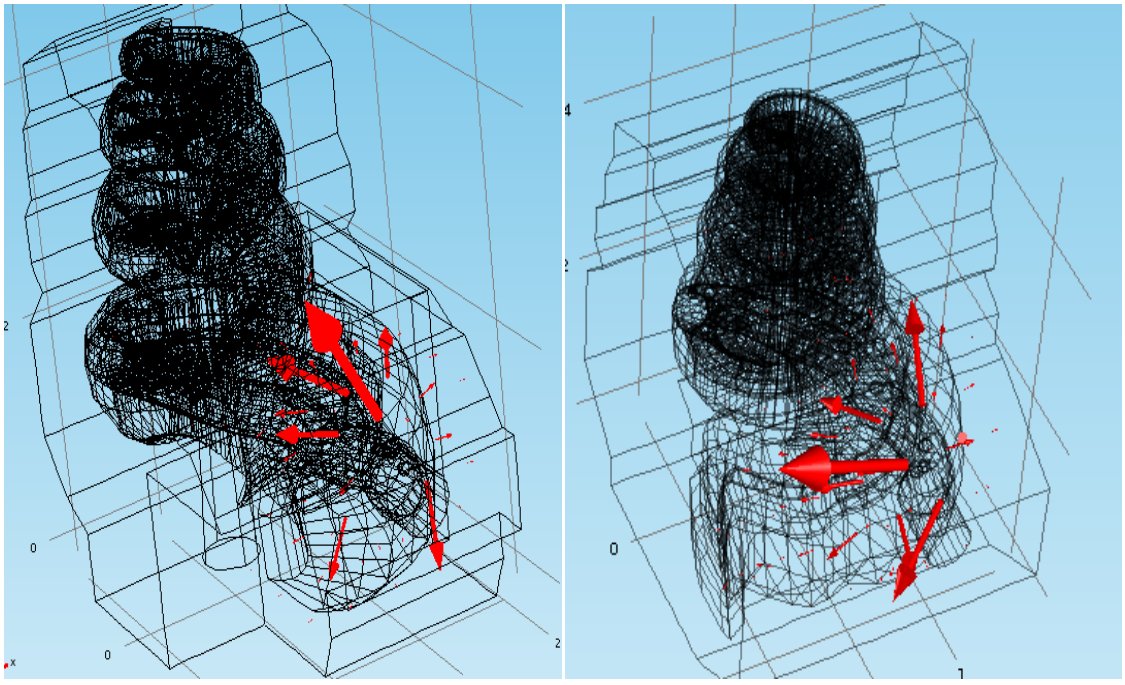

a) b)

Figure 4.7: Current distribution at *e11* - a) Carrier b) Hook, carrier and thin bone capsule. The reduction in accuracy is due to the sinking of current by the hook region

© University of Pretoria

The largest variance occurs at *e11*, which is the most basal electrode. The relative accuracy is reduced almost 3 fold from 1.39, with just the carrier, to 0.52 with the hook and carrier. Figure 4.7 is explanatory of this result as it illustrates that a large portion of the current is shunted toward the hook region (figure 4.7.b). This sinking of the current by the hook region increases the predicted threshold to 501 μA due to a significantly reduced current density at nerve fibers in the vicinity of *e11*.

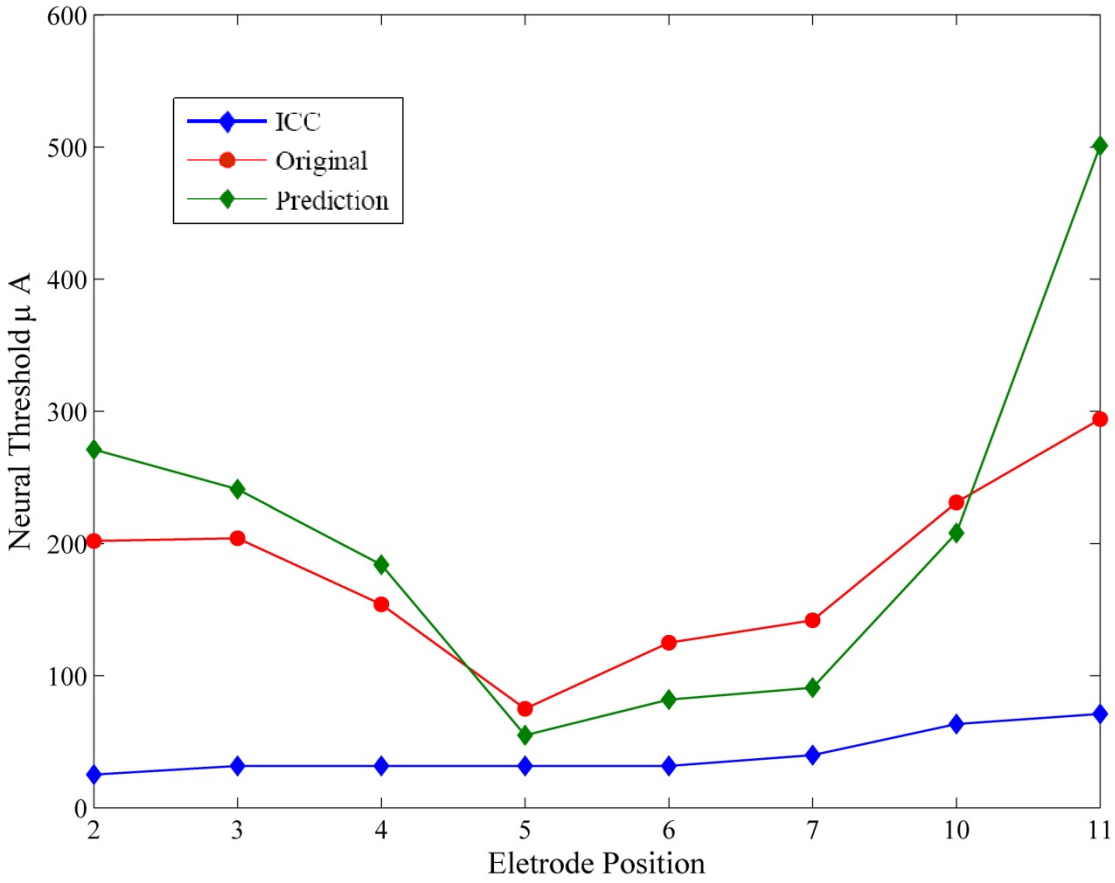

Figure 4.8: Predicted neural response: Hook region, carrier and thin bone capsule

The influence of the hook-carrier combination on the predicted response is illustrated in figure 4.8. The profile of the response is similar to that of the carrier (figure 4.5) indicating that the hook region may only effect the current density within the cochlea for all electrodes, except *e11*. This is favourable for the two most apical electrodes (*e2*,*e3*) as it increases their accuracy, relative to the carrier-only response. The negative impact on *e11* is clear, as at this position the hook region influences both the current density and current distribution.

© University of Pretoria

4.3.5 Hook-Return electrode

The correct positioning of the return electrode has a strong positive impact on the results, with all electrode positions exhibiting an improvement in predicted neural threshold values. The combination of hook region and return electrode has an aggregated Impact Factor of 3.56, which results in the prediction being 3.5 times more accurate than the original. The largest increase in accuracies occurs at the apical (*e2*,*e3*) and basal (*e10*,*e11*) electrodes. *E2* and *e3* are now respectively 3 and 4 times more accurate, with *e10* and *e11* being 5 and 8 times more accurate (Table 4.6).

Table 4.6: Comparative metrics – Hook, return electrode and thin bone capsule

Electrode Position	ICC	Original prediction	Hook- RE	%Error (Original)	%Error (Hook-RE)	Impact Factor
(Apex) 2	25.18	202	81	702	222	3.17
3	31.70	204	77	544	143	3.80
4	31.70	154	76	386	140	2.76
5	31.70	75	61	137	92	1.48
6	31.70	125	76	294	140	2.11
7	39.91	142	82	256	105	2.43
10	63.40	231	99	264	56	4.71
(Base) 11	71.13	294	99	313	39	8.00

© University of Pretoria

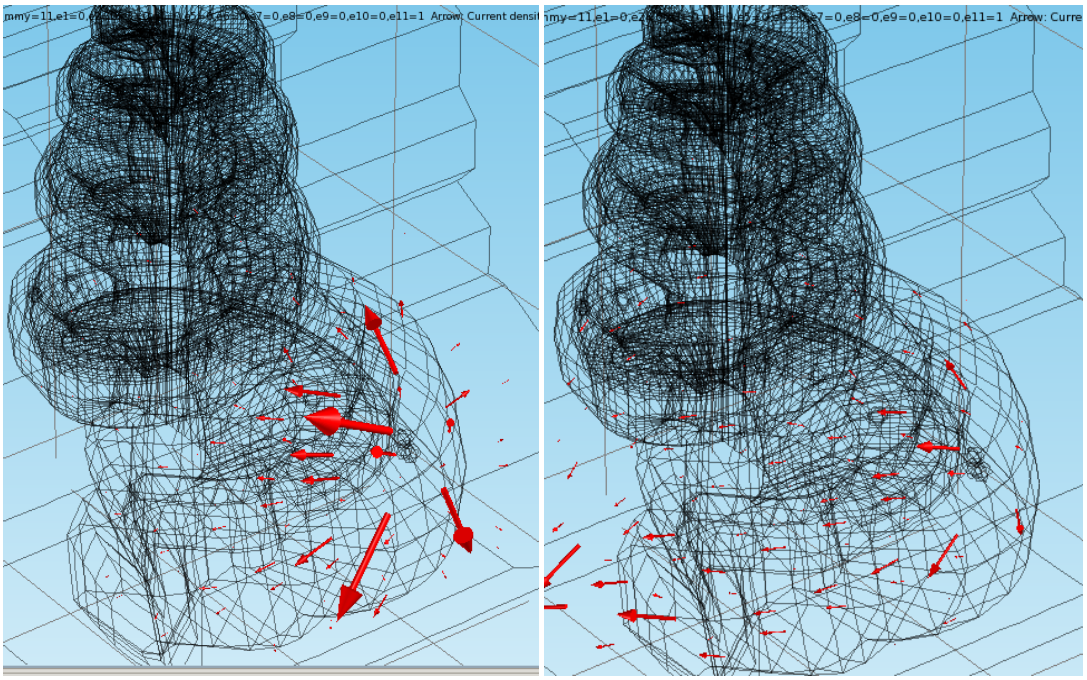

Figure 4.9: Comparison of current paths at e11 with and without the return electrode

This may be explained by a larger portion of the current flowing through the modiolus toward the return electrode. Figure 4.9b is an illustration of this concept and shows a clear permeation of the current from *e11* toward the return electrode. The resulting current density around the nerve fibers is thus much higher in comparison to figure 4.9a, where the entire bone capsule is set to ground. This causes dispersion and grounding of the current in multiple directions.

© University of Pretoria

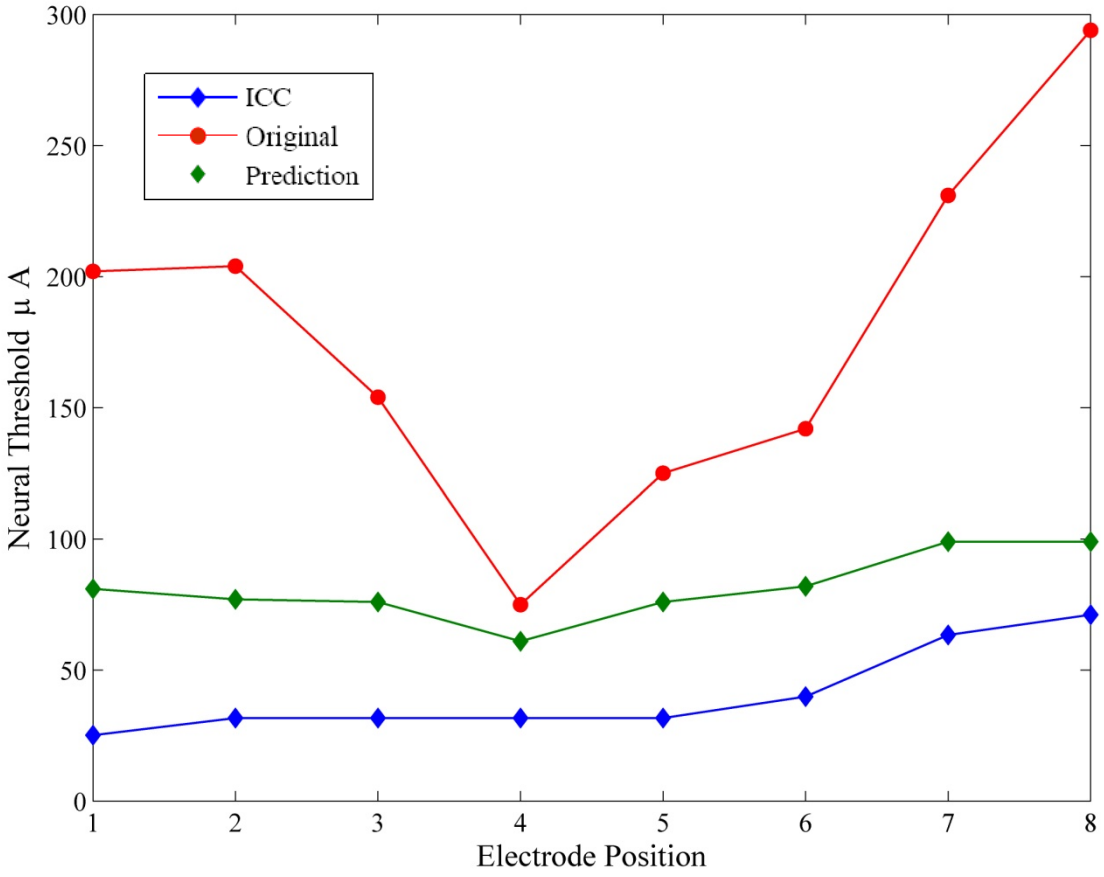

Figure 4.10: Predicted Neural response: Hook region, return electrode and thin bone capsule

Figure 4.10 illustrates the improvement in the accuracy when the return electrode is modelled and positioned correctly. There is a clear change in both the magnitude and profile of the response. The predicted neural thresholds (green line) are lower at all electrode positions with the profile bearing a closer resemblance to the ICC data (blue line). This indicates that the return electrode causes an increase in current density around the nerve fibers and channels the current in such a manner that it flows primarily within and through the cochlear structures.

© University of Pretoria

4.3.6 Carrier – Return Electrode

The silicon carrier is modelled in conjunction with the return electrode and thin bone capsule. This combination yields the most accurate predictions with an overall Impact Factor of 4.56, with the results being close to 5 times more accurate than the original prediction. The accuracy for the 3 apical electrodes (*e2, e3, e4*)is slightly lower than the hook-return-electrode model but all other electrode positions have increased accuracy. *E11* has the highest Impact Factor of the data set (11.2) with an absolute difference of only 20 μA relative to the ICC data.

Table 4.7: Comparative metrics – Carrier, return electrode and thin bone capsule

Electrode Position	ICC	Original prediction	Carrier - RE	%Error (Original)	%Error (Carrier-RE)	Impact Factor
(Apex) 2	25.18	202	83	702	230	3.06
3	31.70	204	85	544	168	3.23
4	31.70	154	81	386	156	2.48
5	31.70	75	43	137	36	3.83
6	31.70	125	62	294	96	3.08
7	39.91	142	68	256	70	3.63
10	63.40	231	92	264	45	5.86
(Base) 11	71.13	294	91	313	28	11.22

© University of Pretoria

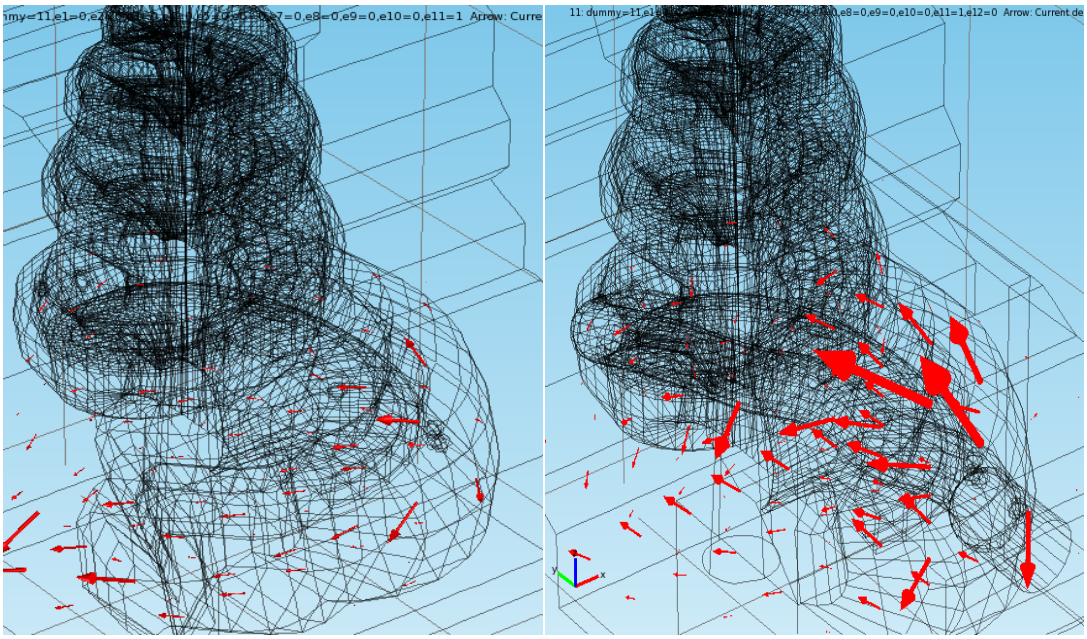

Figure 4.11: Comparison of the current spread with and without the carrier showing a greater proportion of the current being directed toward the modiolus, in the vicinity of e11, when the carrier is included

© University of Pretoria

Figure 4.11 qualifies the improvement in accuracy at *e11* by comparing the current spreads of the hook-return-electrode configuration to that of the carrier-return-electrode configuration. It is evident that the carrier channels the current in a more favourable manner, with a significant increase in current density around the nerve fibers. This results in an increase in Impact Factor from 8 to 11.22 at *e11*. There is also a marked improvement in accuracy at *e5* with an absolute difference in threshold of 11.3 µA relative to the ICC data. The Impact Factor also increases to 3.83 at *e5* compared to 1.48 in the hook-return-electrode scenario. This increase in accuracy is explained by figure 4.12.

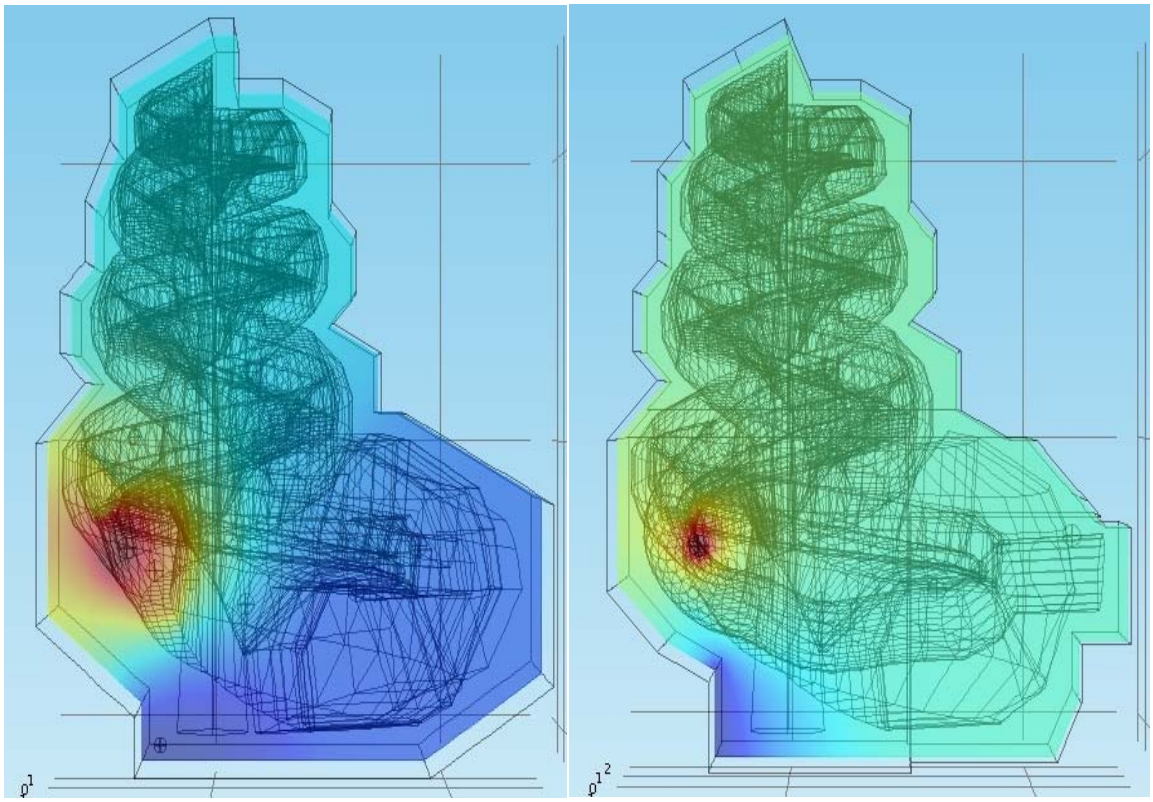

a) b)

Figure 4.12: Comparison of the voltage spread at *e5* with and without the carrier

The images are formulated in Comsol and represent voltage distributions around *e5*. Each one is 'slice' along the Y-Z plane centered at the origin on the x-axis. Figure 4.12a is absent of the carrier and has a broader spread around e5 compared to figure 4.12b which includes the carrier. The concentrated voltage helps focus the current toward the modiolus resulting in a higher current density around the nerve fibers which leads to a reduction in predicted threshold. It is the insulative nature of the carrier which causes the localisation of the voltage and positive influence on the current path.

© University of Pretoria

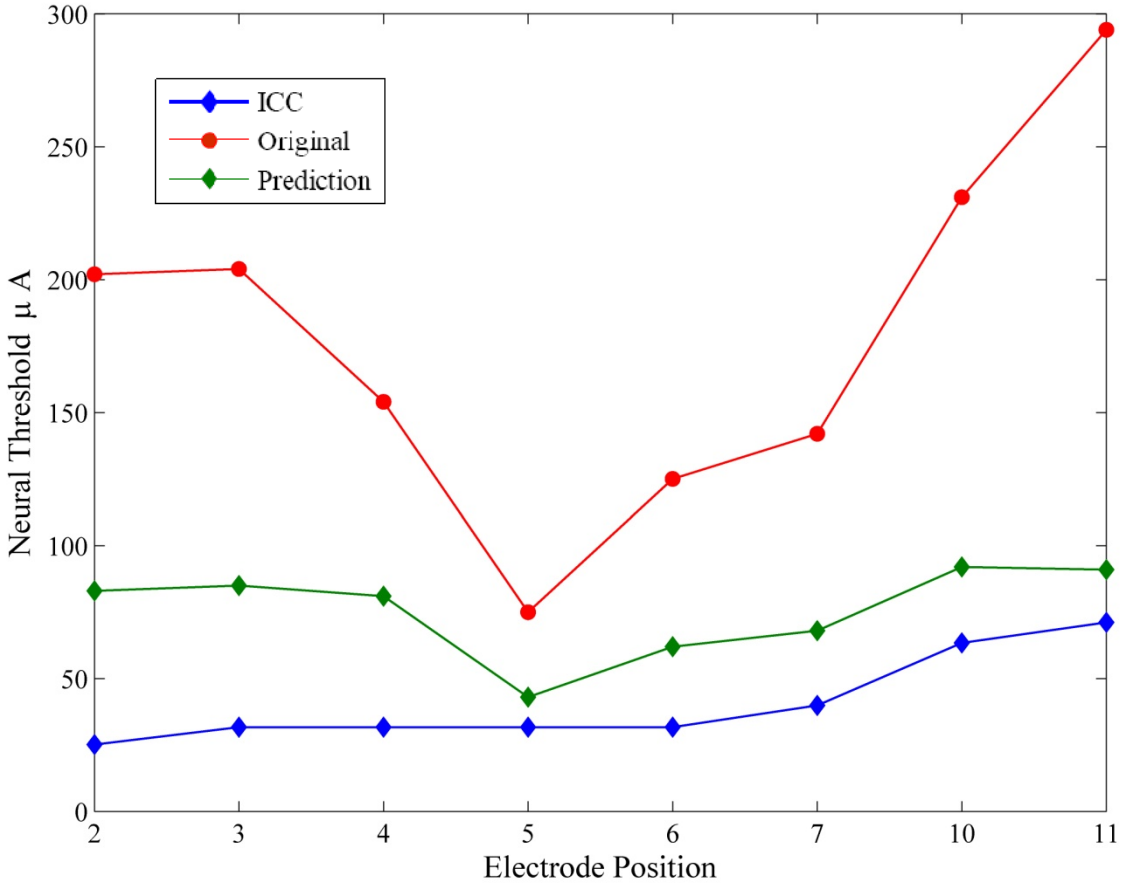

Figure 4.13: Predicted neural response: Carrier, return electrode and thin bone capsule

Figure 4.13 illustrates the most accurate prediction produced in this study. It exhibits thresholds that are closest to the ICC values at positions *e5, e6, e7,e10* and *e11.* The apical electrodes (*e2,e3,e4*) have thresholds which are slightly higher when compared to the hook-return-electrode. This suggests that modelling the hook region does exert some positive influence on the apical electrodes. A possible cause for this may be that it sinks current in such a manner, that the current traverses a path that is in closer proximity to the nerve fibers, than in the case of the electrode carrier. The carrier's insulative properties and the orientation of the electrodes in the apical region may encourage the current to flow superiorly and not laterally or inferiorly to axons or dendrites in the apical region.

© University of Pretoria

4.3.7 Hook, carrier and return electrode

Table 4.8 shows the data generated by the final model. This model is inclusive of the thin bone capsule, electrode carrier, hook region and return electrode. It has an overall Impact Factor of 3.92, between that of the hook-re (3.56) and carrier-re (4.55). At the basal end, the model favours the influence of the hook region over the insulating effect of the carrier as the Impact Factor at e11 drops from 11.22 down to 8.29, which is comparable to that of the hook-re model.

Table 4.8: Comparative metrics - Hook, carrier, return electrode and thin bone capsule

Electrode Position	ICC	Original prediction	Final	%Error (Original)	%Error (Final)	Impact Factor
(Apex) 2	25.18	202	81	702	222	3.17
3	31.70	204	79	544	149	3.64
4	31.70	154	77	386	143	2.70
5	31.70	75	46	137	45	3.03
6	31.70	125	68	294	115	2.57
7	39.91	142	74	256	85	2.99
10	63.40	231	97	264	53	4.99
(Base) 11	71.13	294	98	313	38	8.29

The sinking of the current by the hook region and consequent increase in neural threshold for *e11* is explained by Figure 4.14h. A large portion of the current is shunted toward the hook, away from the modiolus causing a decrease in effective current density. Figure 4.14g illustrates the current paths from *e10* and supports the notion of current escaping toward the hook in the basal region of the cochlea.

The collective figure illustrates the current paths and current densities across all eight electrode positions (*e2,e3,e4,e5,e6,e7,e10,e11*). The common theme of the images is that the return electrode causes a significant increase in the effective current density as the current paths cause the current to circulate through the cochlea before exiting and grounding at the return electrode. This highlights the importance for the correct positioning of the return electrode as it has a controlling influence on the current paths and subsequent neural thresholds.

© University of Pretoria

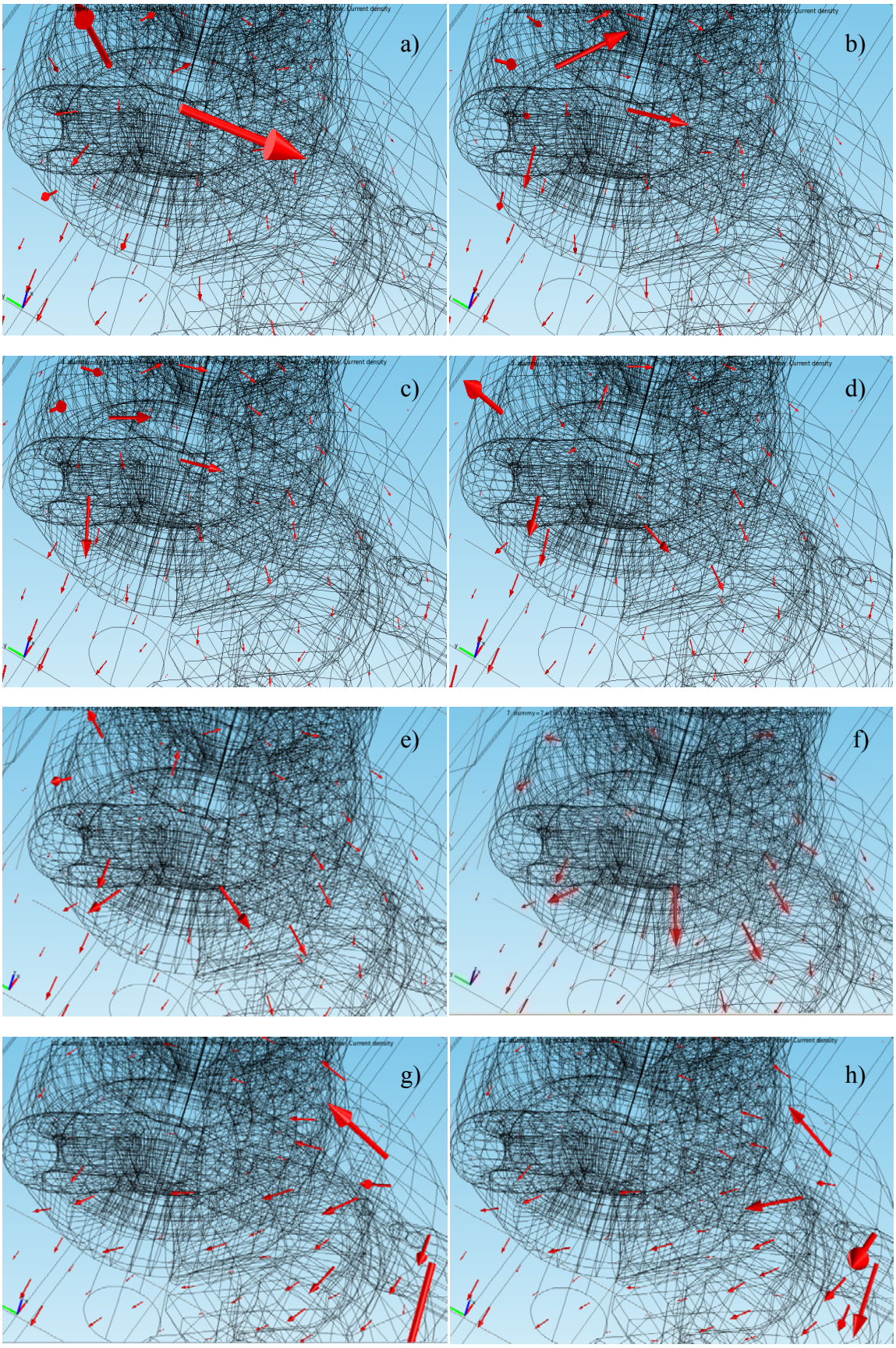

Figure 4.14: Current distributions around each active electrode starting at the apex with *e2* (a) and ending at the base with *e11* (b)

© University of Pretoria

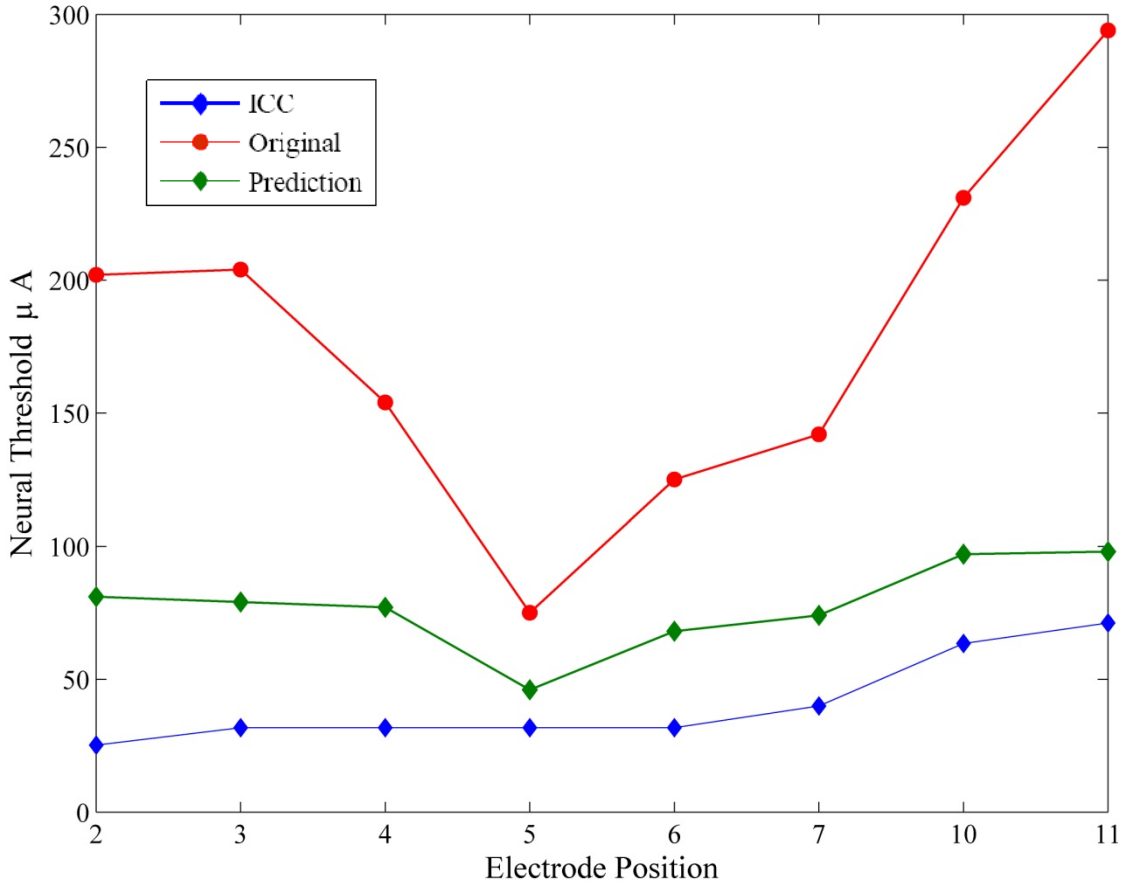

Figure 4.15: Predicted Neural response: Hook, carrier, return electrode and thin bone capsule

Figure 4.15 depicts the neural prediction (green line) after combining most of the investigative parameters into a single model. The overall profile has a closer correlation with the carrier-return electrode result, indicating that the carrier exercises greater control over the neural prediction than the hook region. In comparison to the original (red line) and ICC data (blue line), the prediction is in closer proximity to the EABR, which is an encouraging result.

© University of Pretoria

4.3.8 Insertion trauma and neural degeneration

In this section the possibility of neural degeneration and its effect on neural thresholds is investigated. The scala media contains neurotoxic endolymph which could cause nerve fibers to degenerate should this fluid leak out onto the fibers. The electrode carrier breaches the wall of the scala media in the vicinity of neurons 75-120, with the neurons being in close proximity to electrodes e2, e3 and e4. It is assumed that the endolymph could have caused the dendric portions of these neurons to degenerate, hence the neural model is configured to simulate this effect by removing the first four nodes for neurons 75-120.

Figure 4.16 illustrates the perforation of the scala media (red) by the carrier. The electrodes close to the breach (*e2,e3,e4*) are highlighted with the modiolus and nerve fibers depicted in blue. Figure 16b highlights the proximity of nerve fibers, 75-120, to the area of insertion trauma and it is assumed that the neurotoxic endolymph leaks onto theses fibers post insertion.

© University of Pretoria

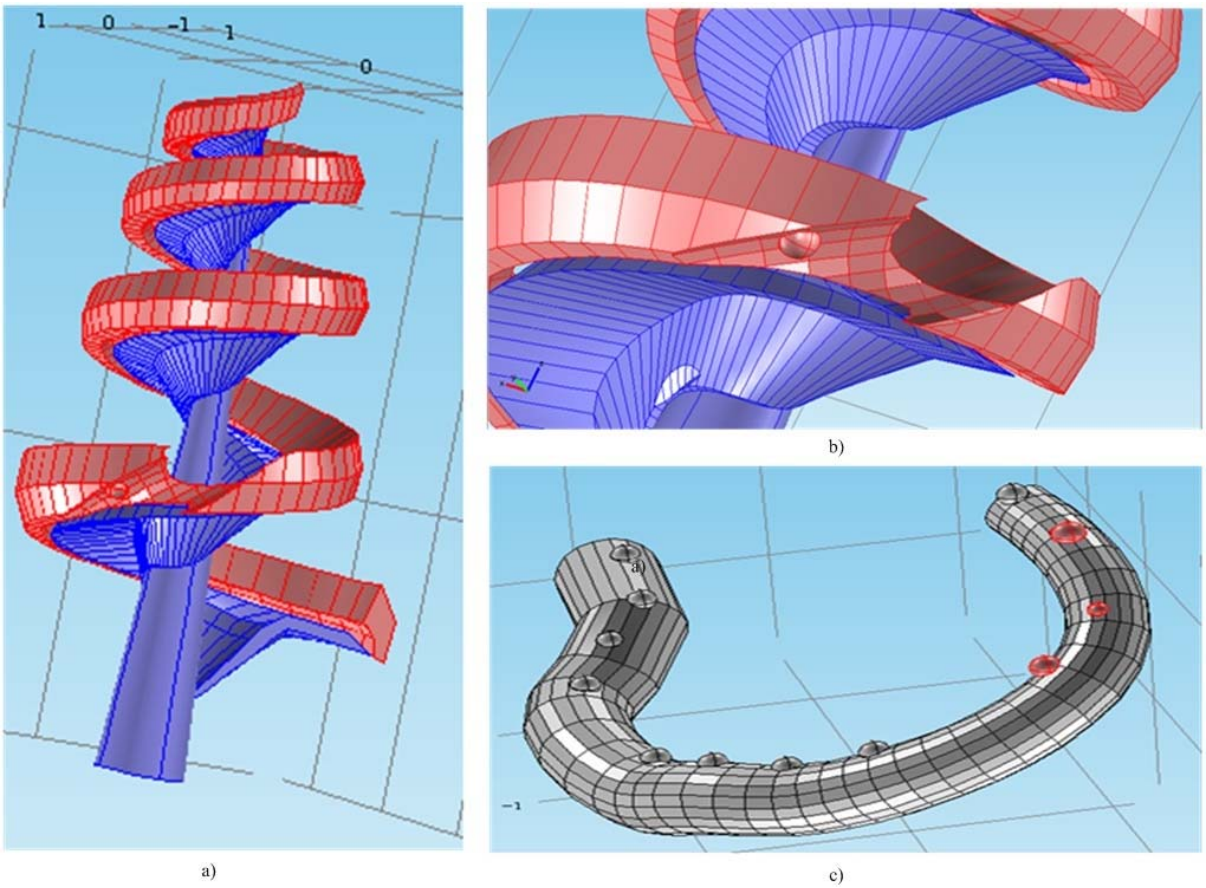

Figure 4.16: Areas of insertion trauma. Figure a. shows the area of the scala media breached by the carrier. Figure b. close up of the breach. Figure c. highlights the electrodes in proximity to the breach

The neural model is adjusted to incorporate degeneration for nerve fibers 75-120. The voltage distribution from the 'Final' model is then applied to neural model, thus adding neural degeneration to the existing parameters (thin bone, hook, carrier, return electrode).

Table 4.9: Neural thresholds for Normal nerve fibers vs. Degenerated nerve fibers

Electrode	Threshold (Normal)	Threshold (Degenerated)
(Apex) 2	81	81
3	79	79
4	77	77
5	46	46
6	68	68
7	74	74
10	97	97
(Base) 11	98	98

© University of Pretoria

Table 4.9 illustrates that modelling the effect of neural degeneration has had no effect on the predicted neural thresholds. In order to qualify and explain these results, a Matlab script was written to determine which neuron/s fire at the minimum threshold relative to the stimulation of each electrode.

Table 4.10: Neurons that fire at minimum threshold (Degenerated case)

Electrode	**Neuron that fires at minimum threshold**													
e2	92	93	94	95	96	97	98	99	100	101	102	103	104	105
e3	94	95	96	97	98	99	100							
e4	94	95	96	97	98	99	100	101						
e5	57													
e6	48	49												
e7	39	40												
e10	95	96	97											
e11	94	95	96	97	98									

Table 4.10 indicates that the minimum threshold is reached simultaneously by at least two neurons, except at *e5* where it is exclusive to one neuron. This may be explained by the proximity of *e5* to neurons 57-60.

© University of Pretoria

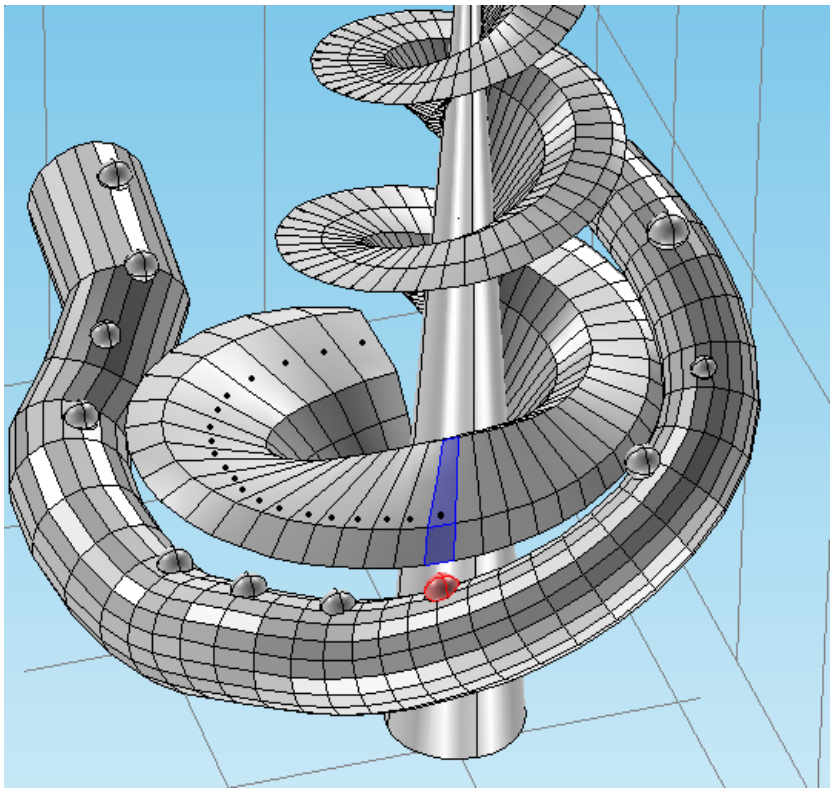

Figure 4.17: The proximity of *e*5 to nerve fibers 57-60

Each of the Comsol nerve fibers seen above represents 3 modelled fibers, which in turn represents 60 actual nerve fibers. The 19 black dots translate to the nerve fibers being stimulated lying in the range of 57-60 (blue) in the neural model. The targeted stimulation is assisted both by the proximity of the electrode to the nerve fiber and the isolative influence of the carrier.

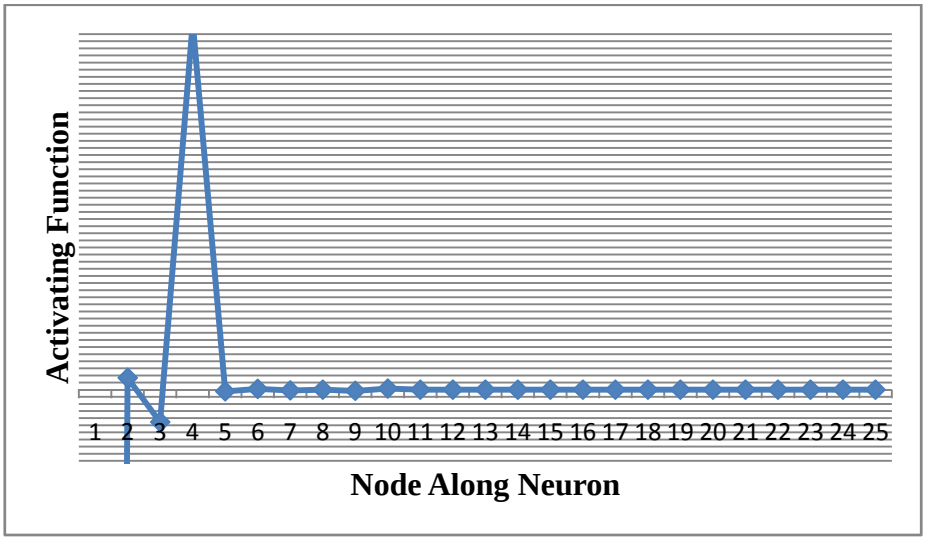

Figure 4.18: Activating Function for neuron 57

© University of Pretoria

As an indicative measure, the activating function for neuron 57 was determined in order to gauge whether stimulation occurs in the axonal, somatic or dendric portion of the fiber. The dendrite is represented by nodes 1-3, the soma node 4 and the axon nodes 6-27. Figure 4.18 suggests that stimulation could have occurred in either the dendric or somatic portion of the fiber as the activating function is positive in these two regions. Neuron 57 is not within the 'degenerated range' (75-120) hence, we may conclude that excitation is likely to occur in the dendric portion of the nerve.

Figure 4.19 represents the activating function for neuron 94 which lies in the 'degenerated range' and suggests that excitation can only occur in the somatic (node 4) or axonal portion (slight activation occurs at node 26 which is part of the axon) of the nerve. This may help explain the results of Table 4.9, as the activating function is independent of the neural degeneration parameter, which supports the notion that excitation will occur in the soma or axon regardless of whether the dendrite is present. An acceptance of this postulate would support the results in table 4.9 across electrodes *e2,e3,e4,e10 and e11.* This is supported by (Miller et al. 1999).

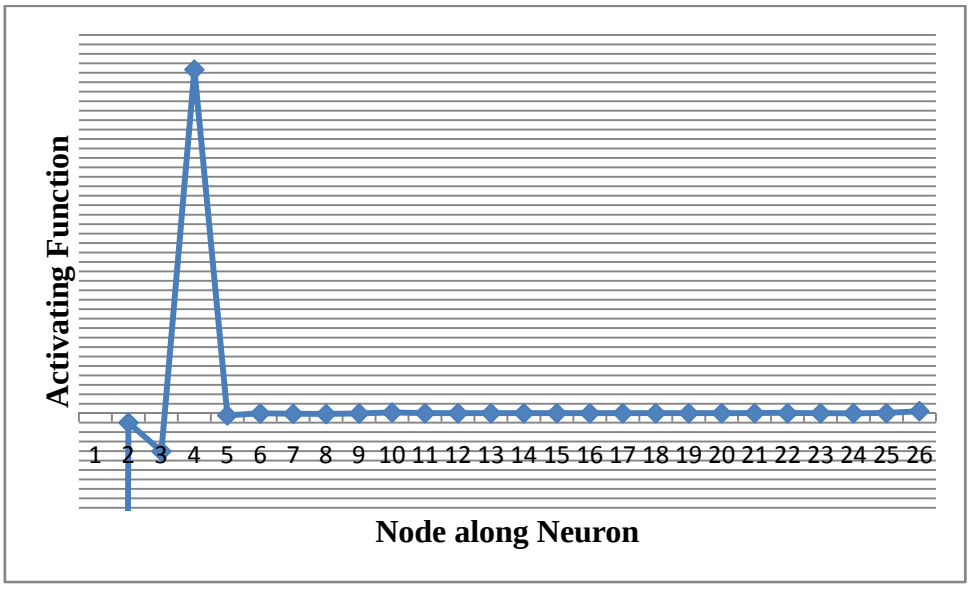

Figure 4.19: Activating Function for neuron 94

© University of Pretoria

4.3.9 Final Results – Comparison to generic model

For the subject-specific model to be comparable to models with a more general morphology and configuration, the detail had to be reduced. This was achieved by modelling an electrode array placed in the center of the scala tympani, replacing the subject-specific array. This array is ideal in the sense that it does not damage the scala tympani, whereas the array of the modelled subject perforated the upper wall of the scala tympani. The electrodes were modelled as 110 µm spheres with no carrier. This resembles banded electrode contacts as there is no insulative material restricting radial current flow (Malherbe 2009). Figure 4.20 illustrates the modelling of the generic model.

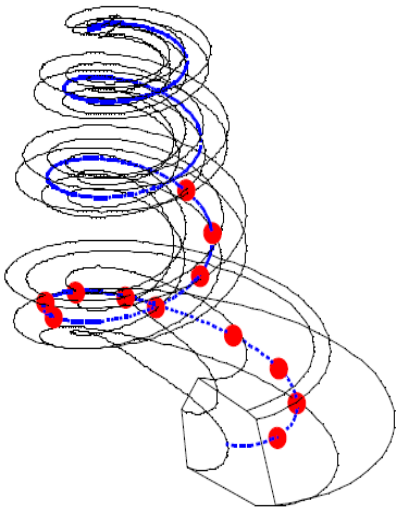

Figure 4.20: Electrode array placed in the middle of the scala tympani. The scala tympani is outlined in Black, with the electrode contacts in red. Blue line indicates the center line of the scala tympani (Malherbe 2009)

Table 4.11 Comparative metrics of final detailed model to a generic model

Electrode Position	ICC	Original prediction	Generic	Final	%Error (Generic)	%Error (Final)	Impact Factor
(Apex) 2	25.18	202	81	81	238	222	3.17
3	31.70	204	113	79	310	149	2.12
4	31.70	154	159	77	455	143	0.96
5	31.70	75	270	46	806	45	0.18
6	31.70	125	255	68	821	115	0.42
7	39.91	142	271	74	692	85	0.44
10	63.40	231	480	97	761	53	0.40
(Base) 11	71.13	294	357	98	502	38	0.78

© University of Pretoria

The model is stimulated in the same fashion as the subject-specific model with table 4.11 indicating the comparative results. The aggregated Impact Factor of the final subject-specific model is 3.35 relative to the generic prediction (1.06). It is more accurate at all electrode positions.

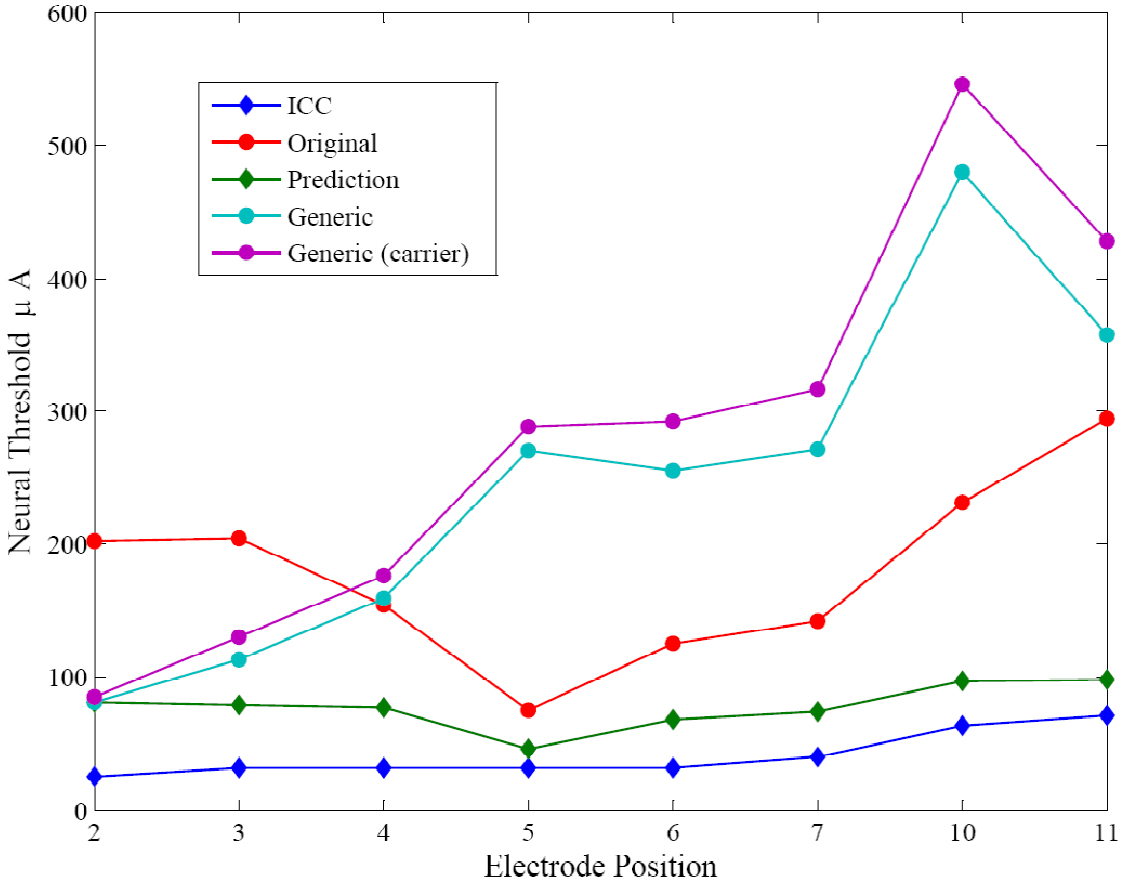

Figure 4.21: Comparison of subject-specific model prediction to generic model prediction. The final set of results shows that the revised subject-specific model has the most accurate prediction thus far.

Figure 4.21, is in essence, a summary of the results for this study. It highlights the increased accuracy in prediction when using a subject-specific model. The generic model is 3.35 (3.83 with carrier) times less accurate in its prediction, although the two are closely matched in their predictions at the apical end (*e2*,*e3*). The impact of the improvements made to the original model (red line) are also evident as the prediction (green line) is now much closer in both trend and absolute value to the ICC data (dark blue line).

© University of Pretoria

The effect of the added parameters is also captured in figure 4.22 which illustrates the ratio between the model data and the ICC response data. The optimum result would be when the model has a constant ratio for all electrode contacts and a value of one. Neither the new (blue) or original (red) models exhibit this profile but the blue line shows a marked improvement. It has a mean of 2.0 (closer to one) and has a relatively flat profile in comparison to the original, which has a mean of 4.6. The σ^2 of the new model is 0.4 while the original model has a σ^2 of 3.26. This highlights that the new model tracks the profile of the ICC response data more accurately than the original.

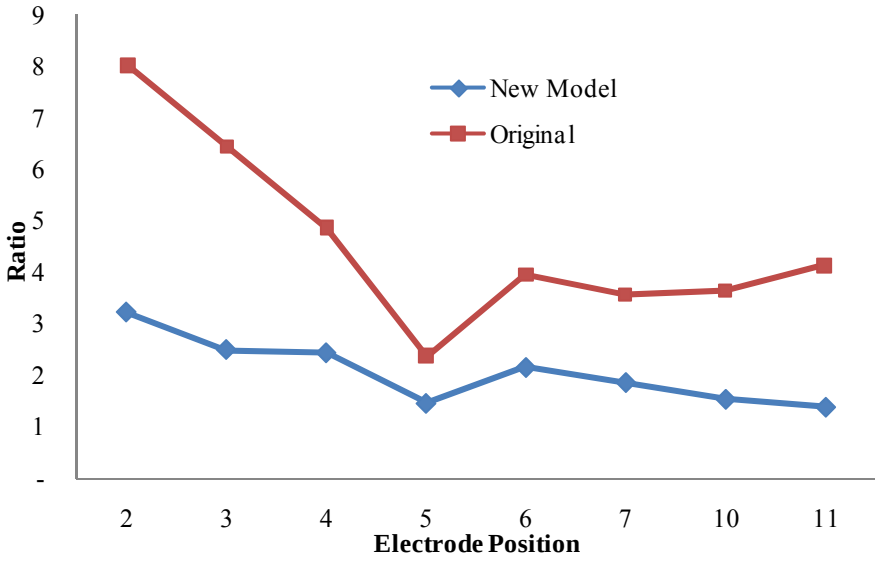

Figure 4.22: Ratio between model predictions and ICC response data (Table 4.11 data used in calculating the ratios)

This concludes the results chapter, which presented the results after each additional model parameter was implemented. A comparison was also made against the ICC data, original prediction and generic prediction. A discussion of the results and their implications follows in chapter 5.

© University of Pretoria

CHAPTER 5 DISCUSSION

5.1 INTRODUCTION

This study investigated the impact of structural additions to a subject-specific model of the guinea pig cochlea, with the objective of improving the model's ability to predict subject-specific ICC data. The accuracy was qualified and assessed against the original model (Malherbe 2009) and a generic model's prediction. The Impact Factor was used as a measure of the improvement in the model, as parameters were added. This chapter discusses the importance of each parameter and also discusses the implications of the findings, in the broader context of clinical application within the field of cochlear implants. Clinical audiology using animal subjects and how this research may be translated to improve hearing in humans is also discussed. The findings are also used to answer the research questions and support the hypothesis.

The chapter starts with an explanation for each set of results and their implications are discussed. The hypothesis and research questions are then discussed and validated through examination of the findings, after which a general discussion sheds light on the translational aspect of the research. A summarising conclusion highlights the inferences that can be deduced from the material presented in this chapter.

5.2 EXPLANATION AND IMPLICATION OF RESULTS

This section starts with a summary of each result, with references to literature before explaining the result in greater detail and deducing its implications. A critical evaluation is then given for each parameter in the context of improving the model's accuracy. The parameters discussed are: thin bone capsule, carrier, hook region, return electrode and neural degeneration. Finally, the comparative results for the subject-specific model and generic model are discussed.

5.2.1 Thin bone capsule

Modelling of the thin bone capsule has proven to have an adverse effect on the prediction with an Impact Factor of 0.89. This implies that on average, the parameter has reduced the accuracy of the prediction across electrode positions.

© University of Pretoria

The guinea pig cochlea is surrounded by a thin bone capsule and air filled bulla, which forms part of the larger osseous labyrinth. The original model (Malherbe 2009) represented this bone capsule as a solid cylinder of infinite proportion, with the outer boundaries set to ground in order to simulate the effect of the distant return electrode for MP stimulation. Bone has a conductivity of 0.156 $S.m^{-1}$, which is much lower than that of the cochlear ducts. The infinite volume of bone surrounding the cochlea would thus affect the impedance seen by the currents and the respective current paths. It was thus deemed credible to model this structure with greater accuracy.

The bone was reduced to a thin layer, 200 µm in diameter, with this envelope now forming the cochlear casing. Each one of the outer boundaries was set to ground, effectively forming a uniformly distributed return electrode. The results show an improvement in the predicted neural thresholds only at electrodes *e5* and *e7*. The remaining electrode positions all show a reduction in accuracy. There is a trend for the results to deteriorate closer to the basal or apical electrodes. The most apical (*e2*) and basal electrodes (*e11*) have the lowest impact factors, 0.73 and 0.68 respectively. These two electrodes are furthest away from the modiolus and closest to the outer wall of the thin bone capsule. The current is likely to be short circuited towards the ground plates (Figure 4.1). Although the same may be said for the case of the infinite bone surrounds, the effect is more pronounced with the thin bone capsule due to its finite and relatively small thickness. The absolute impedance seen by the electrodes and ground, increases with an increase in bone thickness (length). The infinite bone capsule presents a less attractive current path due to its higher impedance. The thin bone capsule is far more effective in sinking current, drawing it away from the modiolus. Thus, there should be a higher current density at the boundary of the thin bone capsule compared to the infinite bone cylinder. This explains the increase in thresholds at *e2* and *e11*.

The centrally located electrodes (*e4*,*e5*,*e6*) are in closer proximity to the nerve fibers, thus the thresholds at these locations are either comparable or lower than the original predictions, giving them a slightly improved Impact Factor. The relative variance in the thresholds is small, suggesting that the shape of the thin bone capsule may have only a slight effect on the current paths and thus the effective current densities at these locations.

The results are expected to be skewed as the return electrode is modelled incorrectly for this case and the results are only presented to provide a complete set of results. The bone

© University of Pretoria

capsule, however, is included in all other permutations of the model as it encases the cochlea.

5.2.2 Electrode Carrier

The implementation and modelling of the electrode carrier has had a positive effect on the results with an Impact Factor of 1.36. There is an improvement in accuracy across six electrodes (*e4,e5,e6,e7,e10,e11)* with only *e2* and *e3* experiencing a reduction in accuracy. These results imply that the electrode carrier is an integral component of the subject-specific model.

The silicon carrier has very high impedance and was modelled due to its potential impact on the current spread in the cochlea, due to its insulative effect. Figure 4.4 illustrates its ability to limit the shunting of current between electrodes, as almost no current flows toward adjacent electrodes from either *e7* or *e11.* It is also capable of focusing the current in a more controlled fashion, as is exhibited by Figure 4.4b. E11 directs current ly and toward the modiolus when the carrier is present, but shunts a large portion laterally in the absence of the carrier (Figure 4.1c).

These two properties help explain the results, where they have positive effects on most of the electrode positions except at *e2* and *e3* where the carrier's influence is negative. The orientation of *e2* is such that its superior hemisphere is exposed. It is also situated laterally in the cochlea. These two factors along with the carrier's ability to steer current (upward in this case) and the thin bone capsule does not bode well for an accurate result at *e2*for this scenario. The predicted value is almost 100 μA higher than the original prediction, with figure 4.3 illustrating that majority of the current is shunted away from the nerve fibers toward the ground plate of the bone capsule. A similar understanding may be applied to the result at *e3*.

The neural predictions at the remaining electrodes all respond favourably to the carriers presence for the same reasons mentioned above. *E7* has an Impact Factor of 2.17, the highest of the centrally located electrodes *(e5-e7*). This electrode also has its hemisphere exposed, but lies in closer proximity to the modiolus, thus giving the nerve fibers maximum exposure to its influence. The carrier assists in steering the current toward the nerve fibers, thus increasing the current density and reducing the predicted thresholds which improves the accuracy. Figure 4.4a illustrates that a significant portion of the current

© University of Pretoria

flows over the dendric portion of the nerve fibers situated in the region of *e7*. The same effect leads to a vastly improved accuracy at e11, with a reduction in percentage error of 87%.

5.2.3 Hook Region

Modelling of the hook region has an aggregated Impact Factor of 0.85, the lowest of the parameters discussed thus far. This suggests that modelling the hook region is regressive for this particular case, as on average it negatively impacts the accuracy of the predictions. A closer inspection of the results, however, implies the opposite.

The hook region proved to be a complex structure to model due to its curvature, tapering, lack of cross-sectional μCT representation and difficulty in meshing certain geometrical components in Comsol. The issue of meshing these geometries was resolved by modelling only the scala tympani, scala vestibuli, spiral ligament and Reissners membrane. This was necessary as Comsol experienced significant boundary conflicts when meshing adjacent geometries of different scales e.g. scala media, stria vascularis and Basilar membrane. The other challenges lie beyond the scope of this study.

The addition of the hook region may yield the worst aggregated impact factor (0.85) but it is the only parameter that increases the accuracy at the apical end of the electrode array (*e2, e3*). Its addition improves the Impact Factor of the thin bone capsule at *e2* and *e3* from 0.73 and 0.86 to 0.82 and 0.99 respectively. When integrated in conjunction with the carrier and thin bone capsule, it improves the accuracy at these two positions from 0.65 and 0.77 to 0.72 and 0.82. This is an average increase of 10% to the apical Impact Factors whenever the hook is added.

The positive influence on the apical Impact Factors is explained by the hook region's high conductivity. By acting as a current sink, it draws a differential current towards it that would otherwise flow laterally toward the bone capsule. This increases the effectiveness of the current, as the current paths now result in a slightly higher current density in the vicinity of the nerve fibers.

Its low aggregated impact factor of 0.85 is largely accounted for by its negative influence at *e11*. When added to the carrier, it reduces the impact factor from 1.39 at *e11* to 0.52, although at all other positions its inclusion is either positive or with negligible negative influence. The current sinking trait works adversely at the basal end as it draws current

© University of Pretoria

away from the modiolus, thus increasing the threshold. Seeing that this is the only parameter that positively influences the predictions at the apical end, the results imply that the hook region is a necessary component in the subject-specific model, as the specificity of its positive influence outweighs the negative impact it has for all permutations.

5.2.4 Return Electrode

The return electrode significantly improves the accuracy of the predictions and although simple to implement, it has the greatest positive impact on the results. This implies that the addition of a discrete return electrode is a fundamental general improvement to subject-specific and generic models.

It achieves this impact through its direct influence on the current paths, as exhibited by figures 4.9, 4.11 and 4.14. This is due to the fact that there is now only one ground, located just under the skin of the guine pig, close to the insertion, positioning it in the basal region of the cochlea. Figure 4.9, which illustrates the effect on the current paths clearly shows that the return electrode channels current through the cochlea. The effective current densities around the nerve fibers and modiolus is increased which results in lower neural thresholds across all electrode positions. Its effect is quantified by impact factors of 3.56, 4.55 and 3.92 for the hook, carrier and hook-carrier models. These are between 2.6 and 3.3 times higher than the previous best model (thin bone &carrier) with drastically reduced percentage errors across all electrode positions.

5.2.5 Neural degeneration and Insertion Trauma

Insertion trauma and the possible neural degeneration associated with this, has had no effect on the results or accuracy of prediction. This suggests that the nerve fibers in the region of simulated degeneration, were stimulated in their axons regardless of whether neural degeneration occurred or not.

This may be explained by the current densities being higher at the axonal portions of the nerve fibers. The broad excitation spread elicited by MP stimulation aggregates the current densities most effectively at the modiolus, as illustrated by Figures 4.14a-c. This causes the nerve fiber to fire only at the soma or axon and not the dendrite.

Neural degeneration did not affect the results of this specific subject model because of the location of the electrode contacts. However, whether it is a required component of the model is inconclusive since it might have a significant influence if the neural degeneration

© University of Pretoria

occurs in a section of the cochlea where the electrode contacts are positioned toward the lateral walls of the cochlea (Hanekom 2001a)

5.2.6 Comparison to generic model

The result of the comparison confirms the hypothesis that a subject-specific model is to a generic model when predicting ICC data.

The subject-specific model is more accurate due to its increased structural resolution. The modelling and correct positioning of the return electrode is the most important addition, with the carrier also playing an influential role. The hook region gives improved accuracy to the apical predictions, while the thin bone capsule and neural degeneration have negligible positive influence on their own.

5.3 GENERAL DISCUSSION

The results of this study suggest that a subject-specific model of the guinea pig cochlea is able to predict ICC data with greater accuracy than a generic model. It has also been shown that the complexity of the model, in terms of granular detail, has a direct influence on the accuracy of the prediction. This section exposes how the model may be used to steer the development of technology and enhance the perceptions of human cochlear implantees.

Animal models have been used extensively to help understand some of the underlying processes governing neurophysiology (Miller et al. 1983; Nagel 1974; Stypulkowski & Van den Honert 1984).The guinea pig provides a good comparator for the way in which humans process and respond to physical stimuli in the auditory system, due to a similarity in the physiologies. The work completed in this study forms the basis for understanding some of the subject-specific variances that occur across cochlear implantees. These variances cause inconsistency in the level of hearing restoration, particularly in speech intelligibility and music perception. The current method employed by audiologists to navigate this variance is to use a series of psychophysical and behavioural tests (Brown et al. 1994; Gordon, Papsin, & Harrison 2004; Miller et al. 2008).The tailoring of the implant in this manner helps to customise the implant on a subject-specific basis, but is extremely time consuming, difficult to conduct on children and has to be repeated frequently. ICC data may be used to supplement this process by indicating a level that is

© University of Pretoria

audible[26], allowing for interpolation of T and C-levels and reducing processing time by indicating threshold levels for corresponding electrodes. An objective measure of T-levels is crucial to the audiologist when the cochlear implant user is very young, developmentally delayed or disabled as these conditions inhibit behavioural mapping. Predicting C-levels could also help measure the safety margin before electrochemical processes at the electrodes produce potentially noxious products. Total power consumption, an important parameter for behind-the-ear or fully implantable devices could also be calculated from predicted C-levels (Frijns, Briaire, & Grote 2001).

This presents a reasonable case for models that can predict an ICC response on a subject-specific basis, as the models could be used to estimate the way the subject would respond to changes in electrode configuration, insertion depth or stimulation intensity. These changes could then be interpreted and their influence on threshold levels assessed without invasive surgery or extensive behavioural testing. The results of this study have shown that such a model is plausible and effective in its representation of subject-specific ICC data.

There are some challenges associated with this, however, when migrating from guinea pig to human models. The anatomical and volume conduction component of the guinea pig model can be replicated in humans. Although the physical dimensions, shape and surrounds of the cochlea are different, the same method may be applied. The one aspect that may prove challenging is the degradation in image quality, as the conventional CT scans used to image live human subjects have lower resolution than the μ-CT scans used to construct the guinea pig model. The impact of this degradation in a subject-specific context needs to be investigated and qualified.

A challenge of greater concern is soliciting credible ICC data from humans. The technique of inserting a probe into the IC, as used in the current study, is not transferable to humans. The only viable alternative is to obtain EABR through use of surface electrodes placed at various points on the skull. This method is accepted but gives only a coarse representation of the actual EABR, as the data is usually tainted by muscle artefacts. It cannot provide single fiber data as was used in this study.

The development of ECAP measurement techniques has allowed for a compromise between the single nerve fiber IC responses and the far field EABR surface electrode

[26] It is likely that one needs more fibers to respond in order to elicit a detectable / perceivable response, hence the ICC responses (single fiber) may not give a true indication of audible thresholds

© University of Pretoria

method. The electrically evoked compound action potential (ECAP) is captured at the periphery using the passive cochlear electrodes to record the distribution around an active one. It is a gross potential that represents the collective response of single auditory nerve fibers. The single fiber response, as is the one in the current study, is vital in bridging the gap between the physical reactions of the nerve fibers to the clinically obtainable gross potentials(Miller et al. 2008). The ECAP is an accumulated and synchronous response of multiple fibers, whose amplitude is believed to be proportional to the number of individual fibers that are firing.

A fundamental difference between ICC and ECAP data is that ICC data exposes central neural activity as it is a measure of neural responses in the brainstem. ECAP on the other hand is indicative of peripheral neural activity and is exempt of any central integration or processing. It has the advantage of being in close proximity to the source of neural excitation, but introduces the potential for interference by stimulus artefacts. Studies have shown that ECAPs can also be influenced by the shape of the evoking stimulus (Macherey et al. 2006; van Wieringen et al. 2008).

Similarly to ICC, ECAPs are valued for their potential to predict stimulus thresholds in cochlear implantees in cases where behavioural mapping is a challenge. They are also similar in the sense that they give an indication of only the range where a sound is audible and not the actual T-level. Perhaps the most pertinent trait of ECAPs, in the context of this study, is that they exhibit strong inter-subject variability. A study by (Miller et al. 2008) measured ECAP data across 17 implantees and found that in certain cases the ECAP correlated closely with the T-levels and in other cases it was recorded close to or higher than the C-level. This validates the need for a subject-specific representation, should one attempt to model the ECAP response. The study also introduces the notion that central temporal integration varies greatly amongst subjects which is supported by(Brown et al. 2000). The authors define temporal integration as a lowering of the psychophysical threshold due to the integrated effect of multiple stimulation pulses, which causes the behavioural thresholds to be lower than that of ECAP thresholds.

Although there are challenges associated with ECAP data, it does offer a viable reflection of neural thresholds in humans and could be used to bridge the gap between the single-fiber animal model, used in this study, and a gross response human model. The critical aspect then is to adapt the current model to predict ECAP data on a subject-specific basis.

© University of Pretoria

The impact of the inherent physical variations of the cochlear geometries, bone capsule and hook region as well as the induced variations of the carrier and return electrode have been accounted for in this study. It has also been proven that the inclusion and acknowledgment of these variations has significant impact on the predictive ability of the model. This aspect of the modelling process is easily transferable to a human subject.

The complexity arises in the neural representation, as the current model utilises a single-nerve fiber response i.e. the Generalised Schwartz and Eikhof (GSEF) model. The model provides a good measure of individual nerve fiber behaviour and thresholds but is incapable of simulating the collective response of a population of fibers. A correct prediction of ECAP data requires this collective representation. The membrane kinetics of each neural model (GSEF, HH etc.) is different and for a model to be clinically applicable it should ideally predict both trends as well as absolute values of specific phenomena. The choice of the GSEF model in this case proved to be a good one since it performs well on both accounts. Thus, the fact that other models of membrane kinetics such as the HH model will probably predict other threshold values, does not in fact matter, because the choice of the GSEF model in this case is adequate (accurate to within 36 μA on average). It may be necessary to select another model if the work is translated to human models, depending on how each model fares in predicting both trends in and absolute values of thresholds.

A more sophisticated neural model would require the interaction between different nerve fibers to be taken into account when determining population characteristics such as neural threshold. The preliminary work of (Jonsson.R, Hanekom.T, & Hanekom.J.J 2007) aims to capture the relationships between adjacent fibers through representation of ephaptic excitation. Ephaptic stimulation is defined as the excitation of a neuron by the surrounding environment as a consequence of other neural activity..It is often the case in cochlear implantees that neural responses are synchronous, which results in increased extracellular currents that may cause the firing of a neuron that wouldn't ordinarily fire due to the stimulus alone.. The study concludes that ephaptic stimulation is relevant and evident as it has a significant effect at intensities close to threshold. The authors suggest that future work incorporates this ephaptic neural model with a volume conduction model of the implanted cochlea.

© University of Pretoria

The existing subject-specific model coupled with a more sophisticated neural model, like the one mentioned above, should favour a more accurate prediction of ECAP data. The improved model could then be used to assess the impact of biophysical changes on neural and perceptual responses in humans, provided it replicates the predictive accuracy attained in this study. The realisation of such a model would bring the research community one step closer to being able to predict and understand perceived auditory responses in humans. This would, however, require a thorough understanding of central processing stages as these bridge the gap between physical responses (ICC, ECAP) and perception.

© University of Pretoria

CHAPTER 6: CONCLUSION

It has been shown in this study that a subject-specific model of the guinea pig cochlea is capable of predicting ICC data more accurately than a generic model. The study has also provided insight into the impact of certain subject-specific variances and how these influence the accuracy of the model. To this extent the study can conclude that modelling the correct position of the return electrode for MP stimulation is the most important factor in approving the accuracy of the model. This is due to its direct influence on the current paths, causing a higher current density around the modiolus, consequently reducing neural thresholds. The electrode carrier is also a critical component when constructing a subject-specific model, as it helps to direct and steer the current due to its insulative properties. Finally, the hook region is important as it improves the accuracy of the prediction at the apical end due to its high conductivity. This causes it to draw current over the neurons toward the hook area, effectively increasing the current density and lowering neural thresholds. It is the only added parameter that improves the accuracy of the prediction in the apical region.

A consideration of these three parameters improves the accuracy of the model by 4.5 times relative to the original and makes it 3.5 times more accurate than a generic prediction. This finding strongly supports the hypothesis and proves correct, that a subject-specific model is better at predicting neural responses than a generic one. The validation of this subject-specific approach will allow the model to be used as a research tool to predict the way an individual subject would respond to changes in electrode configuration, insertion depth and stimulus intensity.

The future work entails the translation of this research so that it is applicable to humans. The migration from the animal model would involve the use of ECAP data as opposed to ICC as ECAPs provide a better physical representation in humans than surface electrode EABR. The volume conduction portion of the model should be directly translatable to humans, with inclusion of the added parameters accounted for in this study. The main concern would be the degradation of the image quality from which the subject-specific geometries are constructed. A more important translative requirement is the adaption of the neural model such that it captures the behaviour of a population of nerve fibers, as opposed to the single nerve fiber model used in this study. One of the shortcomings of this study was that only one subject-specific model was assessed. In order to validate the modelling

© University of Pretoria

method, ranking of important parameters and results, the same procedure needs to be carried out across several subjects. This would prove whether the subject-specific method is effective and whether the influential parameters of this study are applicable on a broad basis.

© University of Pretoria

REFERENCES

Adunka, O. & Kiefer, J. 2006, "Impact of electrode insertion depth on intracochlear trauma", *Otolaryngology - Head and Neck Surgery*, vol. 135, no. 3, pp. 374-382.

Aubert, L. R. & Clarke, G. P. 1994, "Reliability and predictive value of the electrically evoked auditory brainstem response", *British Journal of Audiology*, vol. 28, no. 3, pp. 121-124.

Baskent, D. & Shannon, R. V. 2003, "Speech recognition under conditions of frequency-place compression and expansion", *Journal of the Acoustical Society of America*, vol. 113, no. 4 I, pp. 2064-2076.

Beitel, R. E., Snyder, R. L., Schreiner, C. E., Raggio, M. W., & Leake, P. A. 2000, "Electrical cochlear stimulation in the deaf cat: Comparisons between psychophysical and central auditory neuronal thresholds", *Journal of Neurophysiology*, vol. 83, no. 4, pp. 2145-2162.

Berenstein, C. K., Mens, L. H. M., Mulder, J. J. S., & Vanpoucke, F. J. 2008, "Current steering and current focusing in cochlear implants: Comparison of monopolar, tripolar, and virtual channel electrode configurations", *Ear and Hearing*, vol. 29, no. 2, pp. 250-260.

Bierer, J. A. 2007, "Threshold and channel interaction in cochlear implant users: Evaluation of the tripolar electrode configuration", *Journal of the Acoustical Society of America*, vol. 121, no. 3, pp. 1642-1653.

Bierer, J. A. & Middlebrooks, J. C. 2002, "Auditory cortical images of cochlear-implant stimuli: Dependence on electrode configuration", *Journal of Neurophysiology*, vol. 87, no. 1, pp. 478-492.

Blamey, P. 1997, "Are spiral ganglion cell numbers important for speech perception with a cochlear implant?", *American Journal of Otology*, vol. 18, no. 6 SUPPL..

Blamey, P., Arndt, P., Bergeron, F., Bredberg, G., Brimacombe, J., Facer, G., Larky, J., Lindstram, B., Nedzelski, J., Peterson, A., Shipp, D., Staller, S., & Whitford, L. 1996b, "Factors Affecting Auditory Performance of Postlinguistically Deaf Adults Using Cochlear Implants", *Audiology and Neuro-Otology*, vol. 1, no. 5, pp. 293-306.

Blamey, P., Arndt, P., Bergeron, F., Bredberg, G., Brimacombe, J., Facer, G., Larky, J., LindstrÃ¶m, B., Nedzelski, J., Peterson, A., Shipp, D., Staller, S., & Whitford, L. 1996a, "Factors Affecting Auditory Performance of Postlinguistically Deaf Adults Using Cochlear Implants", *Audiology and Neuro-Otology*, vol. 1, no. 5, pp. 293-306.

© University of Pretoria

Boëx, C., Baud, L., Cosendai, G., Sigrist, A., Kós, M., & Pelizzone, M. 2006, "Acoustic to electric pitch comparisons in cochlear implant subjects with residual hearing", *JARO - Journal of the Association for Research in Otolaryngology*, vol. 7, no. 2, pp. 110-124.

Bonham, B. H. & Litvak, L. M. 2008, "Current focusing and steering: Modeling, physiology, and psychophysics", *Hearing Research*, vol. 242, no. 1-2, pp. 141-153.

Boons, T., Brokx, J. P. L., Dhooge, I., Frijns, J. H. M., Peeraer, L., Vermeulen, A., Wouters, J., & van Wieringen, A. 2012, "Predictors of spoken language development following pediatric cochlear implantation", *Ear and Hearing*, vol. Article in Press.

Briaire, J. J. & Frijns, J. H. M. 2000, "3D mesh generation to solve the electrical volume conduction problem in the implanted inner ear", *Simulation Practice and Theory*, vol. 8, no. 1-2, pp. 57-73.

Briaire, J. J. & Frijns, J. H. M. 2005, "Unraveling the electrically evoked compound action potential", *Hearing Research*, vol. 205, no. 1-2, pp. 143-156.

Briaire, J. J. & Frijns, J. H. M. 2006, "The consequences of neural degeneration regarding optimal cochlear implant position in scala tympani: A model approach", *Hearing Research*, vol. 214, no. 1-2, pp. 17-27.

Brown, C. J., Abbas, P. J., Fryauf-Bertschy, H., Kelsay, D., & Gantz, B. J. 1994, "Intraoperative and postoperative electrically evoked auditory brain stem responses in nucleus cochlear implant users: Implications for the fitting process", *Ear and Hearing*, vol. 15, no. 2, pp. 168-176.

Brown, C. J., Abbas, P. J., & Gantz, B. 1990, "Electrically evoked whole-nerve action potentials: Data from human cochlear implant users", *Journal of the Acoustical Society of America*, vol. 88, no. 3, pp. 1385-1391.

Brown, C. J., Hughes, M. L., Luk, B., Abbas, P. J., Wolaver, A., & Gervais, J. 2000, "The relationship between EAP and EABR thresholds and levels used to program the Nucleus 24 speech processor: Data from adults", *Ear and Hearing*, vol. 21, no. 2, pp. 151-163.

Carlyon, R. P., MacHerey, O., Frijns, J. H. M., Axon, P. R., Kalkman, R. K., Boyle, P., Baguley, D. M., Briggs, J., Deeks, J. M., Briaire, J. J., Barreau, X., & Dauman, R. 2010, "Pitch comparisons between electrical stimulation of a cochlear implant and acoustic stimuli presented to a normal-hearing contralateral ear", *JARO - Journal of the Association for Research in Otolaryngology*, vol. 11, no. 4, pp. 625-640.

Chandler, W. K. & Meves, H. 1970, "Rate constants associated with changes in sodium conductance in axons perfused with sodium fluoride", *Journal of Physiology*, vol. 211, no. 3, pp. 679-705.

Chatterjee, M. 1999, "Effects of stimulation mode on threshold and loudness growth in multielectrode cochlear implants", *Journal of the Acoustical Society of America*, vol. 105, no. 2 I, pp. 850-860.

Chatterjee, M., Galvin III, J. J., Fu, Q. J., & Shannon, R. V. 2006, "Effects of stimulation mode, level and location on forward-masked excitation patterns in cochlear implant

© University of Pretoria

patients", *JARO - Journal of the Association for Research in Otolaryngology*, vol. 7, no. 1, pp. 15-25.

Cheng, A. H. D. & Cheng, D. T. 2005, "Heritage and early history of the boundary element method", *Engineering Analysis with Boundary Elements*, vol. 29, no. 3, pp. 268-302.

Chiu, S. Y., Ritchie, J. M., Bogart, R. B., & Stagg, D. 1979, "A quantitative description of membrane currents in rabbit myelinated nerve", *Journal of Physiology*, vol. Vol. 292, pp. 149-166.

Clough, R. W. 1990, "Original formulation of the finite element method", *Finite Elements in Analysis and Design*, vol. 7, no. 2, pp. 89-101.

Colletti, L., MandalÃ , M., Zoccante, L., Shannon, R. V., & Colletti, V. Infants versus older children fitted with cochlear implants: Performance over 10 years. International Journal of Pediatric Otorhinolaryngology .
Ref Type: In Press

Dettman, S. J., Pinder, D., Briggs, R. J. S., Dowell, R. C., & Leigh, J. R. 2007, "Communication development in children who receive the cochlear implant younger than 12 months: Risks versus benefits", *Ear and Hearing*, vol. 28, no. SUPPL.2.

Dorman, M. F., Spahr, T., Gifford, R., Loiselle, L., McKarns, S., Holden, T., Skinner, M., & Finley, C. 2007, "An electric frequency-to-place map for a cochlear implant patient with hearing in the nonimplanted ear", *JARO - Journal of the Association for Research in Otolaryngology*, vol. 8, no. 2, pp. 234-240.

Drullman, R. & Bronkhorst, A. W. 2004, "Speech perception and talker segregation: Effects of level, pitch, and tactile support with multiple simultaneous talkers", *Journal of the Acoustical Society of America*, vol. 116, no. 5, pp. 3090-3098.

Eggermont, J. J., Ponton, C. W., Don, M., Waring, M. D., & Kwong, B. 1997, "Maturational delays in cortical evoked potentials in cochlear implant users", *Acta Oto-Laryngologica*, vol. 117, no. 2, pp. 161-163.

Escude., James, C., Deguine, O., Cochard, N., Eter, E., & Fraysse, B. 2006, "The size of the cochlea and predictions of insertion depth angles for cochlear implant electrodes", *Audiology and Neurotology*, vol. 11, no. SUPPL. 1, pp. 27-33.

Faulkner, A. 2006, "Adaptation to distorted frequency-to-place maps: Implications of simulations in normal listeners for cochlear implants and electroacoustic stimulation", *Audiology and Neurotology*, vol. 11, no. SUPPL. 1, pp. 21-26.

Finley, C. C., Holden, T. A., Holden, L. K., Whiting, B. R., Chole, R. A., Neely, G. J., Hullar, T. E., & Skinner, M. W. 2008, "Role of electrode placement as a contributor to variability in cochlear implant outcomes", *Otology & neurotology : official publication of the American Otological Society, American Neurotology Society [and] European Academy of Otology and Neurotology*, vol. 29, no. 7, pp. 920-928.

Finney, E. M., Fine, I., & Dobkins, K. R. 2001, "Visual stimuli activate auditory cortex in the deaf", *Nature Neuroscience*, vol. 4, no. 12, pp. 1171-1173.

© University of Pretoria

Fitzhugh, R. 1969, "Nbuifnbujdbm!npefmt!pg!fydjubujpo!boe!qspqbhbujpo!jo!ofswf," in *Schwan, H.P. (Ed.), Biological Engineering*, McGraw-Hill, New York, pp. 1-85.

Friedland, D. R., Venick, H. S., & Niparko, J. K. 2003, "Choice of ear for cochlear implantation: The effect of history and residual hearing on predicted postoperative performance", *Otology and Neurotology*, vol. 24, no. 4, pp. 582-589.

Friesen, L. M., Shannon, R. V., Baskent, D., & Wang, X. 2001, "Speech recognition in noise as a function of the number of spectral channels:
Comparison of acoustic hearing and cochlear implants", *Journal of the Acoustical Society of America*, vol. 110, no. 2, pp. 1150-1163.

Frijns, J. H. M., Briaire, J. J., & Grote, J. J. 2001, "The importance of human cochlear anatomy for the results of modiolus-hugging multichannel cochlear implants", *Otology and Neurotology*, vol. 22, no. 3, pp. 340-349.

Frijns, J. H. M., Briaire, J. J., & Schoonhoven, R. 2000, "Integrated use of volume conduction and neural models to simulate the response to cochlear implants", *Simulation Practice and Theory*, vol. 8, no. 1-2, pp. 75-97.

Frijns, J. H. M., De Snoo, S. L., & Schoonhoven, R. 1995, "Potential distributions and neural excitation patterns in a rotationally symmetric model of the electrically stimulated cochlea", *Hearing Research*, vol. 87, no. 1-2, pp. 170-186.

Frijns, J. H. M., De Snoo, S. L., & Ten Kate, J. H. 1996, "Spatial selectivity in a rotationally symmetric model of the electrically stimulated cochlea", *Hearing Research*, vol. 95, no. 1-2, pp. 33-48.

Frijns, J. H. M., Mooij, J., & Ten Kate, J. H. 1994, "Quantitative approach to modeling mammalian myelinated nerve fibers for electrical prosthesis design", *IEEE Transactions on Biomedical Engineering*, vol. 41, no. 6, pp. 556-566.

Fu, Q. J. & Shannon, R. V. 1999, "Effects of electrode configuration and frequency allocation on vowel recognition with the nucleus-22 cochlear implant", *Ear and Hearing*, vol. 20, no. 4, pp. 332-344.

Fu, Q. J., Shannon, R. V., & Galvin III, J. J. 2002, "Perceptual learning following changes in the frequency-to-electrode assignment with the Nucleus-22 cochlear implant", *Journal of the Acoustical Society of America*, vol. 112, no. 4, pp. 1664-1674.

Gantz, B. J., Woodworth, G. G., Knutson, J. F., Abbas, P. J., & Tyler, R. S. 1993, "Multivariate predictors of audiological success with multichannel cochlear implants", *Annals of Otology, Rhinology and Laryngology*, vol. 102, no. 12, pp. 909-916.

Geers, A. E. 2004, "Speech, Language, and Reading Skills after Early Cochlear Implantation", *Archives of Otolaryngology - Head and Neck Surgery*, vol. 130, no. 5, pp. 634-638.

Gelfand, S. A. 2004, *Hearing: An introduction to psychological and physiological acoustics*, 4th edn, New York: Marcel Dekker.

© University of Pretoria

Gibson, W. C. 2008, *The Method of Moments in Electromagnetics* Chapman & Hall/CRC.

Goldstein, M. H. & Kiang, N. Y. S. 1958, "Synchrony of neural activity in electric response evoked by transient acoustic stimuli.", *Journal of the Acoustical Society of America*, vol. 30, pp. 107-114.

Gordon, K. A., Papsin, B. C., & Harrison, R. V. 2004, "Toward a battery of behavioral and objective measures to achieve optimal cochlear implant stimulation levels in children", *Ear and Hearing*, vol. 25, no. 5, pp. 447-463.

Greenwood, D. D. 1990, "A cochlear frequency-position function for several species - 29 years later", *Journal of the Acoustical Society of America*, vol. 87, no. 6, pp. 2592-2605.

Gyo, K. & Yanagihara, N. 1980, "Electrically and acoustically evoked brain stem responses in guinea pig", *Acta Oto-Laryngologica*, vol. 90, no. 1-2, pp. 25-31.

Hanekom, T. 2001a, *Modelling of the electrode-auditory nerve fibre interface in cochlear prosthesis,* PhD thesis, University of Pretoria.

Hanekom, T. 2001b, "Three-dimensional spiraling finite element model of the electrically stimulated cochlea", *Ear and Hearing*, vol. 22, no. 4, pp. 300-315.

Hanekom, T. 2005, "Modelling encapsulation tissue around cochlear implant electrodes", *Medical and Biological Engineering and Computing*, vol. 43, no. 1, pp. 47-55.

Hardie, N. A. & Shepherd, R. K. 1999, "Sensorineural hearing loss during development: Morphological and physiological response of the cochlea and auditory brainstem", *Hearing Research*, vol. 128, no. 1-2, pp. 147-165.

Hassanzadeh, S., Farhadi, M., Daneshi, A., & Emamdjomeh, H. 2002, "The effects of age on auditory speech perception development in cochlear-implanted prelingually deaf children", *Otolaryngology - Head and Neck Surgery*, vol. 126, no. 5, pp. 524-527.

Ho, S. Y., Wiet, R. J., & Richter, C. P. 2004, "Modifying cochlear implant design: Advantages of placing a return electrode in the modiolus", *Otology and Neurotology*, vol. 25, no. 4, pp. 497-503.

Hodgkin, A. L. & Huxley, A. F. 1952, "A quantitative description of membrane current and its application to conduction and excitation in nerve", *The Journal of physiology*, vol. 117, no. 4, pp. 500-544.

Jiang, M., Wang, G., Skinner, M. W., Rubinstein, J. T., & Vannier, M. W. 2003, "Blind deblurring of spiral CT images", *IEEE Transactions on Medical Imaging*, vol. 22, no. 7, pp. 837-845.

Jonsson.R, Hanekom.T, & Hanekom.J.J 2007, "Initial results from a model of ephaptic excitation in the electrically excited peripheral auditory nervous system", *Hearing Research* no. 237, pp. 49-56.

© University of Pretoria

Kileny, P. R., Zwolan, T. A., Telian, S. A., & Boerst, A. 1998, "Performance with the 20 + 2L lateral wall cochlear implant", *American Journal of Otology*, vol. 19, no. 3, pp. 313-319.

Kitano, H. 2002b, "Systems biology: A brief overview", *Science*, vol. 295, no. 5560, pp. 1662-1664.

Kitano, H. 2002a, "Computational systems biology", *Nature*, vol. 420, no. 6912, pp. 206-210.

Klop, W. M. C., Boermans, P. P. B. M., Ferrier, M. B., Van Den Hout, W. B., Stiggelbout, A. M., & Frijns, J. H. M. 2008, "Clinical relevance of quality of life outcome in cochlear implantation in postlingually deafened adults", *Otology and Neurotology*, vol. 29, no. 5, pp. 615-621.

Koks, D. 2006, in *Explorations in Mathematical Physics*, Springer Science, p. 147.

Kubo, T., Yamamoto, K., Iwaki, T., Matsukawa, M., Doi, K., & Tamura, M. 2001, "Significance of auditory evoked responses (EABR and P300) in cochlear implant subjects", *Acta Oto-Laryngologica*, vol. 121, no. 2, pp. 257-261.

Kunisue, K., Fukushima, K., Kawasaki, A., Maeda, Y., Nagayasu, R., Kataoka, Y., Kariya, S., Fukutomi, Y., Takami, H., & Nishizaki, K. 2007, "Comprehension of abstract words among hearing impaired children", *International Journal of Pediatric Otorhinolaryngology*, vol. 71, no. 11, pp. 1671-1679.

Leake, P. A., Snyder, R. L., Hradek, G. T., & Rebscher, S. J. 1993, "Chronic intracochlear electrical stimulation in neonatally deafened cats: Effects of intensity and stimulating electrode location", *Hearing Research*, vol. 64, no. 1, pp. 99-117.

Lee, D. S., Lee, J. S., Oh, S. H., Kim, S. K., Kim, J. W., Chung, J. K., Lee, M. C., & Kim, C. S. 2001, "Cross-modal plasticity and cochlear implants", *Nature*, vol. 409, no. 6817, pp. 149-150.

Li, P. M. M. C., Wang, H., Northrop, C., Merchant, S. N., & Nadol, J. 2007, "Anatomy of the round window and hook region of the cochlea with implications for cochlear implantation and other endocochlear surgical procedures", *Otology and Neurotology*, vol. 28, no. 5, pp. 641-648.

Macherey, O., van Wieringen, A., Carlyon, R. P., Deeks, J. M., & Wouters, J. 2006, "Asymmetric pulses in cochlear implants: Effects of pulse shape, polarity, and rate", *JARO - Journal of the Association for Research in Otolaryngology*, vol. 7, no. 3, pp. 253-266.

Malherbe, T. K. 2009, *Development of a method to create subject specific cochlear models for electric hearing,* Masters Thesis, University of Pretoria.

Manrique, M., Cervera-Paz, F. J., Huarte, A., & Molina, M. 2004, "Advantages of cochlear implantation in prelingual deaf children before 2 years of age when compared with later implantation", *Laryngoscope*, vol. 114, no. 8 I, pp. 1462-1469.

Mason, S. M., Sheppard, S., Garnham, C. W., Lutman, M. E., O'Donoghue, G. M., & Gibbin, K. P. "Improving the relationship of intraoperative EABR thresholds to T-level in

© University of Pretoria

young children receiving the Nucleus cochlear implant.", in *Paper presented at Third International Cochlear Implant Conference,Innsbruck, Austria*.

Massoud, T. F., Hademenos, G. J., Young, W. L., Gao, E., Pile-Spellman, J., & Vinuela, F. 1998, "Principles and philosophy of modeling in biomedical research", *FASEB Journal*, vol. 12, no. 3, pp. 275-285.

Mattiussi, C. The finite volume, finite element, and finite difference methods as numerical methods for physical field problems. 113[C], 1-146. 2000.
Ref Type: Serial (Book,Monograph)

McCreery, D., Lossinsky, A., & Pikov, V. 2007, "Performance of multisite silicon microprobes implanted chronically in the ventral cochlear nucleus of the cat", *IEEE Transactions on Biomedical Engineering*, vol. 54, no. 6, pp. 1042-1052.

Middlebrooks, J. C. & Snyder, R. L. 2007, "Auditory prosthesis with a penetrating nerve array", *JARO - Journal of the Association for Research in Otolaryngology*, vol. 8, no. 2, pp. 258-279.

Miller, C. A., Abbas, P. J., Robinson, B. K., Rubinstein, J. T., & Matsuoka, A. J. 1999, "Electrically evoked single-fiber action potentials from cat: Responses to monopolar, monophasic stimulation", *Hearing Research*, vol. 130, no. 1-2, pp. 197-218.

Miller, C. A., Brown, C. J., Abbas, P. J., & Chi, S. L. 2008, "The clinical application of potentials evoked from the peripheral auditory system", *Hearing Research*, vol. 242, no. 1-2, pp. 184-197.

Miller, C. A., Faulkner, M. J., & Pfingst, B. E. 1995, "Functional responses from guinea pigs with cochlear implants. II. Changes in electrophysiological and psychophysical measures over time", *Hearing Research*, vol. 92, no. 1-2, pp. 100-111.

Miller, C. A., Woodruff, K. E., & Pfingst, B. E. 1995, "Functional responses from guinea pigs with cochlear implants. I. Electrophysiological and psychophysical measures", *Hearing Research*, vol. 92, no. 1-2, pp. 85-99.

Miller, J. M., Malone, M. A., Duckert, L. G., & Pfingst, B. E. 1983, "Cochlear prostheses: Stimulation-induced damage", *Annals of Otology, Rhinology and Laryngology*, vol. 92, no. 6 I, pp. 599-609.

Momin, S. R., Melki, S. J., Alagramam, K. N., & Megerian, C. A. 2010, "Spiral ganglion loss outpaces inner hair cell loss in endolymphatic hydrops", *Laryngoscope*, vol. 120, no. 1, pp. 159-165.

Moore, D. R. 1994, "Auditory brainstem of the ferret: Long survival following cochlear removal progressively changes projections from the cochlear nucleus to the inferior colliculus", *Journal of Comparative Neurology*, vol. 339, no. 2, pp. 301-310.

Nadol, J. B., Adams, J. C., & O'Malley, J. T. 2011, "Temporal bone histopathology in a case of sensorineural hearing loss caused by superficial siderosis of the central nervous system and treated by cochlear implantation", *Otology and Neurotology*, vol. 32, no. 5, pp. 748-755.

© University of Pretoria

Nagel, D. 1974, "Compound action potential of the cochlear nerve evoked electrically. Electrophysiological study of the acoustic nerve (guinea pig)", *Archives of Oto-Rhino-Laryngology*, vol. 206, no. 4, pp. 293-298.

Nikolopoulos, T. P., O'Donoghue, G. M., & Archbold, S. 1999, "Age at implantation: Its importance in pediatric cochlear implantation", *Laryngoscope*, vol. 109, no. 4, pp. 595-599.

Niparko, J. K., Tobey, E. A., Thal, D. J., Eisenberg, L. S., Wang, N., Quittner, A. L., & Fink, N. E. 2010, "Spoken language development in children following cochlear implantation", *JAMA - Journal of the American Medical Association*, vol. 303, no. 15, pp. 1498-1506.

Nishimura, H., Hashikawa, K., Doi, K., Iwaki, T., Watanabe, Y., Kusuoka, H., Nishimura, T., & Kubo, T. 1999, "Sign language 'heard' in the auditory cortex", *Nature*, vol. 397, no. 6715, p. 116.

Oxenham, A. J., Bernstein, J. G. W., & Penagos, H. 2004, "Correct tonotopic representation is necessary for complex pitch perception", *Proceedings of the National Academy of Sciences of the United States of America*, vol. 101, no. 5, pp. 1421-1425.

Pfingst, B. E., Bowling, S. A., Colesa, D. J., Garadat, S. N., Raphael, Y., Shibata, S. B., Strahl, S. B., Su, G. L., & Zhou, N. 2011, "Cochlear infrastructure for electrical hearing", *Hearing Research*, vol. 281, pp. 65-73.

Ponton, C. W. & Eggermont, J. J. 2001, "Of kittens and kids: Altered cortical maturation following profound deafness and cochlear implant use", *Audiology and Neuro-Otology*, vol. 6, no. 6, pp. 363-380.

Purves, D., Augustine, G. J., & Fitzpatrick, D. 2001, "The Inner Ear," in *Neuroscience*, 2nd edn, Sinauer Associates.

Rattay, F., Lutter, P., & Felix, H. 2001, "A model of the electrically excited human cochlear neuronI. Contribution of neural substructures to the generation and propagation of spikes", *Hearing Research*, vol. 153, no. 1-2, pp. 43-63.

Rauschecker, J. P. & Shannon, R. V. 2002, "Sending sound to the brain", *Science*, vol. 295, no. 5557.

Rebscher, S. J., Hetherington, A. M., Snyder, R. L., Leake, P. A., & Bonham, B. H. 2007, "Design and fabrication of multichannel cochlear implants for animal research", *Journal of Neuroscience Methods*, vol. 166, no. 1, pp. 1-12.

Rebscher, S. J., Snyder, R. L., & Leake, P. A. 2001, "The effect of electrode configuration and duration of deafness on threshold and selectivity of responses to intracochlear electrical stimulation", *Journal of the Acoustical Society of America*, vol. 109, no. 5 I, pp. 2035-2048.

Robbins, A. M., Koch, D. B., Osberger, M. J., Zimmerman-Phillips, S., & Kishon-Rabin, L. 2004, "Effect of Age at Cochlear Implantation on Auditory Skill Development in Infants

© University of Pretoria

and Toddlers", *Archives of Otolaryngology - Head and Neck Surgery*, vol. 130, no. 5, pp. 570-574.

Rubinstein, J. T. 2004, "How cochlear implants encode speech", *Current Opinion in Otolaryngology and Head and Neck Surgery*, vol. 12, no. 5, pp. 444-448.

Ryugo, D. K., Rosenbaum, B. T., Kim, P. J., Niparko, J. K., & Saada, A. A. 1998, "Single unit recordings in the auditory nerve of congenitally deaf white cats: Morphological correlates in the cochlea and cochlear nucleus", *Journal of Comparative Neurology*, vol. 397, no. 4, pp. 532-548.

Schwartz, J. R. & Eikhof, G. 1987, "Na currents and action potentials in rat myelinated nerve fibres at 20 and 37 degrees C", *Pflug.Arch*, vol. 409, pp. 469-577.

Semaan, M. T. & Megerian, C. A. 2010, "Contemporary perspectives on the pathophysiology of Meniere's disease: Implications for treatment", *Current Opinion in Otolaryngology and Head and Neck Surgery*, vol. 18, no. 5, pp. 392-398.

Sharma, A., Dorman, M. F., & Spahr, A. J. 2002, "A sensitive period for the development of the central auditory system in children with cochlear implants: Implications for age of implantation", *Ear and Hearing*, vol. 23, no. 6, pp. 532-539.

Shepherd, R. K. & Javel, E. 1999, "Electrical stimulation of the auditory nerve: II. Effect of stimulus waveshape on single fibre response properties", *Hearing Research*, vol. 130, no. 1-2, pp. 171-188.

Shepherd, R. K., Linahan, N., Xu, J., Clark, G. M., & Araki, S. 1999, "Chronic electrical stimulation of the auditory nerve using non-charge- balanced stimuli", *Acta Oto-Laryngologica*, vol. 119, no. 6, pp. 674-684.

Shivdasani, M. N., Mauger, S. J., Rathbone, G. D., & Paolini, A. G. 2008, "Inferior colliculus responses to multichannel microstimulation of the ventral cochlear nucleus: Implications for auditory brain stem implants", *Journal of Neurophysiology*, vol. 99, no. 1, pp. 1-13.

Shore, S. E. 2009, "Auditory / Somatosensory Interactions," in *Encyclopedia of Neuroscience*, Academic Press, pp. 691-695.

Snyder, R. L., Bierer, J. A., & Middlebrooks, J. C. 2004b, "Topographic spread of inferior colliculus activation in response to acoustic and intracochlear electric stimulation", *JARO - Journal of the Association for Research in Otolaryngology*, vol. 5, no. 3, pp. 305-322.

Snyder, R. L., Bierer, J. A., & Middlebrooks, J. C. 2004a, "Topographic spread of inferior colliculus activation in response to acoustic and intracochlear electric stimulation", *JARO - Journal of the Association for Research in Otolaryngology*, vol. 5, no. 3, pp. 305-322.

Snyder, R. L., Bonham, B. H., & Sinex, D. G. 2008, "Acute changes in frequency responses of inferior colliculus central nucleus (ICC) neurons following progressively enlarged restricted spiral ganglion lesions", *Hearing Research*, vol. 246, no. 1-2, pp. 59-78.

© University of Pretoria

Snyder, R. L., Middlebrooks, J. C., & Bonham, B. H. 2008, "Cochlear implant electrode configuration effects on activation threshold and tonotopic selectivity", *Hearing Research*, vol. 235, no. 1-2, pp. 23-38.

Snyder, R. L., Rebscher, S. J., Cao, K., Leake, P. A., & Kelly, K. 1990, "Chronic intracochlear electrical stimulation in the neonatally deafened cat. I: Expansion of central representation", *Hearing Research*, vol. 50, no. 1-2, pp. 7-34.

Spahr, A. J., Litvak, L. M., Dorman, M. F., Bohanan, A. R., & Mishra, L. N. 2008, "Simulating the effects of spread of electric excitation on musical tuning and melody identification with a cochlear implant", *Journal of Speech, Language, and Hearing Research*, vol. 51, no. 6, pp. 1599-1606.

Stakhovskaya, O., Sridhar, D., Bonham, B. H., & Leake, P. A. 2007, "Frequency map for the human cochlear spiral ganglion: Implications for cochlear implants", *JARO - Journal of the Association for Research in Otolaryngology*, vol. 8, no. 2, pp. 220-233.

Strelioff, D. 1973, "A computer simulation of the generation and distribution of cochlear potentials", *Journal of the Acoustical Society of America*, vol. 54, no. 3, pp. 620-629.

Stypulkowski, P. H. & Van den Honert, C. 1984, "Physiological properties of the electrically stimulated auditory nerve. I. Compound action potential recordings", *Hearing Research*, vol. 14, no. 3, pp. 205-223.

Suesserman, M. F. & Spelman, F. A. 1993, "Lumped-parameter model for in vivo cochlear stimulation", *IEEE Transactions on Biomedical Engineering*, vol. 40, no. 3, pp. 237-245.

Svirsky, M. A., Teoh, S. W., & Neuburger, H. 2004, "Development of language and speech perception in congenitally, profoundly deaf children as a function of age at cochlear implantation", *Audiology and Neuro-Otology*, vol. 9, no. 4, pp. 224-233.

Sweeney, J. D., Mortimer, J. T., & Durand, D. "Modeling of mammilian myelinated nerve for functional neuromuscular electrostimulation", pp. 1577-1578.

Tavartkiladze, G. A., Potalova, L. A., Kruglov, A. V., & Belov, O. A. 2000, "Effect of stimulation parameters on electrically evoked auditory brainstem responses", *Acta Oto-Laryngologica*, vol. 120, no. 2, pp. 214-217.

Thalmann, R. & Thalmann, I. 1999, "Source and role of endolymph macromolecules", *Acta Oto-Laryngologica*, vol. 119, no. 3, pp. 293-296.

Tobey, E. A., Geers, A. E., Brenner, C., Altuna, D., & Gabbert, G. 2003, "Factors associated with development of speech production skills in children implanted by age five", *Ear and Hearing*, vol. 24, no. 1 SUPPL..

Van Dijk, J. E., Van Olphen, A. F., Langereis, M. C., Mens, L. H. M., Brokx, J. P. L., & Smoorenburg, G. F. 1999, "Predictors of cochlear implant performance", *Audiology*, vol. 38, no. 2, pp. 109-116.

van Wieringen, A., Macherey, O., Carlyon, R. P., Deeks, J. M., & Wouters, J. 2008, "Alternative pulse shapes in electrical hearing", *Hearing Research*, vol. 242, no. 1-2, pp. 154-163.

© University of Pretoria

Verbist, B. M., Ferrarini, L., Briaire, J. J., Zarowski, A., dmiraal-Behloul, F., Olofsen, H., Reiber, J. H. C., & Frijns, J. H. M. 2009, "Anatomic considerations of cochlear morphology and its implications for insertion trauma in cochlear implant surgery", *Otology and Neurotology*, vol. 30, no. 4, pp. 471-477.

Voie, A. H. 2002, "Imaging the intact guinea pig tympanic bulla by orthogonal-plane fluorescence optical sectioning microscopy", *Hearing Research*, vol. 171, no. 1-2, pp. 119-128.

Vollmer, M., Beitel, R. E., Snyder, R. L., & Leake, P. A. 2007, "Spatial selectivity to intracochlear electrical stimulation in the inferior colliculus is degraded after long-term deafness in cats", *Journal of Neurophysiology*, vol. 98, no. 5, pp. 2588-2603.

Wang, G. & Vannier, M. W. 1998, "Spiral CT image deblurring for cochlear implantation", *IEEE Transactions on Medical Imaging*, vol. 17, no. 2, pp. 251-262.

Westen, A. A., Dekker, D. M. T., Briaire, J. J., & Frijns, J. H. M. 2011, "Stimulus level effects on neural excitation and eCAP amplitude", *Hearing Research*, vol. 280, no. 1-2, pp. 166-176.

Wilson, B. S. Engineering Design of Cochlear Implants. In Zeng FG, Popper AN, Fay RR, eds. Cochlear Implants: Auditory Prostheses and Electric Hearing. New York : Springer, pp. 14-52. 2004.
Ref Type: Generic

Wilson, B. S. & Dorman, M. F. 2008, "Cochlear implants: A remarkable past and a brilliant future", *Hearing Research*, vol. 242, no. 1-2, pp. 3-21.

Wysocki, J. 2005, "Topographical anatomy of the guinea pig temporal bone", *Hearing Research*, vol. 199, no. 1-2, pp. 103-110.

Xu, J., Xu, S. A., Cohen, L. T., & Clark, G. M. 2000, "Cochlear view: Postoperative radiography for cochlear implantation", *American Journal of Otology*, vol. 21, no. 1, pp. 49-56.

Zhou, H. & Van Oosterom, A. 1994, "Application of the boundary element method to the solution of anisotropic electromagnetic problems", *Medical and Biological Engineering and Computing*, vol. 32, no. 4, pp. 399-405.

Zwolan, T. A., Kileny, P. R., Ashbaugh, C., & Telian, S. A. 1996, "Patient performance with the cochlear corporation '20 + 2' implant: Bipolar versus monopolar activation", *American Journal of Otology*, vol. 17, no. 5, pp. 717-723.

© University of Pretoria